PFG

Photogrammetrie Fernerkundung Geoinformation

Organ der Deutschen Gesellschaft für Photogrammetrie, Fernerkundung und Geoinformation (DGPF) e. V.

Jahrgang 2010, Heft 6

Hauptschriftleiter:
Prof. Dr.-Ing. Helmut Mayer

Schriftleiter:
Prof. Dr. rer.nat. Carsten Jürgens, Prof. Dipl.-Ing. Thomas P. Kersten, Prof. Dr. rer.nat. Lutz Plümer und Dr.-Ing. Eckhardt Seyfert

Redaktionsbeirat (Editorial Board): Clement Atzberger, Andrew Frank, Christian Heipke, Joachim Hill, Patrick Hostert, Hans-Gerd Maas, Wolfgang Reinhardt, Franz Rottensteiner, Jochen Schiewe

E. Schweizerbart'sche Verlagsbuchhandlung
(Nägele u. Obermiller) Stuttgart 2010

Deutsche Gesellschaft für Photogrammetrie, Fernerkundung
und Geoinformation (DGPF) e.V.
Gegründet 1909

Die *Deutsche Gesellschaft für Photogrammetrie, Fernerkundung und Geoinformation* (DGPF) e.V. unterstützt als Mitglieds- bzw. Trägergesellschaft die folgenden Dachverbände:

International Society
for Photogrammetry
and Remote Sensing

Deutsche Arbeits-
gemeinschaft für
Mustererkennung e.V.

GeoUnion
Alfred-Wegener-Stiftung

Herausgeber:
© 2010 Deutsche Gesellschaft für Photogrammetrie, Fernerkundung und Geoinformation (DGPF) e.V.
Präsidentin: Prof. Dr. Cornelia Gläßer, Martin-Luther-Universität Halle-Wittenberg, Institut für Geowissenschaften, Von-Seckendorff-Platz 4, D-06120 Halle, Tel.: +49(0)345 55-26020
Geschäftsstelle: Dr. Klaus-Ulrich Komp, c/o EFTAS Fernerkundung Technologietransfer GmbH, Oststraße 2–18, D-48145 Münster, e-mail: klaus.komp@eftas.com

Published by:
E. Schweizerbart'sche Verlagsbuchhandlung (Nägele u. Obermiller), Johannesstraße 3A,
D-70176 Stuttgart. Tel.: 0711 351456-0, Fax: 0711 351456-99, e-mail: mail@schweizerbart.de
Internet: http://www.schweizerbart.de
Gedruckt auf alterungsbeständigem Papier nach ISO 9706-1994

All rights reserved including translation into foreign languages. This journal or parts thereof may not be reproduced in any form without permission from the publishers.
Die Wiedergabe von Gebrauchsnamen, Handelsnamen, Warenbezeichnungen usw. in dieser Zeitschrift berechtigt auch ohne besondere Kennzeichnung nicht zu der Annahme, dass solche Namen im Sinne der Warenzeichen- und Markenschutz-Gesetzgebung als frei zu betrachten wären und daher von jedermann benutzt werden dürften.
Verantwortlich für den Inhalt der Beiträge sind die Autoren.

ISSN 1432-8364

Science Citation Index Expanded (also known as SciSearch®) Journal Citation Reports/Science Edition
Hauptschriftleiter: Prof. Dr.-Ing. Helmut Mayer, Institut für Angewandte Informatik, Universität der Bundeswehr München, D-85577 Neubiberg, e-mail: Helmut.Mayer@unibw.de
Schriftleiter: Prof. Dr. rer.nat. Carsten Jürgens, Ruhr-Universität Bochum, Geographisches Institut, Gebäude NA 7/133, D-44780 Bochum, e-mail: carsten.juergens@rub.de, Prof. Dipl.-Ing. Thomas P. Kersten, HafenCity Universität Hamburg, Department Geomatik, Hebebrandstr.1, D-22297 Hamburg, e-mail: thomas.kersten@hcu-hamburg.de, Prof. Dr. rer.nat. Lutz Plümer, Universität Bonn, Institut für Geodäsie und Geoinformation, Meckenheimer Allee 172, D-53115 Bonn, e-mail: Lutz.Pluemer@ikg.uni-bonn.de und Dr.-Ing. Eckhardt Seyfert, Landesvermessung und Geobasisinformation Brandenburg, Heinrich-Mann-Allee 107, D-14473 Potsdam, e-mail: eckhardt.seyfert@geobasis-bb.de

Erscheinungsweise: 6 Hefte pro Jahrgang.
Bezugspreis im Abonnement: € 191,– pro Jahrgang. Mitglieder der DGPF erhalten die Zeitschrift kostenlos. Der Online-Zugang ist im regulären Subskriptionspreis enthalten.

Anzeigenverwaltung: E. Schweizerbart'sche Verlagsbuchhandlung (Nägele u. Obermiller), Johannesstraße 3A, D-70176 Stuttgart, Tel.: 0711 351456-0; Fax: 0711 351456-99.
e-mail: mail@schweizerbart.de, Internet: http://www.schweizerbart.de
Bernhard Harzer Verlag GmbH, Westmarkstraße 59/59a, D-76227 Karlsruhe, Tel.: 0721 944020, Fax: 0721 9440230, e-mail: Info@harzer.de, Internet: www.harzer.de
Printed in Germany by Tutte Druckerei GmbH, D-94121 Salzweg bei Passau

PFG – Jahrgang 2010, Heft 6
Inhaltsverzeichnis

Themenheft DeSecure

Berichte und Mitteilungen

Zusammenfassungen der „Originalbeiträge" und der Beiträge „Aus Wissenschaft und Technik" (deutsch und englisch) sind auch verfügbar unter www.dgpf.de/neu/pfg/ausgaben.htm

PFG · Photogrammetrie · Fernerkundung · Geoinformation
Jahrgang 2010 · Heft 6

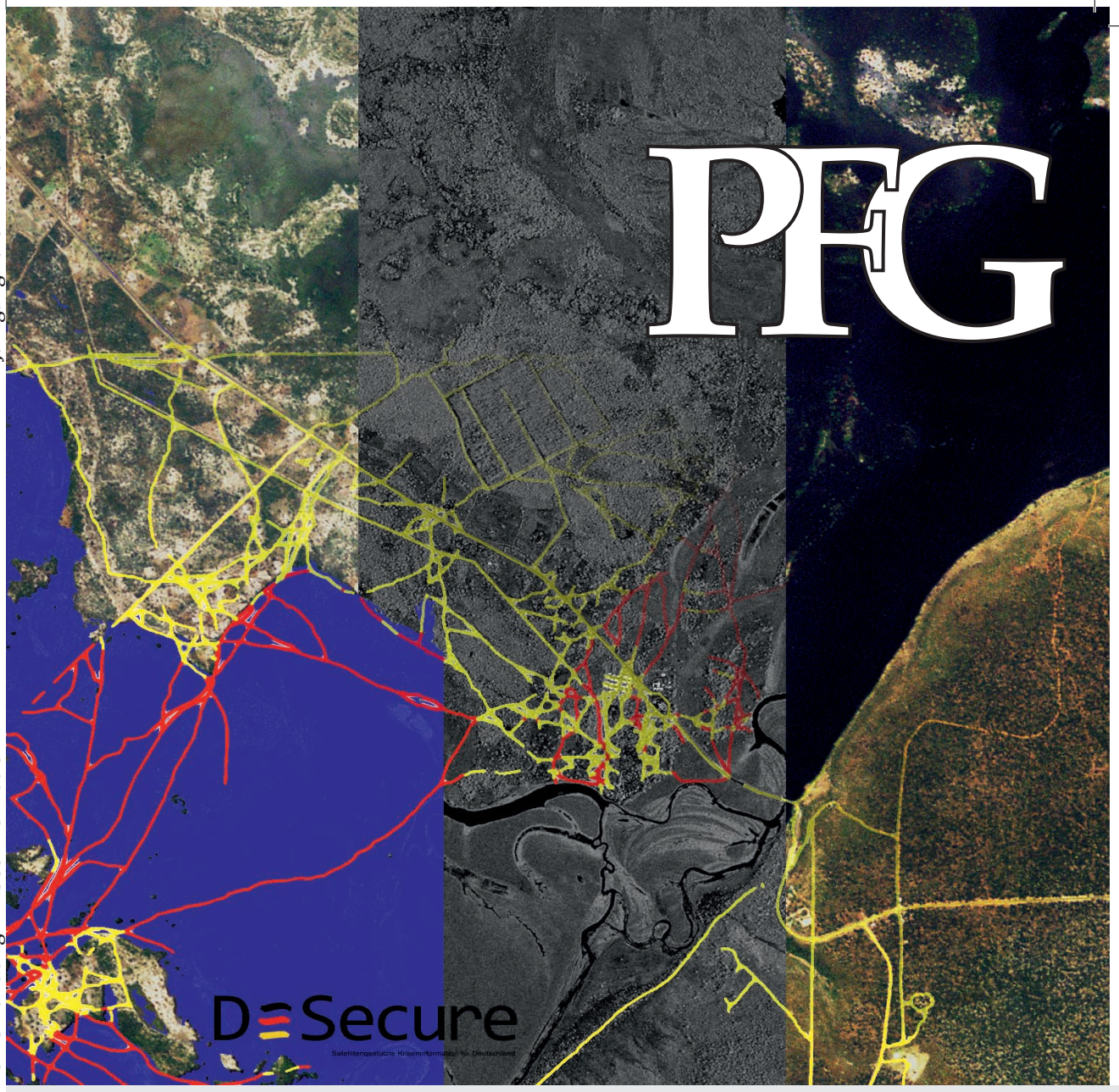

Photogrammetrie Fernerkundung Geoinformation

Jahrgang 2010
Heft 6
Organ der Deutschen Gesellschaft für Photogrammetrie, Fernerkundung und Geoinformation (DGPF) e.V.
Indexed in Science Citation Index Expanded (SciSearch®) Journal Citation Reports / Science Edition

E. Schweizerbart'sche Verlagsbuchhandlung (Nägele u. Obermiller) Stuttgart

PFG_Heft_5_2010.indd 1 07.10.2010 15:18:30 Uhr

PFG 2010 / 6, 425–427
Stuttgart, Dezember 2010

Article

Editorial: DeSecure – Satellitengestützte Kriseninformation für Deutschland

Monika Gähler, Oberpfaffenhofen & Stefan Hinz, Karlsruhe

Mit der weltweiten Zunahme von Naturkatastrophen, humanitären Notsituationen und zivilen Gefahrenlagen steigt auch der Bedarf an zeitnaher, präziser und flächendeckender Lageinformation. Diese aktuellen und umfassenden Informationen können inzwischen zum großen Teil durch Analyse von satellitengestützten Fernerkundungsdaten bereitgestellt werden und wertvolle Informationen im Bereich der Naturkatastrophen-Vorsorge, -Frühwarnung und -Ausbreitung sowie auch zur Schadensabschätzung nach Katastrophen, zur schnellen Übersicht akuter Ereignisse und zum Beobachten von Wiederaufbaumaßnahmen liefern. Hierfür sind Strukturen und Kapazitäten notwendig, die eine schnelle Aufnahme und verlässliche Aufbereitung der Satellitendaten ermöglichen.

Dieses Themenheft der PFG gibt einen Einblick in die Ziele und Ergebnisse des Projektes DeSecure. DeSecure ist ein Verbundprojekt initiiert durch die DLR Raumfahrtagentur mit dem übergeordneten Ziel der Verbesserung der operativen Bereitstellung von satellitengestützten Krisenlageinformationen durch eine Stärkung der in Deutschland verfügbaren methodisch-technischen Notfallkartierungskapazitäten und geht einher mit dem Ausbau der GMES (Global Monitoring for Environment and Security) Aktivitäten auf europäischer Ebene. Hierfür wurde aufbauend auf einer Nutzeranalyse der gesamte Produktionszyklus von satellitengestützter Information (Satellitendatenempfang, -prozessierung, Informationsextraktion und -bereitstellung) im Projektzeitraum (2007–2010) analysiert, Optimierungspotentiale identifiziert und für diese konzeptionelle und praktische Lösungswege erarbeitet und umgesetzt. Die erzielten Verbesserungen werden exemplarisch in den Beiträgen dieses Heftes dargestellt.

Neben dem Deutschen Fernerkundungsdatenzentrum (Projektleitung) waren das Institut für Methodik der Fernerkundung des DLR sowie die Industriepartner Definiens AG, GAF AG, Infoterra GmbH, PRO DV AG und RapidEye AG sowie die Technischen Universitäten Berlin und München beteiligt.

Fig. 1: DeSecure Konsortium.

Durch DeSecure wurden die operativen Notfallkartierungskapazitäten insbesondere beim Zentrum für satellitengestützte Kriseninformation (ZKI) des Deutschen Fernerkundungsdatenzentrums (DFD) im DLR sowie bei den Projektpartnern gesteigert und weiterentwickelt. Aufgabe des ZKI ist die schnelle Beschaffung, Aufbereitung und Analyse von Satellitendaten bei Natur- und Umweltkatastrophen, für humanitäre Hilfsaktivitäten und für die zivile Sicherheit sowie die Bereitstellung der extrahierten Krisenlageinformation in aufbereiteten Produkten. Die bei den Analysen verwendeten Daten, werden zurzeit über verschiedene Mechanismen bereitgestellt, z. B. die „International Charter on Space and Major Disasters“ oder über den Auf- bzw. Ausbau der GMES Aktivitäten auf europäischer Ebene.

© 2010 E. Schweizerbart'sche Verlagsbuchhandlung, Stuttgart, Germany
www.schweizerbart.de
DOI: 10.1127/1432-8364/2010/0064
1432-8364/10/0064 $ 0.75

GMES ist eine gemeinsame Initiative der Europäischen Kommission und der europäischen Raumfahrtagentur ESA für Globale Umwelt- und Sicherheitsüberwachung. Ziel ist es bis zum Jahr 2012, durch eine arbeitsteilige Zusammenarbeit in Europa eine eigenständige, dauerhaft verfügbare, kosteneffiziente und nutzerfreundliche Beobachtungskapazität für politische Entscheidungsträger und Behörden zu schaffen. Nach dem Aufbau der europäischen GMES Kapazitäten bis zum Anfang 2012 sollen die GMES Dienste in den operationellen Betrieb sowie eine evolutionäre Weiterentwicklung übergeführt werden. Dies wird zunächst durch GMES Kerndienste für Land, Ozean und Notfallkartierung geschehen. Um die europäischen GMES Aktivitäten und nationale Kapazitäten in der Informationserzeugung und -bereitstellung besser koppeln zu können, wurden die nationalen Projekte DeCOVER, DeMARINE und DeSecure initiiert.

Ein Schwerpunkt von DeSecure war es demnach auch, die deutschen Anforderungen, Bedürfnisse sowie Kapazitäten für den Bereich der satellitengestützten Krisenlageinformation zu identifizieren, zu definieren sowie weiterzuentwickeln und so die deutschen Interessen gebündelt in die GMES Aktivitäten auf europäischer Ebene einfließen zu lassen. Dabei stand neben der Sammlung der spezifischen Nutzeranforderungen die Integration der deutschen Sensoren TerraSar-X und RapidEye in Krisenkartierungen im Fokus. Hierdurch sollten diese Sensoren den deutschen und europäischen Nutzern besser bekannt gemacht werden. Darüber hinaus wurden durch Universitäten und Industriepartner technisch operative Analysemethoden geschaffen, die u.a. die Anwendungsentwicklung sowie Vermarktung der Daten und Informationsprodukte, auch über den Krisensektor hinaus, stärken.

Das vorliegende Themenheft beleuchtet v.a. die methodischen Weiterentwicklungen der gesamten Prozessierungskette von der Bildaufnahme über die Informationsextraktion als Schwerpunktthema bis hin zur Dissemination der Ergebnisse. Der Artikel von Hoja et al. beschäftigt sich mit der Effizienzsteigerung der Bilddatenakquisition und -Vorverarbeitung unter Berücksichtigung der speziellen Nahe-Echtzeit Anforderungen in Krisensituationen. Die Herausforderungen und Lösungsansätze werden anhand der beiden deutschen Fernerkundungssysteme TerraSAR-X und RapidEye dargestellt. Ebenfalls unter dem Blickwinkel der hocheffizienten Auswertung fokussiert die Arbeit von Kersten et al. auf die semi-automatische Klassifikation von Objekten. Das auf hierarchischen Markov-Zufallsfeldern basierende Verfahren ist generisch angelegt und kann an unterschiedliche Objektklassen und Aufgabenstellungen der krisenrelevanten Informationsextraktion adaptiert werden. Speziell mit Straßen beschäftigt sich dagegen der Artikel von Frey et al. Das modulare System integriert Information aus Geodatenbanken wie Digitale Geländemodelle oder (u. U. nur grob) digitalisierte Straßenachsen und ist in der Lage, das Straßennetz zu bewerten, zu vervollständigen, geometrisch zu verfeinern und schließlich mithilfe aktueller Satellitenbilddaten auf Befahrbarkeit hin zu analysieren. Das anschließend vorgestellte Verfahren von Schmitt et al. beinhaltet einen generischen Ansatz zur Änderungserkennung in multitemporalen SAR-Bildern. Methodisch stützt sich das Verfahren auf die sog. Curvelet-Transformation – grundlegend eine der Fourier-Transformation ähnliche Repräsentation, die jedoch multiskalige curvilineare Strukturen als Basisfunktionen verwendet. Im folgenden Artikel von Herrera et al. wird die inzwischen beinahe weltweit relevant gewordene Thematik der schnellen Überflutungskartierung behandelt. Das vorgestellte Verfahren ist grundsätzlich generisch aufgebaut und kann multiple Datenquellen verarbeiten. Aufgrund der Allwettertauglichkeit von Radar-Fernerkundungssystemen steht in der Arbeit das Flut-Monitoring mit TerraSAR-X im Vordergrund. Der das Themenheft abschließende Artikel von Andresen & Stracke beschäftigt sich schließlich mit der Thematik der nutzergerechten Darstellung und Dissemination (Verbreitung) der Ergebnisse. Besonderes Augenmerk liegt dabei auf der 3D Visualisierung unter quasi-Echtzeit Bedingungen.

Die Editoren haben das Themenheft einerseits initiiert, um der interessierten PFG-Leserschaft einen Überblick über die neuesten Entwicklungen, die Herausforderungen sowie die Komplexität der satellitengestützten Er-

fassung und Analyse von Kriseninformation zu geben, andererseits soll durch die selektive Auswahl der präsentierten Arbeiten auch Einblick in methodische Weiterentwicklungen im Bereich der Bildverarbeitung, Bildanalyse und Visualisierung gegeben werden. Daher wurde auch auf eine gewisse inhaltliche Eigenständigkeit der Artikel geachtet. Wir wünschen viel Freude beim Lesen!

Anschriften der Autoren:

Dr. Monika Gähler, Deutsches Zentrum für Luft- und Raumfahrt e.V., Deutsches Fernerkundungsdatenzentrum, Abteilung Zivile Sicherheit & GeoRisiken, Oberpfaffenhofen, D-82234 Weßling, Tel.: +49-8153-28-3309, Fax: -1445, e-mail: Monika.Gaehler@dlr.de

Prof. Dr.-Ing. Stefan Hinz, Karlsruher Institut für Technologie (KIT), Institut für Photogrammetrie und Fernerkundung, D-76128 Karlsruhe, Tel.: +49-721-608-2314, Fax: -8450, e-mail: stefan.hinz@kit.edu

PFG 2010 / 6, 429–438
Stuttgart, Dezember 2010

Article

Optimised Near-Real Time Data Acquisition and Pre-processing of Satellite Data for Disaster Related Rapid Mapping

Danielle Hoja, Maximilian Schwinger, Anna Wendleder, Oberpfaffenhofen; Peter Löwe, Harald Konstanski, Horst Weichelt, Brandenburg an der Havel & Nadine Kiefl, Jürgen Janoth, Friedrichshafen

Keywords: RapidEye, Infoterra, TerraSAR-X, DLR, Rapid Imaging, Rapid Mapping, Rapid Ordering Process

Summary: In its first part this paper describes exemplarily optimisations of the satellite systems RapidEye and TerraSAR-X. For this purpose a short insight into processes, relevant for data production, will be given. Focus of this will be time constraints typical for disaster related rapid mapping.

Optimisations of geometric pre-processing of satellite data are described in a second part of this paper. For this purpose different software packages available for radar and optical data were compared and analysed respectively. Results were as far as possible optimised.

Zusammenfassung: *Optimierte Nahe-Echtzeit Akquisition und Vorverarbeitung von Satellitendaten zum Zweck der Krisenkartierung.* Dieser Artikel beschreibt im ersten Teil exemplarisch die Optimierung der Satellitensysteme RapidEye und TerraSAR-X. Hierzu wird ein kurzer Einblick in die zur Datenlieferung notwendigen Abläufe bei den Satellitendatenanbietern gegeben. Der Fokus liegt auf den zeitlichen Ansprüchen der schnellen Krisenkartierung. Die Optimierung der Vorverarbeitung der vom Satellitendatenanbieter erzeugten Daten mit dem Schwerpunkt geometrische Entzerrung wird im zweiten Teil des Artikels beschrieben. Hierzu wurden auf dem Markt verfügbare Programme für Radar- und optische Bilder jeweils verglichen, analysiert und soweit möglich Ergebnisse optimiert.

1 Introduction

During a typical disaster-related rapid mapping process several requirements have to be fulfilled by a satellite data provider. As an example, Fig. 1 shows communication and actions during a rapid mapping process between a satellite data provider and the ZKI (Centre for Satellite Based Crisis Information). It does not include actions performed within an entity.

Within the blue highlighted area the following actions are performed:

- The customer, in this case ZKI, communicates an order to the satellite data provider.
- The satellite data provider decides if the order can be answered with catalogued data or if new data has to be acquired.
  - If catalogue data is needed, the data can be served without further actions.
  - If data has to be acquired, the satellite data provider has to
    - Create a schedule for the satellite which includes the ordered data;
    - Command the satellite(s);
    - Satellite(s) acquire(s) the data;
    - Data is down linked to a ground station;
    - Data is transferred to satellite data providers catalogue.

© 2010 E. Schweizerbart'sche Verlagsbuchhandlung, Stuttgart, Germany
www.schweizerbart.de
DOI: 10.1127/1432-8364/2010/0065
1432-8364/10/0065 $ 2.50

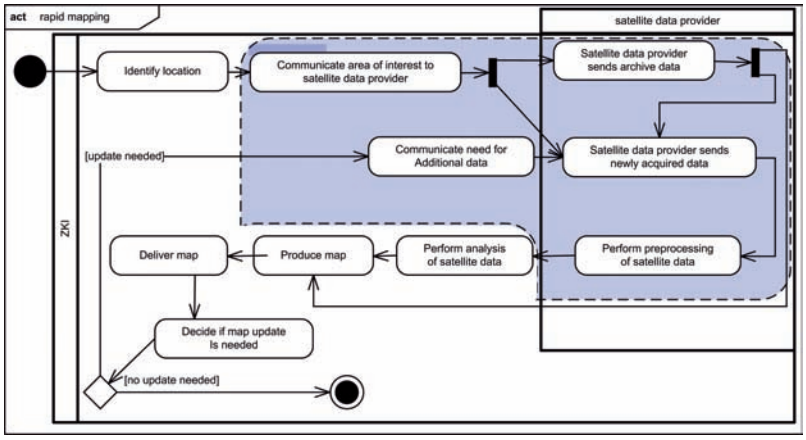

Fig. 1: Rapid Mapping Process as activity diagram. The blue highlighted area describes content which is discussed in this article.

- Data is pre-processed and delivered to the customer.

A rapid mapping process is differentiated from a normal mapping process mainly by its time constraints. To deliver information about a disaster in near real time (NRT) is vital to save lives of people involved. Near real time means the whole process only takes the time needed for processing and transfer. For satellite application this includes the time constraint arising from the satellites visibility by a ground station, which is limited by the number of used ground stations and the satellites orbit. Only if a satellite is visible to a ground station it can be commanded and data can be down linked from the satellite.

2 Typical Rapid Mapping Products

To find the right focus, typical products have to be identified and requirements which lead to this product to be devised.

After a disaster comes into focus a first product need is a **reference map**. Requirements for this map which are of importance within our focus are scale (1 : 200 000 to 1 : 25 000) and availability (worldwide within 6 hours), also the maps have to include a timestamp and geo-reference. In Fig. 2 the steps needed for creation of a reference map are depicted. The map has to be created from pre-damage data acquired prior to the disaster.

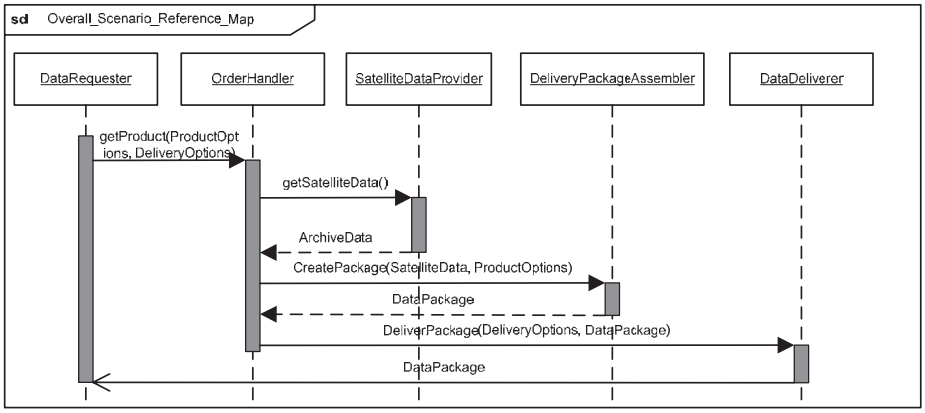

Fig. 2: Interactions typical for generation of a reference map for disaster scenarios.

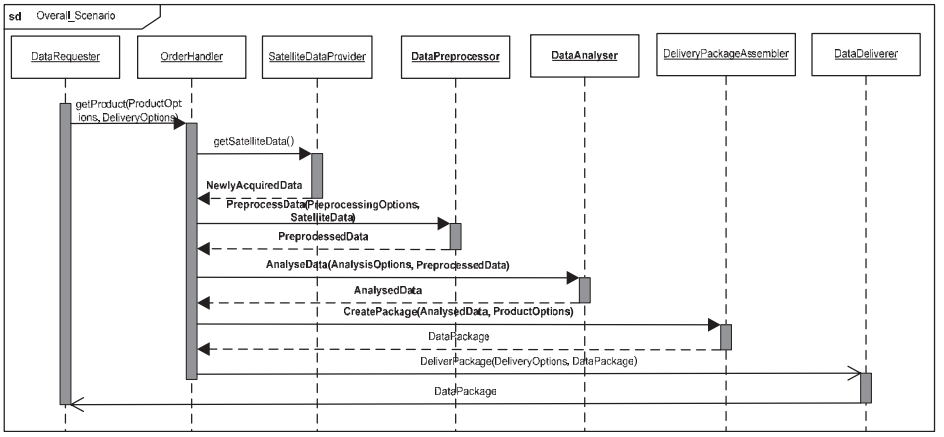

Fig. 3: Interactions typical for generation of a damage map.

A map concerning the special circumstances of a disaster is the next map needed. This map shall be called **damage map**. In Fig. 3 the much more complex actions needed for creation of a damage map are depicted. The differences from requirements of a reference map are scale (1 : 50 000 to 1 : 10 000) and availability (24 hours after ordering).

The main difference between a reference map and a damage map is the data needed to produce these maps. A reference map is a standard map of the area of interest. It has been created prior the disaster and is not disaster specific. The damage map uses satellite images created after the disaster. It is disaster specific and is analysed in detail (as depicted in Fig. 3).

The implementation of the scenarios leading to a damage map shall now be described for the satellite data providers RapidEye and Infoterra.

3 RapidEye

The effective and rapid imaging of large area disasters as applied in the DeSecure project requires imaging activites immediately following the disaster event. The RapidEye satellite constellation of five identical satellites is well suited for disaster mapping tasks as it provides multispectral imaging in 6.5 m resolution, a swath width of 77 km and a high area revisit rate. The capability of RapidEye's image acquisition workflows to successfully handle distaster-related special imaging orders were verified and repeatedly demonstrated within the DeSecure project.

3.1 *The RapidEye Mission*

The RapidEye Satellite constellation was successfully launched in August of 2008. All five satellites were successfully deployed and are in phase. Detailed information about the RapidEye system is given in (Tyc et al. 2008).

3.2 *Standard RapidEye Image Ordering and Processing Workflow*

RapidEye uses a flexible ordering and processing workflow. The workflow begins when an image order is entered by a Customer Service Representative (CSR) into the RapidEye Order Handling System (OHS). The OHS provides the order information for the following processing steps.

Following a positive decision during the next planning session, the tasked imaging schedule is uploaded to the satellite constellation from the RapidEye facility in Brandenburg an der Havel, Germany. After image acquisition, the collected data is downloaded via

a receiving station located in Spitsbergen, Norway. The image data is transferred to the Brandenburg facility for further processing. Derived image products are in turn generated and provided via a „drop-box“ for FTP access to the customer.

Special Order Requests for Disaster Imaging for DeSecure

To enable the rapid imaging on short notice, such as to map natural disasters, a dedicated workflow was defined (RapidEye Special Order Request) to enable the processing of short term image orders of high priority. For this, at the beginning of each planning session the stack of incoming orders is checked for Special Orders. If this applies, the acceptance and prioritisation of the Special Orders is ensured by the (human) operators.

The originally scheduled trials and subsequent evaluation of the Special Order Process were rendered obsolete by real world scenarios: The Special Order Process underwent its first successful application in February 2009 for the mapping of bush fires in Australia.

Daily Imaging Tasking Planning (Fig. 4)

After initially starting out with a single daily planning cycle, RapidEye conducts planning sessions twice every day since 2009 to schedule the imaging tasking of the satellite fleet. The daily planning schedule is as follows:

06:00 UTC: The planning of imaging from 13:00 UTC to 24:00 UTC is done, based on existing image orders and global cloud forecasts. This planning focuses on the imaging activities covering both South and North America.
14:00 UTC: Planning of imaging from 00:00 UTC till 13:00 UTC on the following day, based on image orders and the latest cloud forecasts. This planning phase focuses on Australia, Asia, Europe and Africa.

The results of each planning are subsequently handed to the satellite control centre to be uploaded to the individual satellites via the RapidEye facilities in Brandenburg an der Havel, Germany.

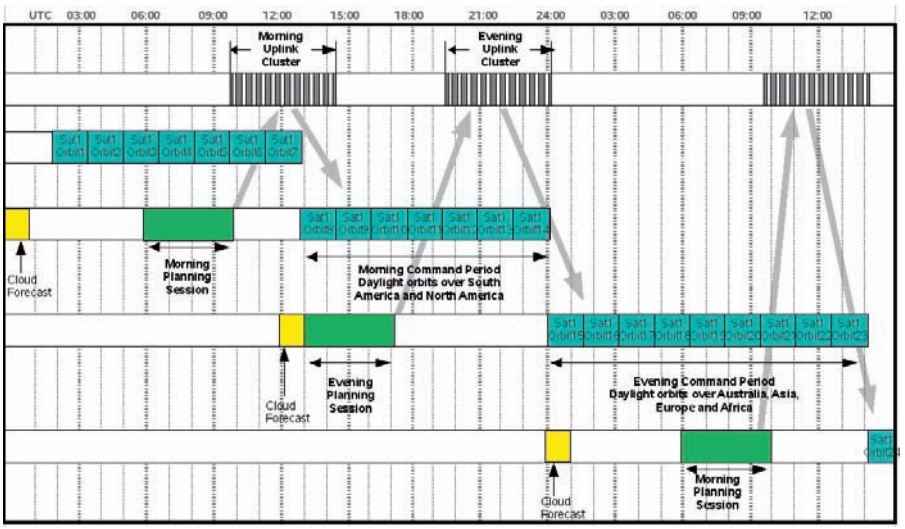

Fig. 4: RapidEye daily image acquisition planning workflow. Each planning phase (6:00 UTC and 14:00 UTC) is followed by the upload of an updated imaging schedule to the satellites. Upon successful image acquisition, the imagery data is downloaded via a ground station on Spitzbergen (Svalbard), Norway.

Time Constraints

The time span between the "go" decision to image an area of interest and the actual imaging event can range between 90 minutes to 13 hours. The reason for this is the time difference in universal time between the overpass of the tasked satellite over the ground station in Brandenburg and the next overpass over the area of interest.

Fig. 5 gives the times in universal time (UTC) when the satellite constellation passes areas of interest during the daylight hours. After successful image acquisition, the data download via Spitsbergen and transfer to the RapidEye facilities in Brandenburg, Germany, can take up to 60 minutes.

3.3 *Test Cases*

The Special Order Request workflow was successfully applied to provide imagery for the following six worldwide disaster imaging activities within the scope of the DeSecure project.

- 2009 February, Australia: Bush Fires
- 2009 April and 2010 April, Namibia: Caprivi flooding events
- 2009 June, Greece: Bush Fires
- 2010 March, Haiti: Earthquake
- 2010 April, Chile: Earthquake / Tsunami
- 2010 April, Gulf of Mexico: Oil spill

3.4 *RapidEye Conclusion*

RapidEye's Special Order Request work flow for rapid imaging for large disasters has been successfully tried and tested within the DeSecure project. Instead of a planned test run, the work flow performance was confirmed in real world situations due to sudden demand. Caused by system design constraints, minimal response/turnaround times from placing an order until imagery delivery (for special order completion) exist. It was confirmed that the system can successfully provide imagery data to the Svalbard station within a time frame from 90 minutes to 13 hours after a positive planning decision. Within additionally up to 60 minutes the image data were available in RapidEye for processing and delivery to the customer. The specified response times were always met when the Special Order Process was used for six different disaster imaging tasks on several continents in the DeSecure project.

The work flow for Special Order Requests was and still is under permanent review and optimisation. Improvements could be achieved in the order submission to RapidEye, the implementation of orders into the planning system, the improvement of processing speed and the delivery process of image data to the customer.

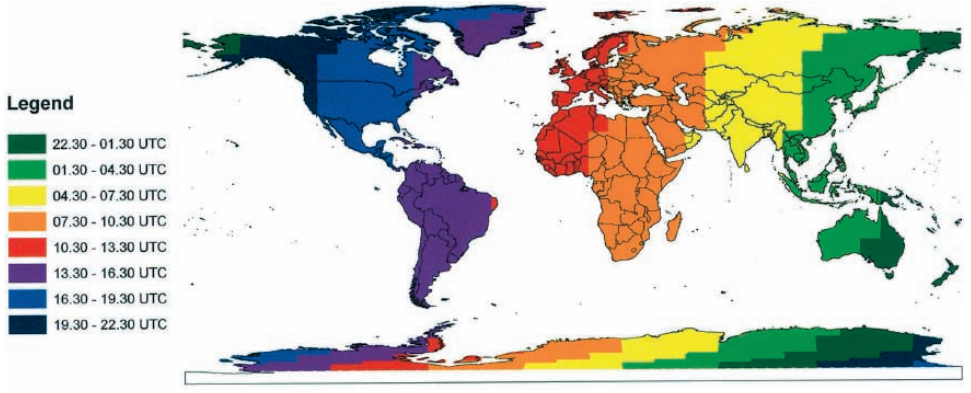

Fig. 5: Daily timeslots for satellite passes: Schematic overview of the daily imaging times by the the RapidEye satellite constellation. Example: The imaging of central and western Europe can only occur between 10:30 und 13:30 universal time. The imaging of Haiti (Caribbean) or the Gulf of Mexico only occurs between 13:30 to 16:30 hours universal time.

4 TerraSAR-X

In case of a crisis situation rapid delivery of remote sensing data is of utmost importance to serve the user community with early information to support crisis intervention. TerraSAR-X due to its weather independent SAR instrument is well suited for disaster mapping applications and offers different imaging modes ranging from very high resolution SpotLight mode (1 m) to StripMap mode (3 m) up to medium resolution ScanSAR mode (18.5 m). In the frame of the DeSecure project the near-real time data acquisition capability of the combined TerraSAR-X Ground Segment operated by DLR and the Commercial TerraSAR-X Service Segment operated by Infoterra were analysed in order to identify and implement potential improvements to provide customers more rapidly with data and first results. The focus was on optimising the entire processing chain from data ordering up to delivery to the final customer.

4.1 *The TerraSAR-X Mission*

TerraSAR-X is a German radar satellite. It carries a high frequency X-band SAR sensor which can be operated at different imaging modes including high resolution SAR imagery that had not been available by commercial missions from space before. The mission has been implemented as a Public Private Partnership (PPP) between the German Ministry of Education and Science (BMBF), German Aerospace Centre (DLR) and EADS Astrium GmbH.

DLR operates the satellite control system and the payload ground segment for receiving, processing, archiving and distribution of the X-band SAR data. DLR is also responsible for instrument calibration, the operations and the scientific use of TerraSAR-X data.

Infoterra holds the exclusive commercial exploitation rights, operates the commercial service segment and provides all commercial customers access to TerraSAR-X data. Due to its high resolution TerraSAR-X data are subject to a sensitivity check according to the German Satellite Security Act (SatDSiG). This law aims to protect the foreign policy and security interests of Germany.

4.2 *TerraSAR-X Overall Response Time*

TerraSAR-X overall system response times for tasking, sensing, reception and delivery of SAR Image Products are presently determined by a system architecture composed of one spacecraft in orbit and two ground stations, one dedicated for data reception located in Neustrelitz, Germany, and one station dedicated for command uplink, located in Weilheim, Germany. Therefore, orbital geometry, geographic latitude of area of interest and nominal incidence angle ranges of TerraSAR-X dictate the frequency with which an area of interest can be imaged by the satellite, with variations ranging from 1.5 to 11 days. Once

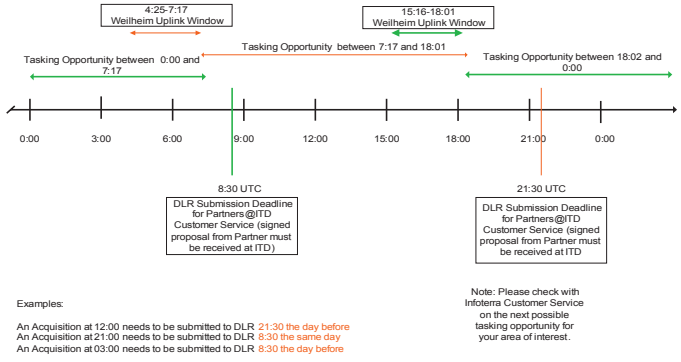

Fig. 6: TerraSAR-X timelines and submission deadline.

one or several accesses over a given site have been identified, the earliest possible access is identified in relation to its submission deadline. This deadline is the last possible opportunity to schedule a particular acquisition in the next 6-18 hours. The Fig. 6 illustrates the principle.

Two deadlines per day for placing orders exist at 8:30 UTC and 21:30 UTC. These deadlines correspond to tasking opportunities within the next 6 to 18 hours. It is important to note here that it is the sensing time of a selected acquisition (and therefore, its geographic location in the world) that determines the corresponding submission deadline.

Once the requested image has been acquired it will be down loaded via the Neustrelitz Groundstation and in case of a NRT request immediately processed to L1B products based on the available predicted orbit product. The final image products are then delivered to a customer pick up point.

4.3 *Optimisation of the TerraSAR-X Order Workflow*

The existing ordering and processing workflows have been analysed in the frame of the DeSecure project. The analysis has revealed that improvements could mainly be realised in following areas:

- Improved operational procedures to handle customer registration.
- Possibility to order long uninterrupted strips of TerraSAR-X StripMap data instead of single StripMap scenes.
- Automisation of the order workflow to reduce manual operator interaction.
- Improved order status handling to foster the overall system performance.
- Optimised sensitivity check according to German Satellite Security Act (SatDSiG).
- Automated delivery process to accelerate the submission of final products.

Consequently, the identified areas for improvement were implemented in the Commercial Service Segment operated by Infoterra and the TerraSAR-X Ground segment operated by DLR.

Several real life tests were conducted to assess and document the achievements that could be gained. The results show that a considerable speed-up can be realised by the implemented new features.

4.4 *TerraSAR-X Conclusion*

The TerraSAR-X order and processing workflow for NRT applications has been analysed in detail and several areas for improvement were identified and subsequently implemented in the existing infrastructure leading to substantial time savings. In particular, following conclusions can be drawn from the available test results:

Even with only one satellite in orbit and one receiving station it could be shown that for most areas in Europe image data can be provided within a few hours, when a tasking opportunity has been established, and a NRT Product is sufficient. Outside Europe the overall response time is mainly depending on the next possible acquisition opportunity.

For the test cases analysed the time from downlink to delivery of the final orthorectified image results in about 2 hours which can be regarded as an excellent result.

5 Optimised Satellite Data Pre-Processing

For an efficient use of geo-information before or during a crisis of any kind, all information should be provided in a geographic information system (GIS). This requires the data to be orthorectified. This is a pre-processing step which has to be done for every satellite image.

Different established methods exist already for the orthorectification of satellite data; both for optical (e. g., RapidEye) and SAR scenes (e. g., TarraSAR-X). In the project DeSecure different software packages were analysed with regard to geometric accuracy, degree and potential of automatisation, computing times and therewith near-real time capabilities, the extendibility and potential for optimisation, user friendliness, and which satellite data are

supported by each program. When a potential for optimisation was detected, it was carried out within the project. For the comparison different test cases were processed with all software packages and the results were analysed qualitatively and quantitatively.

5.1 *Orthorectification of Optical Satellite Data*

For the orthorectification of optical satellite data four software packages (Tab. 1) were evaluated (Hoja et al. 2008). All results were collected yielding in a "methods-sensors matrix". For most common optical satellite data, all software packages create results of high accuracy in less than 45 minutes. Therefore the selection of the program to be used can be done by other criteria, e. g., which program one is used to or computing times. Especially, we emphasise to use a program, which is already existent and you are used to its handling. In this case, the failure probability is lowest and you can expect fast and reliable results in crisis situations.

For the mapping of crisis situations a large number of satellite sensors resp. their data is used. The integration into a processing chain is only possible, when all necessary information like satellite orientation or rational polynomial coefficients (RPC) are delivered in a known and unchanged format. Each change of the data format as often done tacitly by the data provider results in a (time) costly error search and therewith a delay of the orthorectification.

5.2 *Orthorectification of SAR Satellite Data*

Common methods for SAR geocoding as used by the project partners (Enhanced Geocoding Processor EGEO and TerraSAR-X Ground Service Segment TSXX) were evaluated similarly to the optical analysis in regard to accuracy and optimisation potential.

The performance of the EGEO processor (Huber et al. 2004) was analysed with ALOS PALSAR, RADARSAT I and II scenes. First the sensors were implemented in EGEO. The orthorectification of the test scenes with high resolution lasted 18 to 21 minutes. Lower resolutions induce shorter computing times. The time demand of rapid mapping is therefore met. The results of the orthorectified RADARSAT II scenes show very good position accuracy. However the processing of the orthorectified ALOS PALSAR and RADARSAT II scenes achieve a deficient accuracy. Reason is the imprecise position of the orbit. Further results show that improvements can only be achieved with the help of ground control points (GCP).

In a theoretical analysis the orbit measurement accuracy and the digital elevation model (DEM) quality were identified as the two main factors influencing the geo-location accuracy of SAR images. Both factors were further ana-

Tab. 1: Overview of analysed software packages.

Software package	Availability	Orthorectification with orientation data	Orthorectification with RPC	Computing time [min]	Image matching
XDibias	Research	OK	OK	15 to 45	OK
Erdas Imagine	Commercially	OK	OK	5	NO
ENVI	Commercially	OK	OK	30	OK
PCI Geomatics	Commercially	OK	OK	5 bis 10	NO
HALCON	Commercially	NO	NO	–	OK
MIL	Commercially	NO	NO	–	OK

lysed for TerraSAR-X data also with respect to NRT scenarios. In order to analyse the influence of the DEM quality, test sites with different terrain conditions were selected (flat to alpine terrain). The analysis for all test sites confirmed the theory: DEM with a small height error result in an enhancement of the geo-location accuracy of the orthorectified TerraSAR-X product.

In a second step the orbit measurement accuracies for TerraSAR-X were investigated. They differ in delivery time and accuracy. Thus, the best accuracy is available with the science orbit, which is available approx. 5 days after acquisition. The orbit with the lowest accuracy is a prediction of the orbit (predicted orbit) and available directly after downlink of the data. The rapid orbit is available approx. 15 hours after the last satellite contact and provides a very good accuracy of 2 m and better (Fritz & Eineder 2009). The results showed that the geo-location accuracies reached with the science and the rapid orbit were very similar. The difference between this two orbit precisions is nearly not measurable (approx. 0.5 meters). For NRT processing of TerraSAR-X scenes always the predicted orbit is used. The geo-location accuracy reached for the predicted orbit is strongly variable (5 to 34 meters). However, the accuracy is much better than the specification (~700 meters). For the tests conducted in this study the bad orbit accuracy did not result in strong artefacts caused by the not fitting DEM. Thus, the orthorectified products with the predicted orbit might be a first input for further NRT applications. Nevertheless, for cases where a good geo-location accuracy of the images is essential for further processing, it might be more efficient to use directly the rapid orbit.

Another possibility is to use GCP in order to enhance the pixel location accuracy if the orbit accuracy is not sufficient. Different tests were performed resulting in an improvement of the horizontal accuracy of the images in the NRT case. This is valid for manually selected points as well as for the use of points provided within a data base. It has to be considered that point identification and precise point determination in SAR images is often difficult and time consuming and requires reference data.

5.3 *Image-to-Image Registration*

Image-to-image registration (Matching) of satellite data of different acquisition dates serves the geocoding (automatic GCP detection), but is also an important pre-processing step for change detection after a crisis to provide the high relative accuracy of the images. For the image matching different procedures are available (investigations within the project DeSecure):

- Matching of optical data (Evaluation of existing methods).
- Matching SAR data (Development of an automated process, analysis of the optimisation potential for „chip matching“).
- Registration of optical with SAR data (Development of automated methods).

An evaluation of image matching software tools was realised with regard to accuracy and optimisation potential. Four software packages (Tab. 1) were analysed. Main result is that XDibias delivers the highest accuracy and is easy to use due to available scripts. XDibias is the only package that uses a local least squares matching and not only a correlation-based matching like all commercially available programs. Therefore, the most reliable results are produced by XDibias; however, computing time is higher than for all other software packages.

A prototype for a fully automatic orientation of SAR images was developed. The goal is to determine a precise orbit for geocoding by image-to-image matching between a NRT image and a reference SAR image. The approach uses a new algorithm for feature extraction developed in computer vision by Lowe (2004). No prior information about the position of the images or the overlapping parts is needed. The point operator extracts points with scale- and rotation-invariant descriptors (SIFT features). After this the points are matched by using the SIFT parameter descriptors with an extended matching scheme. The resulting points of the reference image are used as GCP for an adjustment of the SAR imaging geometry of the NRT image. This achieves results equivalent to a high precision orbit. The results show that the approach can be used for a wide range of scenes with differ-

ent SAR sensors, different incidence angles, different overlap extensions, and even different SAR frequencies. The results are very reliable but depend on well structured image content.

Another method to improve the geocoding besides image-to-image registration is the reusage of GCP points for the orthorectification of recurring acquisitions of an area by a so-called chip matching, which is based on an image-to-image matching approach. For each GCP a small area is cut from the image and saved in a database together with its coordinates. Almost the same pixel location accuracy was achieved for orthorectified images based on the science orbit information and orthorectified images based on the predicted orbit accuracy and GCP collection. Different polarisations or seasonal changes did not affect the matching results significantly. But the tests showed that the impact of the incidence angle is significant.

Finally, two different methods (mutual information, MI, and scale-invariant feature transform, SIFT) for image-to-image registration were developed and combined to extend their applicability to multi-modal SAR-optical and SAR-SAR registration. The performance of MI for very high resolution (VHR) remote sensing images was analysed and several methods were assessed to improve accuracy, applicability and processing time of VHR images acquired over dense urban areas. The potential of the methods to improve the orthorectification by image-to-image registration could be shown. Additionally, improvements in the SIFT processing chain were proposed resulting in an optimised technique for multi-modal SAR images (Suri & Reinartz 2010, Schwind et al. 2010).

Within the limit of the project DeSecure a large amount of optimisations was completed both, within the workflow of the satellite data systems RapidEye and TerraSAR-X, and regarding the orthorectifiing preprocessing, which has to be done for all satellite images.

References

Fritz, T. & Eineder, M., 2009: TerraSAR-X Basic Product Specification Document. – TX-GS-DD-3302, Issue 1.6.

Hoja, D., Schneider, M., Müller, R., Lehner, M. & Reinartz, P., 2008: Comparison of orthorectification methods suitable for rapid mapping using direct georeferencing and RPC for optical satellite data. – International Archives of the Photogrammetry, Remote Sensing and Spatial Information Sciences **37:** 1617–1624.

Huber, M., Hummelbrunner, W., Raggam, J., Small, D. & Kosmann, D., 2004: Technical Aspects of Envisat ASAR Geocoding Capability at DLR. – ENVISAT/ERS Symposium, Salzburg, Austria.

Lowe, D., 2004: Distinctive image features from scale-invariant keypoints. – International Journal of Computer Vision **60** (2): 91–110.

Schwind, P., Suri, S., Reinartz, P. & Siebert, A., 2010: Applicability of the SIFT Operator to Geometric SAR Image Registration. – International Journal of Remote Sensing, **31** (8): 1959–1980.

Suri, S. & Reinartz, P., 2010: Mutual Information-based Registration of TerraSAR-X and Ikonos Imagery in Urban Areas. – IEEE Transactions on Geoscience and Remote Sensing **48** (2): 939–949.

Tyc, G., Steyn, J., Hannaford, N., Gebbie, J., Stocker, B., Baker, A. & Oxfort, M., 2008: RapidEye – A cost-effective earth observation constellation. – IAC-08-B4.3.03 International Astronautics Conference 2008.

Addresses of the Authors:

Danielle Hoja, Anna Wendleder & Maximilian Schwinger, DLR e.V., Münchner Straße 20, 82234 Weßling, Tel.: +49-8153-28-1418, Fax: -1443, e-mail: Vorname.Nachname@dlr.de

Peter Löwe, Harald Konstanski & Horst Weichelt, RapidEye AG, Molkenmarkt 30, D-14776 Brandenburg an der Havel, Tel.: +49-331-8904-334, Fax: -101, e-mail: loewe@rapideye.de

Nadine Kiefl & Jürgen Janoth, Infoterra GmbH, Claude-Dornier-Strasse, D-88090 Immenstaad, Tel.: +49-7545-8-4291 e-mail: Juergen.Janoth@infoterra-global.com

Manuskript eingereicht: Juni 2010
Angenommen: September 2010

PFG 2010 / 6, 439–449
Stuttgart, Dezember 2010

Article

A General Framework for Fast and Interactive Classification of Optical VHR Satellite Imagery Using Hierarchical and Planar Markov Random Fields

Jens Kersten, Monika Gähler & Stefan Voigt, Oberpfaffenhofen

Keywords: Markov random fields, optical remote sensing, region labeling, crisis mapping

Summary: In this paper a general framework for fast and interactive classification of very high resolution satellite imagery for emergency and crisis mapping applications as well as several other applications is proposed. Multiscale image information as well as hierarchical and spatial context information is incorporated into the classification process using a hybrid Markov model, which combines a hierarchical directed as well as a planar undirected Markov random field (MRF). Classification is carried out using the standard non-iterative maximum a posteriori (MAP) and marginal posterior mode (MPM) inference. Additionally, a modified MAP computation, which is able to outperform the original methods under certain conditions, is proposed. Here uncertain image information, for example from class transition areas, is not incorporated during the inference procedure. The effectiveness of both the framework and the modified MAP inference is demonstrated by two examples.

Zusammenfassung: *Ein allgemeines Rahmenwerk für eine schnelle und interaktive Klassifikation hochauflösender optischer Satellitenbilder mittels hierarchischen und planaren Markov-Zufallsfeldern*. In diesem Artikel wird ein Rahmenwerk von Methoden für eine rasche und interaktive Klassifikation hochauflösender optischer Satellitenbilder im Rahmen von Notfall- und Krisenkartierungen sowie einer Vielzahl anderer Anwendungen vorgestellt. Mittels eines hybriden Markov-Modells, welches ein hierarchisches, gerichtetes und ein ungerichtetes, planares Markov-Zufallsfeld (MRF) kombiniert, werden Bildinformationen auf mehreren Skalen sowie hierarchische und räumliche Kontextinformationen in den Klassifikationsprozess einbezogen. Die Klassifikation erfolgt mittels der bekannten Maximum a Posteriori (MAP) sowie der Marginal Posterior Mode (MPM) Inferenz. Des Weiteren wird ein modifizierter MAP Ansatz vorgestellt, welcher unter bestimmten Voraussetzungen bessere Ergebnisse als die ursprünglichen Methoden liefern kann. Dabei wird „unsichere" Bildinformation, wie zum Beispiel aus Bereichen, welche Mischklassen aufweisen, nicht in den Inferenzprozess einbezogen. Die Effektivität des Rahmenwerks sowie der modifizierten MAP Berechnung wird an zwei Beispielen demonstriert.

1 Introduction

This paper focuses on the challenge of interactive classification of very high resolution optical satellite imagery for emergency and crisis mapping applications. Due to near real time processing requirements, classification is here restated as a task of semantic annotation of square image regions. Furthermore, the transferability of the approach to various crisis scenarios and therefore to several other applications is desired. Representatives for recurrent tasks during crisis scenarios are given with the classification of water surfaces (flood events), urban (earthquakes) and burned areas (fires). The fact, that nearly every crisis situation is unique, often hinders an application of automatic image analysis methods and demands an application of manual processing steps in terms of visual interpretation. This

© 2010 E. Schweizerbart'sche Verlagsbuchhandlung, Stuttgart, Germany
www.schweizerbart.de
DOI: 10.1127/1432-8364/2010/0066
1432-8364/10/0066 $ 2.75

work aims on the combination of fast image analysis methods and the inherent image understanding of an image analyst, in order to minimize visual interpretation steps and to derive robust and reproducible results.

Contextual information can improve classification accuracy significantly, if such information can be well modeled (Khedam & Belhadj-Aissa 2003). Bayesian models form a natural framework for integrating both statistical models of image behaviour and prior knowledge about the contextual structure of semantic classes. The contextual structure is often modeled as a Markov random field (MRF). In order to capture the intrinsic hierarchical nature of remote sensing data, several efficient Markov image modeling approaches defined on tree structures were proposed during the last two decades (Bouman & Shapiro 1994, Fieguth et al. 1998, Lafferté et al. 2000, Wilson & Li 2003, Choi et al. 2008). In order to cope with the surrounding conditions accompanied by crisis mapping scenarios, a hierarchical Markov model is proposed in this article. The motivation for using such a model is to provide a general interactive and computational effective framework for classification or pre-classification of multispectral satellite imagery.

Compared to earlier approaches the proposed framework uses hierarchical semantic networks in order to capture the hierarchical nature of remote sensing data. Therefore, the definition and modeling of arbitrary thematic classes in arbitrary scales as well as the relationship between the classes in adjacent scales is provided. The general formulation of the framework aims on the transferability of this approach to several different image contents, thematic problems as well as products of different sensors. Due to the initial lack of training data the model parameters are learned in a sequential manner.

The article is organized as follows: In Section 2, the proposed general framework is introduced. In Section 3, the utilized hierarchical and planar Markov models as well as the parameter estimation and inference are presented. The relevance and efficiency of the proposed framework is demonstrated in Section 4 and discussed in Section 5. Conclusions are drawn in Section 6.

2 Description of the Framework

Modeling image characteristics in a hierarchical manner has shown to be valuable for many applications, e. g., image labeling and object detection (Awasthi et al. 2007), multiband segmentation of astronomical images (Collet & Murtagh 2004) as well as the unsupervised detection of flood-induced changes in SAR data (Martinis et al. 2010). As pointed out in (Pérez et al. 2000), MRFs defined on causal tree structures always enable computationally efficient and exact inference of the unknown class labels, which is quite appealing for an application in the field of rapid mapping. Motivated by this, the proposed model is defined on a causal quadtree.

Image classification should be possible even when no additional information like vector data or a digital elevation model (DEM) is available. Hence, only the image itself as well as the image analyst is required for the application of the framework. The complete workflow is illustrated in Fig. 1 and can be described as follows: 1) A quadtree image representation is instantiated at first. The size of the smallest region can be defined individually depending on the spatial resolution of the im-

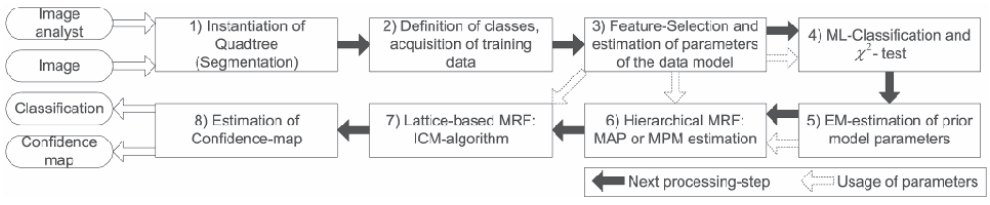

Fig. 1: Workflow for the proposed framework.

age as well as the structure of the thematic classes. 2) The framework allows an interactive definition of arbitrary semantic classes in different scales, i. e., the modeling of a hierarchical semantic network. For each class, the image analyst has to provide training data. 3) Based on the training data the parameters of Gaussian mixture models (data model) are estimated. Relevant features are identified through feature selection. 4) A constrained maximum likelihood classification is carried out in order to obtain training data (labeled regions) for the estimation of the prior model parameters via expectation maximization (step 5)). 6) Non-iterative hierarchical MAP or MPM inference is carried out using the parameters estimated in step 3 and 5. 7) A subsequent optimization step by incorporating spatial context concerning the finest quadtree level using a planar undirected MRF is carried out. 8) In order to obtain information concerning the confidence of the labeling process, a confidence map is computed.

Since some processing steps are optional, the classification can be carried out using several different combinations of methods. The steps 1, 2 and 3 are always required. Based on these computations the following combinations of processing steps are possible: (4), (4, 7), (4, 5, 6, (8)) and (4, 5, 6, 7, (8)), where step 8 is always optional. Interaction with the image analyst is required in the following steps: 1 (definition of the size of the smallest image regions), 2 (definition of classes and acquisition of training data), 3 (define the number of features and check estimation result), 4 (definition of the probability of error for the chi²-test) and 7 (definition of the weight of the context term).

3 Markov Image Modeling

Compared to other approaches, this framework allows to model arbitrary semantic classes in different scales as well as inter- and intra-scale context dependencies between the classes. In this section a complete overview of the methodology, namely hierarchical and lattice-based MRFs is given.

3.1 *Hierarchical Markov Image Models Defined on the Quadtree*

Problem Definition and Statistical Modeling

Given a set of variables (x,y), where x represents the unknown class labels and y the observed image data, the estimation of the "best" realization of x given y is desired. In a statistical process (x,y) represent occurrences of the vectors of random variables (X,Y). The so called Markovian independencies of (X,Y) are represented by an independence graph, which here is defined by a quadtree. As illustrated in Fig. 2, the components of X are indexed by the nodes of the quadtree, and additionally each (or a subset) of these nodes is associated with a component of the observation vector Y.

The set of all nodes of the quadtree is denoted S, and the set of nodes at a single level l is denoted S^l, with $l = 0,\ldots,N$. The root node of the tree is denoted $S^0=r$. Each node $s\in S^{l=1,\ldots,N}$ has a unique parent node s^- and each node $s\in S^{l=0,\ldots,N-1}$ is equipped with a set of four child nodes t. Assuming both a first order top-down Markov chain structure, where each node in S^l depends only on its ancestor in S^{l-1}, as well as a standard site-wise factorization for the observation model $P(y|x)$, the joint distribution $P(x,y)$ is given as the factorization of local functions

$$P(x,y) = P(x_r)\prod_{s\neq r} P(x_s \mid x_{s^-})\prod_{s\in S} P(y_s \mid x_s) \quad (1)$$

and is entirely defined by the root prior $P(x_r)$, the parent-child transition probabilities $\{P(x_s|x_{s^-})\}_{s\neq r}$ and the data conditional likelihoods $\{P(y_s|x_s)\}_{s\in S}$.

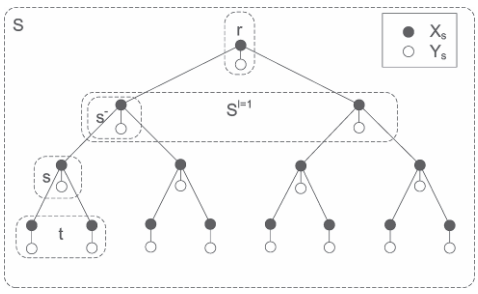

Fig. 2: Independence graph (the quadtree is illustrated as a dyadic tree).

Data Model

The proposed framework allows the definition of arbitrary semantic classes in arbitrary scales (i. e., quadtree levels). The classes are represented by Gaussian mixture models, where each involved level is treated independently. Various features like first and second order statistics, ratios like the well known NDVI, several colour space representations as well as texture and texture related features are available. An image element from a satellite image with four spectral channels can therefore be described by 70 features. In order to limit the computational efforts and to identify redundant and irrelevant features, the suboptimal feature selection method Sequential Forward Floating Search (SFFS) (Pudil et al. 1994) is utilized. The method starts with an empty set of features. Each iteration the most significant feature is added followed by a backtracking phase, where the optional exclusion of features is carried out for as long better variable subsets of the corresponding sizes are identified. The criterion for the evaluation of a distinct feature subset during the feature selection procedure is here defined as the mean Mahalanobis distance between the mixture components. Compared to the well known Bhattacharyya and Kullback-Leibler distance, we observed more reasonable and consistent results using the Mahanalobis distance.

Due to the fact that the true number of components of the desired mixture model is unknown, a split-based expectation maximization (EM) algorithm is applied. The decision, weather to split a component or not, depends on a multivariate normality criterion based on the Mahalanobis distance of a sample measurement vector from a certain Gaussian component center (Ververidis & Kotropoulos 2008). Using this criterion merging of components becomes obsolete.

Prior Model

For the prior model a Potts-like distribution is used in (Bouman & Shapiro 1994). This model favours identity between a node s and its parent node s^-. Since the proposed framework supports the definition of arbitrary semantic classes in each level, the definition of the involved transition probabilities is a more difficult task. Hence, an EM algorithm as described in (Feng et al. 2002) is utilized here to estimate the model parameters. A minimization of efforts concerning the acquisition of training data for the EM learning is achieved by a preliminary maximum likelihood (ML) classification based on the class feature densities of the data model. In order to avoid the incorporation of misclassifications, a chi^2 test of the form

$$\chi^2_{f,\alpha} \geq (y_s - \mu_x)^T \Sigma_x^{-1} (y_s - \mu_x) \qquad (2)$$

is applied, where f is the degree of freedom, α is the probability of error, y_s is the feature vector of node s and μ_x, Σ_x are the parameters of the Gaussian distribution of class x. Thus, the class label information of an image element s is involved in EM parameter estimation, if the right side of inequation (2) is smaller or equal than the corresponding quantile.

Inference

Since a distinct top-down pass through the quadtree hierarchy is a Markov chain in scale, a Viterbi-like algorithm (Forney 1973) can be applied for the exact and non-iterative inference of the class labels. The MAP estimate minimizes the probability that any image region will be misclassified. Wrong classifications are here penalized without any consideration about how many misclassifications occurred in total. A cost function which incorporates this aspect and is generally better behaved (Laferté et al. 2000) yields the MPM estimator. For further details concerning the derivation of the algorithms, the reader is referred to (Pérez et al. 2000) and (Laferté et al. 2000).

The data conditional likelihoods are modeled using multivariate Gaussian mixture models. Hence, missclassifications of image regions which e. g., represent class transition areas may be likely even when context information is included. Therefore, similar to a maximum likelihood classification, a chi^2 test (2) is proposed in order to detect image regions which exhibit low conditional likelihoods for all classes during the inference procedure. If the null hypothesis of this test is refused, only

the prior model is incorporated for the inference of the class label of the appropriate image region. The chi² test is carried out in a preliminary computation step, which leads to the following MAP estimation:

1. Preliminary step. $\forall\ s \in S$, *iff* the null hypothesis of test (2) holds exclusively for one thematic class: classify s based on the data model. Else: $x_s = -1$.

2. Bottom-up pass.
Initialization (leaves $s \in S^N$) with $P(y_s|x_s) = 1$, *if* $xs = -1$:

$$P_s(x_{s-}) = \max_{x_s} P(y_s \mid x_s) P(x_s \mid x_{s-}) \tag{3}$$

$$x_s^*(x_{s-}) = \arg\max_{x_s} P(y_s \mid x_s) P(x_s \mid x_{s-}) \tag{4}$$

Recursion ($s \in S^{N-1} \ldots S^1$) with $P(y_s|x_s) = 1$, *if* $xs = -1$:

$$P_s(x_{s-}) = \max_{x_s} P(y_s \mid x_s) P(x_s \mid x_{s-}) \prod_{t \in s^+} P_t(x_s) \tag{5}$$

$$x_s^*(x_{s-}) = \arg\max_{x_s} P(y_s \mid x_s) P(x_s \mid x_{s-}) \prod_{t \in s^+} P_t(x_s) \tag{6}$$

3. Top-down pass.
Initialization (root r) with $P(y_s|x_s) = 1$, *if* $xs = -1$:

$$\hat{x}_r = \arg\max_{x_r} P(y_r \mid x_r) P(x_r) \prod_{t \in r^+} P_s(x_r) \tag{7}$$

Recursion ($s \in S^1 \ldots S^N$):

$$\hat{x}_s = x_s^*(\hat{x}_{s-}) \tag{8}$$

Until now, this modified inference is realized for the MAP criterion.

Marginal Posterior Entropy

Since a classification result may serve as a basis of decisions for civil and humanitarian relief organisations, a quantification of the uncertainty of the labeling process is highly recommended. As stated in (Pérez et al. 2000), the knowledge of the marginal posteriors allows to assess for each image region s the degree of confidence that can be associated to the estimated value. Therefore, the entropy H_s of the marginal posteriors can be computed as follows:

$$H_S(x_s \mid y) = -\sum_{k=1}^{K} P(x_s = k \mid y) \log_2 P(x_s = k \mid y), \tag{9}$$

where $k = 1,\ldots K$ is the class index. Based on equation (9) a confidence map can be computed for the whole image. Image regions, which exhibit significant marginal posterior entropy are good indicators of misclassified image regions (Feng et al. 2002).

3.2 *Lattice-based Markov Image Modeling*

The above described hierarchical approach allows the modeling of relationships between semantic classes in adjacent scales but does not incorporate spatial context (i. e., intra-scale context). Furthermore, it is often stated that the prior quadtree structure induces non-stationarity in space (Laferté et al. 2000) due to the fact that spatially adjacent image regions may not have common neighbors at coarser scales. This leads to "blocky" artefacts in the estimation result. In order to remove these artefacts and to further improve the classification result, a subsequent incorporation of spatial context by using an undirected lattice-based MRF is proposed here.

Each image region $s \in S^N$ (i. e., all leave nodes of the quadtree) is connected with its four immediately adjacent regions leading to a first order neighborhood system. This limitation is reasonable under the consideration that the spatial dependencies between image regions rapidly decrease when the distance between the regions increases.

Gibbs random fields (GRF) provide global image models by specifying a probability mass function of the following form:

$$P(x) = Z^{-1} \exp(-U(x)), \text{ with } U(x) = \sum_{c \in C} V_c(x) \tag{10}$$

where C is the set of all cliques, Z is a normalization constant (i. e., partition function),

V denotes the neighborhood system and $U(x)$ is the Gibbs energy function. This function is defined as the sum of clique potentials $V_c(x)$ over all possible pairwise cliques. The application of the Hammersley-Clifford theorem (Besag 1974) allows the expression of the joint distribution over the labels X and the observations Y using Gibbs energy functions. The maximization of the posterior probability (MAP) is hereinafter equivalent to the minimization of the following energy function (Dubes & Jain 1989):

$$U(X,Y) = \sum_{1\le i\le I}\sum_{1\le j\le J}\left[\begin{array}{l} U_{data}\left(y_{(i,j)}\middle|x_{(i,j)}\right)+ \\ U_{context}\left(x_{(i,j)}\middle|\left\{x_{(g,h)},(g,h)\in N_{(i,j)}\right\}\right)\end{array}\right], \tag{11}$$

where (ij) describes the position of the image element and $N_{(i,j)}$ denotes the neighborhood of element $s_{(i,j)}$. The energy term $U_{data}(\cdot)$ represents the class statistics and corresponds to the negative data conditional likelihoods of the data model (section 3.1). The energy term $U_{context}(\cdot)$ describes the interregional class dependence and is defined as follows:

$$U_{context}\left(x_{(i,j)}\middle|\left\{x_{(g,h)},(g,h)\in N_{(i,j)}\right\}\right) = \sum_{(g,h)\in N_{(i,j)}} \beta\cdot\delta_k\left(x_{(i,j)},x_{(g,h)}\right), \tag{12}$$

where β is a weighting factor and δ_k is the Kronecker delta function:

$$\delta_k\left(x_{(i,j)},x_{(g,h)}\right)=\begin{cases}-1, & if\ x_{(i,j)}=x_{(g,h)}\\ 0, & if\ x_{(i,j)}\neq x_{(g,h)}\end{cases} \tag{13}$$

The well known ICM algorithm (Besag 1986) is used to carry out the minimization of the energy function (11).

4 Examples and Results

In order to demonstrate the practicability and the relevance of the framework, two examples are examined. In the first experiment the classification of a scene representing a rural region near the city of Dresden, Germany is carried out. Because of the non-complex image content, several characteristics of the framework can be pointed out. A more realistic experiment is given with the second example (northeast Namibia). Here the image content is characterized by inhomogeneous areas and tiny structures like streets and houses.

4.1 *Example 1: Dresden, Germany*

The first example is given with a subset (512 × 512 pixels) from a multispectral IKONOS scene, which represents a rural region near Dresden, Germany. The image has the following product characteristics: pansharpened multispectral (four channels: blue, green, red, near-infrared), standard geometrically corrected, ground sampling distance (GSD) of PAN: 0.87 m cross scan and 0.92 m along scan, ground resolution: 1 m (cubic convolution), acquired on August 6th, 2007. The smallest image region size is defined by 2 × 2 pixels, which leads to a quadtree with nine levels.

The annotation of all image regions in the finest quadtree level to one of the following classes is desired: *dark field*, *vegetation*, *alley*, *street or green field*. Data models are trained in the three finest levels of the quadtree, where class *alley* is not modeled in the coarsest level, since the size of the square image regions is too large (8 × 8 pixels) to represent this class properly. Due to a reference provided by visual interpretation, the impact of context incorporation can be evaluated.

For each scale the feature selection algorithm identified a relevant feature subset, which basically consists of features from different colour space representations, e. g., the well known HLS or CIELUV colour space. Due to the simple image content, all derived classification results are very similar (Tab. 1). However, the overall accuracy increases with every processing step, which confirms the visual comparison of the results.

As expected, the non contextual ML classification yields the worst results. Confusions mainly occur between class *vegetation* and *green field* (Fig. 3.3). An application of the lattice-based MRF (β = 100.0) on the ML result (ML-MRF) causes the well known

smoothing effect but cannot cope adequately with image areas, where many misclassifications occur in the ML result (Fig. 3.6). The MAP (Fig. 3.5) and the MPM (Fig. 3.4) estimator provide similar results, where the latter is slightly better. The lattice-based ML-MRF

Tab. 1: Overall Accuracys of different processing steps.

Domain	Regular 2d-grid (MRF)		Quadtree		Quadtree and 2d-grid	
Estimator	ML (3)	ML-MRF (6)	MAP (5)	MPM (4)	MPM-MRF (7)	Mod. MAP-MRF (8)
Overall accuracy	93.4 %	95.5 %	94.7 %	94.8 %	96.0 %	96.7 %

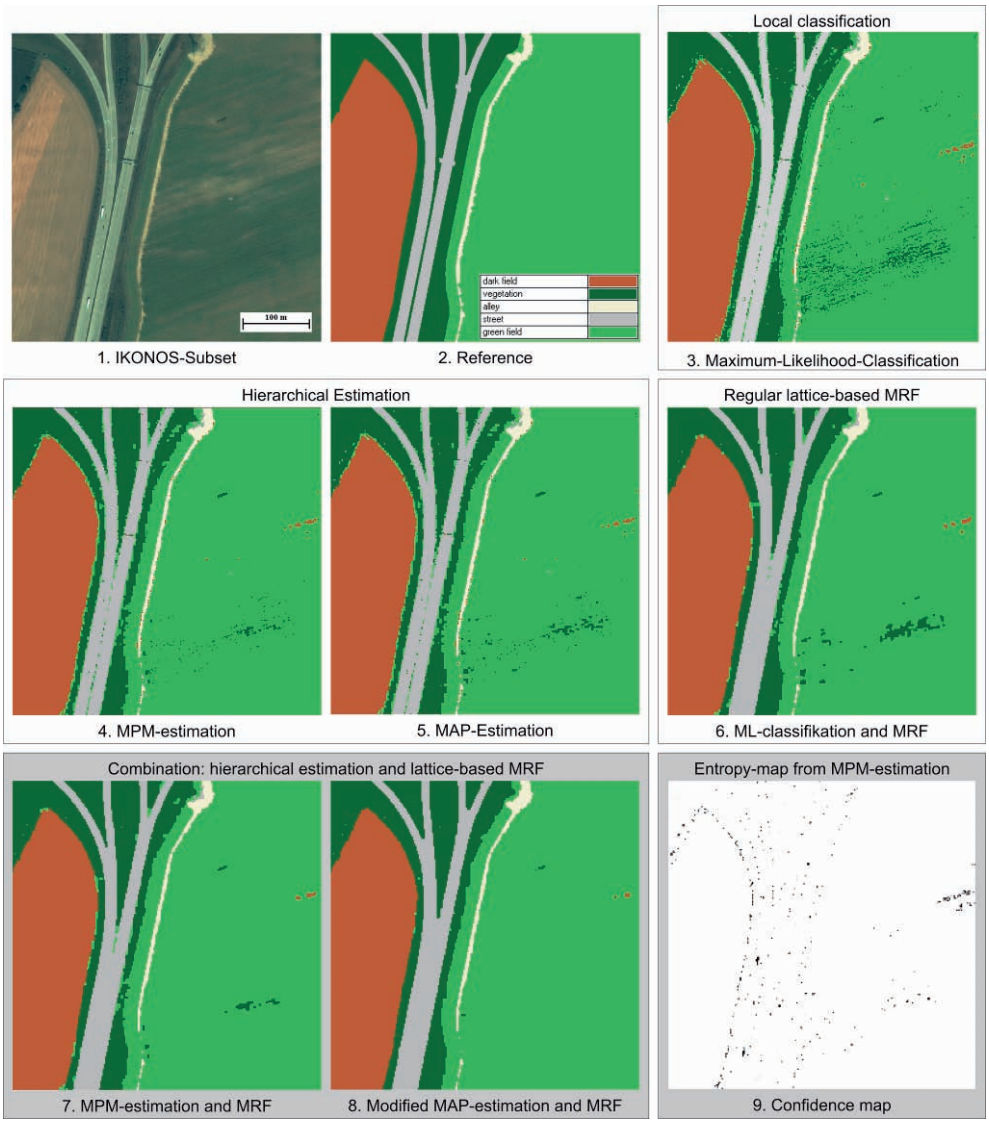

Fig. 3: Example 1: Intermediary results (white boxes) and final results (grey boxes). The local ML-classification (3) as well as (6) were derieved for comparison.

approach provides slightly better classification results than MAP or MPM estimation (see Tab. 1) but takes significantly more computational time than the non-iterative hierarchical approaches. A better classification result is carried out with the combination of the hierarchical MPM estimation and the subsequently applied grid-based MRF (MPM-MRF). The overall accuracy for the modified MAP estimation with $\alpha = 0.3$ is 95.7 %. However, this approach has shown to enforce the "blockiness" of the result. A subsequent MRF smoothing leads to a quite satisfying result with an overall accuracy of 96.7 % (Fig. 3.8). The confidence map shows the image regions, which may be misclassified using the MPM estimator (Fig. 3.9): The darker the regions the higher the uncertainty of the classification. This corresponds to the obviously visible misclassifications in the MPM result.

4.2 *Example 2: Caprivi Region, Northeast Namibia*

The second dataset is a multispectral QUICKBIRD scene from the Caprivi region, located in the northeast of Namibia, acquired on October 10th, 2009. The image has the following product characteristics: multispectral (four channels: blue, green, red, near-infrared), product level: standard imagery, ground resolution: 2.4 m. The size of the chosen subset is 1375 × 1135 pixels. In order to capture tiny structures like houses and streets, the smallest region-size is defined to be 2 × 2 pixels, which results in a quadtree with 11 levels. The classification of *water*, *streets*, *houses* and a class which represents the *rest* of the image is desired. Therefore, data models trained in two levels, namely the finest level S^{10} as well as level S^{8}, have shown to give good results. In the finest level all introduced classes are modeled. Since houses and streets are too small to represent them on the coarser level, only the class *water* and *rest* is modeled here. Due to similarities of the classes in the spectral domain, a local ML classification of the finest quadtree-level leads to confusions between the classes *water* and *street* as well as between *rest* and *house* (Fig. 4).

The application of the lattice-based MRF on the result of the ML classification as well as on all other intermediary results has shown to degrade the quality of the classification. A low weighting of the context term (e. g., $\beta = 2.0$) leads to a slightly smoothing, but mainly preserves misclassified areas. On the other hand, a relatively high weighting (e. g., $\beta = 15.0$) still preserves missclassified areas and partially leads to the omission of small structures like houses and streets. This effect is also caused by the application of the modified MAP estimation. The hierarchical MPM estimation yields the best result (Fig. 4.4) and is equivalent to the MAP estimation. The confidence map (Fig. 4.3) shows that especially image regions which represent streets as well as the land-water boundary are difficult to classify using the hierarchical MPM estimation.

5 Discussion

The experimental results show that the proposed framework allows an interactive classification of different types of high resolution optical satellite images by incorporating spatial and hierarchical context as well as image data from different levels of aggregation. Depending on the image content and the thematic focus, the desired result is obtained using different combinations of the methods utilized in this framework.

In the first experiment the image is characterized by large homogeneous areas. Here, the complete process chain (Fig. 1) is traversed and the best result is obtained using the modified MAP estimation and a subsequent lattice-based MRF smoothing. Using the original MAP or MPM estimation, the influence of the data model, which obviously cannot handle all image regions adequately, "votes down" the context information in some cases (e. g., the margin of the *dark field* is misclassified as *field*). The modified MAP computation has shown to be very useful to avoid misclassifications especially of mixed image regions in this example but enforces the "blockiness" of the classification result. The additional incorporation of spatial context counteracts this effect. In order to save computational time, a single iteration step of the ICM algorithm could be a

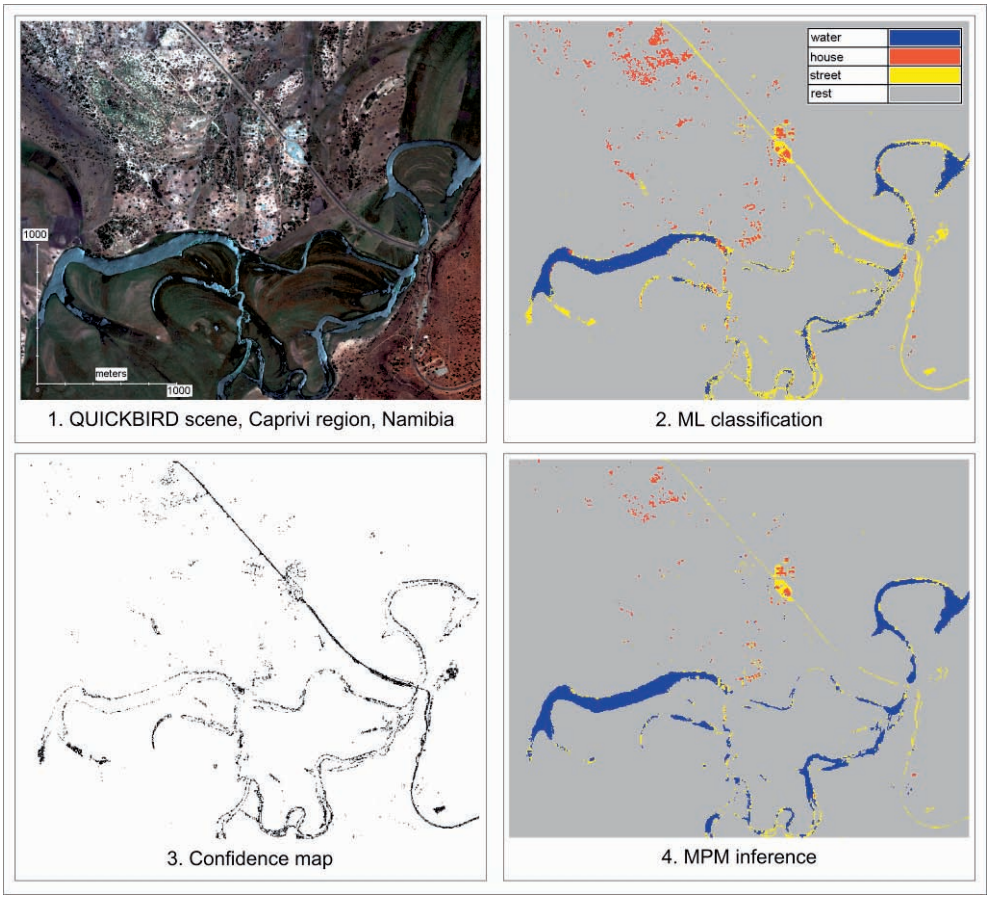

Fig. 4: Results for example 2.

reasonable and sufficient approach for this task. Other ways to tackle this problem are given with the application of the ICM algorithm only for those elements which exhibit other class memberships than their corresponding parent segment (Martinis et al. 2010) or for those elements where the posterior marginal entropy exceeds a defined threshold.

In the second experiment the incorporation of spatial context degrades the classification result since the tiny structures of houses and streets tend to disappear by increasing the weight of the context term. The application of the modified MAP estimation also leads to the omission of tiny structures. These observations lead to the conclusion, that the finest chosen region size (2×2 pixels) is too coarse to capture the tiny structures like houses and streets using square image regions, since these objects exhibit approximately the same respective a slightly bigger size. The original hierarchical MPM estimation yields the best but not the optimal result, whereas confusions between the class *water* and *street* as well as *rest* and *house* (many false positives for the class *street* and *house*) occur. The utilization of data models in more than two levels has shown to degrade the classification result further. The additional incorporation of a data model in level S^9 obviously provides no additional information and leads to more misclassifications. Instead of that, an additional data model in a coarser scale has shown to be useful to solve ambiguities.

The result of the modified MAP estimation in example 2 is an effect of both the limited separability provided by the data model as

well as the chosen class hierarchy. The class *house* and *street* are only modeled in the finest level, whereas the class *rest* dominates the image. Hence, if the data model is not incorporated into the modified MAP computation (chi² test), the class *rest* is favoured for the corresponding image element in the finest level.

Compared to the grid-based estimation, the tree-based non-iterative estimators needed significantly less computational time (experiment 1: ML-MRF: 238 sec., MPM: 82 sec.). It has to be mentioned, that the parameter estimation for the prior model took 363 sec., which is quite acceptable compared to the grid-based MRF approach where the appropriate weight for the context term is usually identified in a trial-and-error manner.

The experiments were carried out using an Intel Xeon CPU with 2.33 GHz and 3.25 GB RAM. The whole framework is implemented in Interactive Data Language (IDL). The usage of other programming languages like C++ can accelerate the computational times further.

6 Conclusion

In this paper, a general approach for interactive classification of optical very high resolution satellite images is proposed. The framework is designed in order to cope with the surrounding conditions of rapid mapping activities and is moreover suitable for the task of satellite image classification in general. Hierarchical and spatial context information as well as image data from different levels of aggregation is incorporated into the classification process using hierarchical and lattice-based Markov random fields.

The experimental results confirm the effectiveness as well as the transferability of the framework on different datasets. Since the thematic classes are parameterized using Gaussian mixture models, the classification of image regions which represent a mixture of classes has shown to be very difficult even when hierarchical context information is incorporated. In order to decrease misclassifications, a new hierarchical MAP estimation is proposed. This modified MAP estimation has shown to outperform the original MAP and MPM estimation under the condition that the square image regions of the finest quadtree level are sufficiently smaller than the image areas of the particular thematic class. The results in (Kersten & Gähler 2010) also confirm these results.

The estimation of model parameters is a crucial task and depends on several aspects. Hence, especially the influence of the cardinality of the training data as well as the features in the feature space domain is addressed in current research activities. Furthermore, the application of the framework on several different image contents and thematic problems is currently evaluated.

The impact of incorporating different hierarchy levels should be analyzed in detail. The robustness of the parameter estimation with respect to other determining factors like the evaluation function applied in the feature selection method will be a topic in further investigations. Furthermore, the potential of detecting true misclassifications using the confidence map should be treated in the future work.

References

Awasthi, P., Gagrani, A. & Ravindran, B., 2007: Image Modeling using Tree Structured Conditional Random Fields. – International Joint Conference on Artificial Intelligence: 2060–2065.

Besag, J., 1986: On the statistical analysis of dirty pictures. – Joint Royal Statistic Society B **48** (3): 259–302.

Besag, J., 1974: Spatial Interaction and the Statistical Analysis of Lattice Systems. – Journal of the Royal Statistical Society, Series B **36**: 192–236.

Bouman, C. & Shapiro, M., 1994: A multiscale image model for Bayesian image segmentation. – IEEE Transactions on Image Processing **3:** 162–177.

Choi, M.J., Chandrasekaran, V., Malioutov, D.M., Johnson, J.K. & Willsky, A.S., 2008: Multiscale stochastic modelling for tractable inference and data assimilation. – Computer Methods in Applied Mechanics and Engineering **197:** 3492–3515.

Collet, C. & Murtagh, F., 2004: Multiband segmentation based on a hierarchical Markov model. – Pattern Recognition **37:** 2337–2347.

Dubes, R. & Jain, A.K., 1989: Random Fields in Image Analysis. – Journal of Applied statistics **16:** 131–164.

Feng, X., Williams, C.K.I. & Felderhof, S.N., 2002: Combining belief networks and neural networks for scene segmentation. – IEEE Transactions on Pattern Analysis and Machine Intelligence **24** (4): 467–483.

Fieguth, P., Karl, W. & Willsky, A., 1998: Efficient multiresolution counterparts to variational methods of surface reconstruction. – Computer Vision and Image Understanding **70** (2): 157–176.

Forney, G.D., 1973: The Viterbi algorithm. – IEEE Proceedings **61:** 268–278.

Kersten, J. & Gähler, M., 2010: A Framework for Satellite Image Classification in the Context of Crisis Mapping using Markov Random Fields. – Remote Sensing and Photogrammetry Society Annual Conference 2010 (accepted).

Khedam, R. & Belhadj-Aissa, A., 2003: Contextual fusion by genetic approach applied to the classification of satellite images. – Remote sensing in transition. Rotterdam' Millpresse.

Laferté, J.M., Pérez, P. & Heitz, P., 2000: Discrete Markov Image Modeling and Inference on the Quadtree. – IEEE Transactions on Image Processing **9** (3).

Martinis, S., Twele, A. & Voigt, S., 2010: Unsupervised extraction of flood-induced backscatter changes in SAR data using Markov image modeling on irregular graphs. – IEEE Transactions on Geoscience and Remote Sensing **48** (12) (accepted).

Pérez, P., Chardin, A. & Laferté, J.M., 2000: Noniterative manipulation of discrete energy-based models for image analysis. – Pattern Recognition **33** (4): 573–586.

Pudil, P., Novovicova, J. & Kittler, J., 1994: Floating Search Methods in Feature Selection. – Pattern Recognition Letters **15** (11): 1119–1125.

Ververidis, D. & Kotropoulos, C., 2008: Gaussian Mixture Modeling by Exploiting the Mahanalobis Distance. – IEEE Transactions on Signal Processing **56** (74): 2797–2811.

Wilson, R. & Li, C., 2003: A class of discrete multiresolution random fields and its application to image segmentation. – IEEE Transactions on Pattern Analysis and Machine Intelligence **25:** 42–56.

Address of the Authors:

Dipl.-Ing. Jens Kersten, Tel.: +49-8153-28-3384, Dr. Monika Gaehler, Tel.: -3309, Dr. Stefan Voigt, German Aerospace Center (DLR), German Remote Sensing Data Center (DFD), D-82234 Oberpfaffenhofen, Fax: -1445, e-mail: Name.Surname@dlr.de

Manuskript eingereicht: Juni 2010
Angenommen: September 2010

PFG 2010 / 6, 451 – 462
Stuttgart, Dezember 2010

Article

A Modular System for Road Updating, Refinement and Classification from Satellite Images

Daniel Frey, Matthias Butenuth, München & Stefan Hinz, Karlsruhe

Keywords: Road Data, Update, Refinement, Classification, Natural Disasters

Summary: The extraction, refinement and verification of intact and damaged infrastructure are important issues for the management of civil crises, e. g., caused by flooding or earthquakes. In this paper, the development of a system for the automated detection of roads, their geometric and semantic refinement as well as classification into different states of accessibility from multi-sensorial imagery is presented. The system is intended to supply information being required for the coordination of rescue teams and the implementation of emergency actions. It is the result of long-term research on different aspects of road extraction, which has been extended and adapted in the context of the bundle project DeSecure to build up a framework providing all relevant information regarding the extent and impact of crises scenarios within shortest timeframes. The results of classification system show the improvement of the fast interpretation of road networks after natural disasters using automatic approaches.

Zusammenfassung: *Ein modulares System zur Aktualisierung, geometrischen Verfeinerung und Klassifikation von Straßen mit Hilfe von Satellitenbildern*. Die Extraktion, geometrische Verfeinerung und Verifikation von intakten und beschädigten Infrastrukturobjekten sind wichtige Fragestellungen bei zivilen Krisen, wie zum Beispiel Überflutungen oder Erdbeben. In diesem Artikel wird die Entwicklung eines Systems beschrieben, das mit Hilfe von multi-sensoriellen und multi-temporalen Bildern eine automatische Detektion von Straßen, eine geometrische und semantische Verfeinerung und eine Klassifikation in verschiedene Zustände der Befahrbarkeit durchführt. Das Ziel des Systems ist die Bereitstellung von Informationen über Straßen, die für die Koordination von Hilfskräften von großer Bedeutung sind. Die präsentierten Ergebnisse basieren auf langfristiger Forschung im Bereich der Straßenextraktion, die im Rahmen des Bündelprojekts DeSecure angepasst und erweitert wurden. Das erweiterte System, bestehend aus den drei Modulen Straßenextraktion, Verfeinerung und Klassifikation liefert ein Rahmenwerk, um sämtliche relevante Informationen über Straßen in kürzester Zeit in Krisenfällen zur Verfügung zu stellen. Die Ergebnisse zeigen, dass mit Hilfe der automatischen Klassifikationsverfahren die benötigte Zeit zur Interpretation von beschädigten Straßen nach Naturkatastrophen erheblich reduziert werden kann.

1 Introduction

A significant increase of natural disasters such as flooding has been observed over the past decades. While it is not absolutely clear, whether the number of disasters has really grown or only appears so because of the advances in world-wide communication and global observation methods, there is no doubt that the disasters' impact on the population has dramatically increased due to the growth of population and material assets (Huadong 2009). The regrettable death of people is accompanied by heavy economic damage, which leads to a long-term backslide of the region hit by the disaster. This situation calls for the development of integral strategies for preparedness and prevention of hazards, fast reaction

© 2010 E. Schweizerbart'sche Verlagsbuchhandlung, Stuttgart, Germany
www.schweizerbart.de
DOI: 10.1127/1432-8364/2010/0067
1432-8364/10/0067 $ 3.00

in case of disasters, as well as damage documentation, planning and rebuilding of infrastructure after disasters.

It is widely accepted in the scientific community that Remote Sensing can contribute significantly to all these components in different ways, especially because of the large coverage by remotely sensed imagery and its global availability. The bundle project DeSecure will build up a framework to provide all relevant information regarding the extent and impact of crises scenarios within shortest timeframes. Time, however, is the overall dominating factor once a disaster has hit a particular region. Several time consuming aspects exists: firstly, available satellites have to be selected and commanded immediately. Secondly, the acquired raw data has to be processed with specific signal processing algorithms to generate images suitable for interpretation. Thirdly, the interpretation of multi-sensorial images, extraction of geometrically precise and semantically correct information as well as the production of (digital) maps need to be conducted in shortest time-frames to support crises management groups.

While the first two aspects are strongly related to the optimization of communication processes and hardware capabilities (at least to a large extend), the main methodological bottleneck is posed by the third aspect: the fast, integrated, and geometrically and semantically correct interpretation of multi-sensorial images. Therefore the development of methods for automatic understanding and interpretation of airborne and space borne optical and radar images to support the fast reaction after disasters is needed. In the following, special focus is on the extraction, analysis and characterization of roads due to their importance for the immediate planning and implementation of emergency actions. Different types of models – physical, stochastic and semantic models – will therefore be used in an integrated approach.

2 Related Work

The extraction of roads from remotely sensed image data has been of considerable interest in recent years, mainly driven by the rapid progress of 2D and 3D geographic information systems as well as navigation systems and their increasing importance in daily life. The advances can be seen in the relevant computer vision literature, for instance in the compendia and overview papers of Grün et al. (1997), Mayer (1999), Baltsavias et al. (2001), Gamba et al. (2003), Gerke et al. (2004), and many others.

Fig. 1: IKONOS image from the Elbe flooding in Germany in 2002.

Despite of numerous technological advances the process of semantic data acquisition still needs lot of manual interaction of a human operator to yield results relevant for practical applications, which is of course both time-consuming and expensive. While this is true for optical images, the situation is even harder for Synthetic Aperture Radar (SAR). SAR is an active and coherent imaging technique which leads to the well-known speckle noise and image derogations due to radar shadow and layover. Thus, the imaged objects are subject to drastic changes in their appearance depending on the radar illumination parameters. Deterministic and stochastic modeling of this varying object appearance is far from being solved today. The scientific challenges of man-made object extraction, in particular roads and buildings, from SAR data can be viewed, for instance, in Baumgartner et al. (1999), Wiedemann & Hinz (1999), Wessel & Hinz (2004), Sörgel et al. (2006), Hedman et al. (2006).

However, besides the drawbacks due to the specific viewing geometry and coherent imaging, SAR holds also some prominent advantages over optical images, which are in particular helpful in crisis situations. For instance, SAR is an active system, which can operate during day and night. It is also nearly weather-independent and, moreover, during bad weather conditions SAR is the only operational system available today.

Hence, under the light of today's and tomorrow's available optical and SAR satellite systems, the development of integrated approaches for object extraction from multi-sensorial images are an attractive alternative to support fast and accurate information extraction. To this end, models and extraction strategies need to be developed that integrate the different geometric and radiometric sensor characteristics attached with stochastic models to accommodate for the inherent modeling and measurement uncertainties.

However, the sole extraction of roads can hardly fulfill the requirement which is needed in case of natural disasters. Using additional road networks from GIS-database can improve the reliability to draw conclusions about the functionality of a road network. Since the geometric accuracy of the road database is essential, methods for refinement are needed. Parametric active contours, often called snakes (Kass et al. 1988, Blake & Isard 1998) can be used for the improvement of the geometrical accuracy. In Butenuth & Heipke (2010) network snakes are applied to a road network. Network snakes have the crucial advantage to perserve the topology of networks. In this paper network snakes are investigeted concerning their performance in natural disaster scenarios. In Gerke et al. (2004), Gerke & Heipke (2008) a quality assessment of existing road data is presented using remotly sensed images. In case of natural disasters the assessment concerning the trafficability of roads is investigated in Frey & Butenuth (2009) for multsensor imagery. The improvement of the assessment using multi-temporal imagery is discussed in Frey & Butenuth (2010).

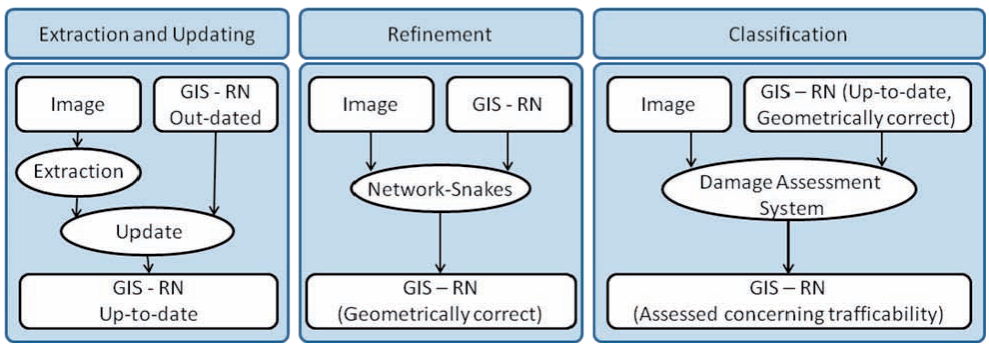

Fig. 2: The three moduls of the system (RN = road network).

3 System and Strategy

3.1 *System*

At the moment, fully automatic approaches for object extraction must still be regarded as a subject of fundamental research, and they seem not to be able to find their way into operational work flows in the very near future. On the contrary, semi-automatic approaches seem more likely to be useful in operational applications. Automatically achieved results nonetheless may provide a basis for efficient checking, editing and improving.

It is assumed in the following that road axes are already available as input data, which might stem from an automatic extraction or an existing road database. These road data, however, might be outdated, geometrically displaced and/or partially semantically wrong. Hence, the framework for the automated detection and classification of roads from multisensorial imagery is conceptually divided into three main parts. The first part comprises the user-assisted updating of roads. It comprises an automated internal evaluation of the input data providing measures about the reliability of road parts. In case of incomplete input data – e. g., of an automatic extraction – this can be used to guide an operator during editing and completing the results, for instance by interactive road tracing. The second part includes road refinement, which basically involves the application of a network snake approach to refine the road network in terms of geometric accuracy. Naturally, during this phase only centerlines of intact road segments can be refined, while those of damaged or flooded roads will usually not improved. Hence, conceptually, this module is only applied to roads which have been identified as "reliable" by the above internal evaluation. The third module, finally, is devoted to classify the whole road network into accessible and damaged/flooded road parts.

In the following, the individual modules (cf. Fig. 2) are described in more detail. However, the system still contains stand-alone modules, which are tested and evaluated only individually. Integrating them into a monolithic software system is not within the scope of this research work. The performance of the individual modules are exemplarily shown at an IKONOS image from the Elbe flooding 2002 (cf. Fig. 1)

3.2 *Road Internal Evaluating and Road Updating*

Existing GIS data nor the results of an automatic object extraction may not be expected to deliver absolutely perfect results and, thus, for meeting predefined application requirement, a human operator must inspect the automatically obtained results. In order to speed up the time- and cost-intensive inspection, the system should provide the operator with confidence values characterizing the system's performance – a so-called internal evaluation. This information can only be derived from redundancies within the underlying data or the incorporated object knowledge. In this context, "object knowledge" means knowledge that is purely described by the object model and not by other external data. The results of internal evaluation are particularly important

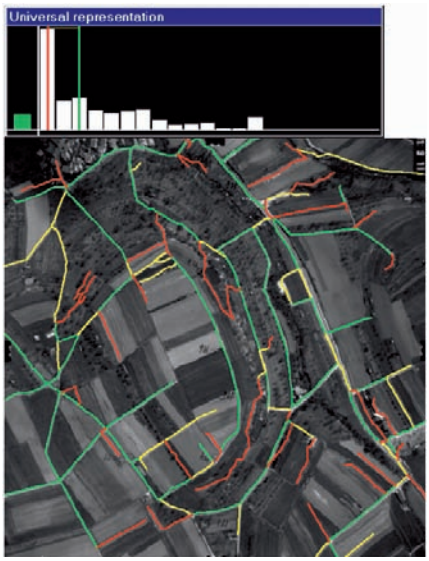

Fig. 3: Overview of self-diagnosis. Top: Length-weighted histogram of evaluation scores (left-most bar indicates mean value = green in this example), thin vertical lines indicate thresholds between categories. Bottom: Overview window.

if the extraction results are combined with other data, e. g., if they are fused with results from other extraction approaches or if they are used for the update of GIS data. On the other hand, they are also very useful for guiding a human operator during post-editing the results of an automatic extraction. In practice, however, this is rarely the case.

Object properties that relate to global characteristics of roads are used in this context. A road network, for instance, must be in accordance with some typical global network characteristics: few connected components, no clusters of junctions outside urban areas, convenient connections between various places depending on the terrain type etc. Such properties are used in Hinz & Wiedemann (2004) to evaluate the reliability of portions of the network with a fuzzy-set theoretic approach.

To allow a quick and effective inspection by a human operator, the evaluated road segments are displayed in an overview window and categorized into three classes: green (to be accepted), yellow (to be checked), and red (to be rejected). In addition, the average quality of the evaluated network and the distribution are displayed (cf. Fig. 3). Whenever a particular road section is sought to be inspected in more detail, it can be selected in a separate cutout to investigate the evaluation details (cf. Fig. 4). Based on the visualization and the quality information, the operator may decide how to handle a particular road section — whether it should be retained, deleted, or edited. Of course, setting the two thresholds between the categories is critical. However, as the test series in Hinz & Wiedemann (2004) show, deriving these thresholds from the statistics of the evaluation scores is a simple but surprisingly effective approach. In particular, in these examples the threshold between the yellow and the category is simply the minimum (zero score), while the threshold between the green and the yellow category is defined as the median of all evaluation scores (see, e. g., Fig. 3).

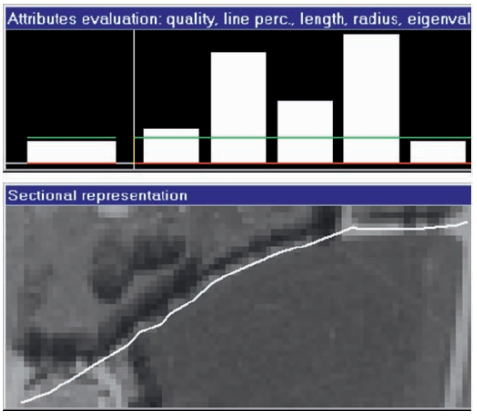

Fig. 4: Detailed inspection of evaluation results of a specific portion of the road network. Bars indicate results of evaluation for each criterion involved ([0 ; 1]).

To analyze the reliability of self-diagnosis, we matched the internally evaluated results to a manually plotted reference (see details and figures in Hinz & Wiedemann 2004). The comparison showed that almost every road section of the green category is a correctly extracted road (above 90%). The self-diagnosis also detects "false alarms" in the extraction with high reliability (80% – 90%). Considering the evaluation of yellow-labeled road sections one can state that these parts of the road network should indeed be investigated by a human operator because the correctness values are generally lower and vary to a notable extent (50% – 75%). It is furthermore interesting to observe what would happen if an operator had checked exclusively the yellow-labeled road sections. Under the assumption that a human operator is able to discern correct and wrong detections without any error, the correctness of the overall result would remain in the range of 95%, while the amount of editing drops down significantly: only 25% to 50% of the whole road network need to be checked.

However, it is important to note that one can improve only the correctness through employing this scheme for internal evaluation. Completeness can only be increased when identifying potential gaps in the extraction and closing them. To this end, the system provides user-assisted tools for road extraction. Semi-automatic, i. e., user-assisted, tools have the advantage that the quality of the results is guaranteed, because a human operator controls the data acquisition process and prevents errors on-line. Yet the overall benefit of such systems depends not only on their sophisticated algorithms but also on adequate tools for editing. Quite a lot of promising approaches for semi-

automatic road extraction have been presented and analyzed in the last decades.

Road trackers and path optimizers are characterized by complementary properties: Road tracking is usually based on a road profile selected by a user for a particular road to be traced. In this way, the specific radiometry of this road is included into the procedure. This is in particular helpful when different roads of varying appearance should be extracted. Such appearance-based constraints are commonly not included in path optimization. Snake algorithms, for instance, need to be fed with a generic image energy, which is derived through more or less complex filtering operations like a gradient amplitude map, Laplacian map, distance transform, etc. On the other hand, road tracking algorithms do not include any topological information about the connectivity of the road network. Disturbances due to background objects or noisy images (like SAR images) lead often to very wiggling tracks or even useless results. In such situations, snakes and in particular network snakes show clear advantages over tracking procedures, since the geometric and topologic constraints involved in the optimization process act as regularization for the noisy data (Butenuth & Heipke 2010).

Fig. 5: User-assisted road tracking in an IKONOS image taken during the Elbe flooding in Germany, 2002. Yellow points: tracked road sections; blue lines/red points: user clicks.

Fig. 5 shows an example for user-assisted tracking of a main road in an IKONOS image taken during the Elbe flooding in Germany, 2002. The yellow parts were traced automatically, while simple user clicks were asked at the blue positions. Here, the operator had to decide whether tracking should just continue or interactive editing is necessary. Tracking could continue at all interruptions except the one shown in the detail of Fig. 5. It illustrates a situation, where cutting-off the tail of the track and manual digitizing of a short road section is necessary due to the occlusion of a small cloud. A detailed description of this algorithm and the variety of options for user interaction can be found in Baumgartner et al. (2002).

At this stage of processing, the road network has been categorized into reliable and unreliable parts, i. e., "green" and "red" road portions only, since the "yellow" parts have been assigned interactively to one of these classes. In addition, potential gaps – which can only occur when applying an automatic road extraction at the beginning of processing – have been closed. In the next section the centerlines of reliable roads are geometrically refined.

3.3 *Road Refinement*

The availability of road data as input information for the assessment requires a high geometric correctness of the road network, in particular for the aimed subsequent classification approach. This prerequisite cannot be ensured in general and, thus, network snakes (Butenuth 2007, Butenuth & Heipke 2010) are used for the geometric refinement of the road network. Network snakes are based on the well-known active contour models (Kass et al. 1988), but in addition to the image energy and internal energy the topology is introduced into the optimization process. This graph-based

active contour method enables a complete topological and shape control during the object delineation. The exploitation of the topology during the iterative optimization process enables to deal with fragmented and blurry object representations in different kinds of imagery (Butenuth & Heipke 2010).

Network snakes are applied to the geometric refinement of road networks to improve and correct the database if necessary. The proposed approach is either able to deal with roads from a database as initialization in an automatic system or, alternatively, within an interactive framework to derive a geometrically optimized road network. In addition, the optimization of roads using network snakes can be accomplished with different kinds of image data such as optical and SAR-data, because the method is able to cope with varying image energy terms in the flexible minimization process. In general, the refinement is accomplished as a preprocessing step using image data representing a status of intact roads. However, in Fig. 6 the network snakes approach is applied to the non-flooded roads starting from the initialization (blue) moving step by step (white) to the true positions of the roads (red) in the optical image. The benefit of network snakes is the exploitation of the topology during the graph-based optimization together with the image energy and the internal energy being a powerful method to deal with noise or disturbances in the imagery when refining road networks. Furthermore, only the local image information at the network has a purposive effect to the correct result, because the region-based image information within the enclosed road network segments is not useable due to the different object classes (e. g., settlement).

3.4 *Road Classification*

The aim of the third module is the assessment of a road network concerning their functionality after a natural disaster. The prerequisite for the road classification is an up-to-date and geometrically correct road network. Most of the industrialized countries offer road databases which fulfill the required geometrical accuracy and up-to-dateness. If there is no appropriate road network available the modules described above can be applied to extract/update roads or refine already existing road networks.

In Fig. 7 a generic overview of the damage assessment system is given. Since the reliability and up-to-dateness of the assessed road network is of prime importance it is necessary to embed all kind of information which is available in near-realtime. Therefore the de-

Fig. 6: Automatic road refinement using network snakes in an IKONOS image taken during the Elbe flooding in Germany, 2002: initialization (blue), optimization steps (white), result (red).

sign of the assessment system has an flexible stucture. The main contribution in the proposed damage assessment system results from different kinds of imagery. Beside optical and radar imagery also additional information such as a DEM can be embedded into the system (Frey & Butenuth 2009). Furthermore the system can cope with imagery at different time points. The useage of multi-temporal data can further improve the results as shown in Tab. 1 (Frey & Butenuth 2010).

The basic idea of the system is the derivation of probabilities from each individual input data whether an road object is trafficable or not. The methods used to infer the probabilities depends on the available input data. In case of optical imagery a multispectral classification is carried out using Gaussian Mixture Models (GMM) (McLachlan & Peel 2000). The road segments given from the GIS-database are classified in various classes such as *intact road*, *not intact road* and all possible kinds of occlusions of the roads such as *forest*, *clouds* or *shadows*. The appearance of the class *not intact roads* depends of the natural disaster. For example in case of a flodding the class *not intact roads* is replaced by the class *water*. The radiometric appearance of the class *intact road* has large variations. This leads to probability density function with a large standard deviation. The difficulties which arise dealing with the broad probability function can be reduced using Gaussian Mixture Models. The complex probability density function composed of several multivariate normal distributions is therefore a more suitable statistical representation of the class *intact road*. Using the Gaussian Mixture Model every road segment is assigned a probability p_{img} belonging to a previous defined class. If a maximum likelihood classification assigns a road segment to class which describes the occlusion of a road (*forest*, *cloud*) than further information has to be exploited. It is possible to utilize the results from the classification of adjacent road segments. Also further input data can give additional hints if the occluded roads are intact or not. In case of flooding the DEM can give additional hints if roads are flooded or not. Belief functions are used to derive the probabilities from these additional informations such as DEM. In case of floodings it is assumed that roads higher than a threshold a_2 are certainly trafficable and lower than

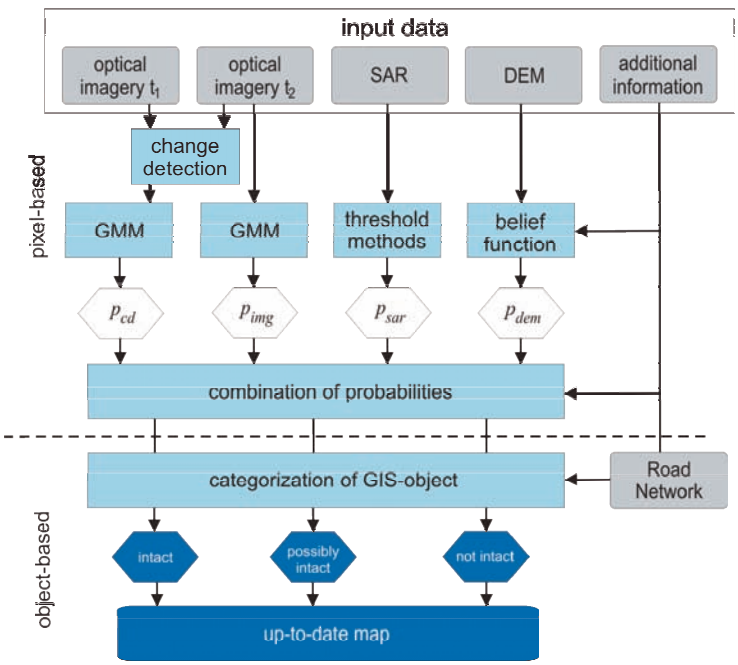

Fig. 7: General damage assessment system.

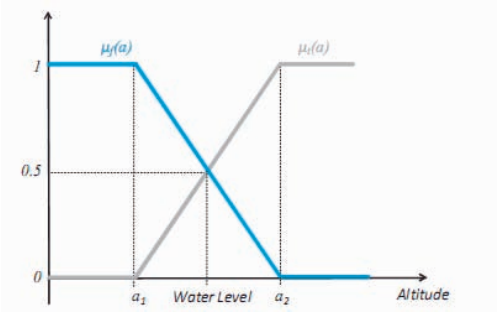

Fig. 8: Belief functions for roads after flooding.

a threshold a_1 are certainly flooded. The probabilities inbetween these theresholds are modelled with a linear function (cf. Fig. 8). The blue function $\mu_f(a)$ shows the belief function that a road is flooded. The gray function $\mu_t(a) = 1 - \mu_f(a)$ stands for the probability that a road is trafficable. By means of the belief functions a probability p_{dem} can be assigned to every road segment.

The availability of mutli-temporal imagery can be used to carry out change detection. In the proposed approach the Multivarate Alteratioin Detection (MAD) method was used, since it is invariant to linear transformation (Nielsen et al. 1998). Therefore linear changing in atmosspheric conditions or sensor calibrations can be neglected. The result of the MAD method are so called MAD variates for each pixel which represents different kind of changes. In case of floodings a training sample is choosen which represents the change from flooded road to a trafficable road or the other way around. By means of the trainings set a supervised classification of the MAD variates using Gaussian Mixture Models is carried out to calculate the probabilities p_{cd}. The probability p_{cd} give additional hints if a road segment is flooded or trafficable at time point t_2. The combination of the probabilities derived from different input data is carried out by a multiplication of the probabilities p_{img}, p_{cd} and p_{dem} embedded into a rule based framework which depends on the natural disaster.

The result of the damage assessment system applied to the Elbe scenario is depicted in Fig. 9. Two IKONOS-scenes from two time points t_1, t_2 and a DEM from ATKIS with an 10 m grid and a geomtrical accuracy of +/− 1m was used as input data. The road segments are categorized into three states *trafficable*, *possibly flooded* and *flooded*. The state *possibly flooded* means that the automatic assessment system could not categorized the road segment within a required certainty.

The obtained results are compared to a manually generated reference. The generation of the reference is carried out by means of the information on image at time t_2. Therefore, it is not a comparison with the real ground truth, but it is the comparison of the automatic approach with the manually interpretation of an human operator. The reference is categorized into three different states *trafficable*, *possibly flooded* and *flooded*. Since the categorization of the automatic system consists of the same states the following four different assignment criteria are determined: 'correct assignment', 'manual control necessary', 'possibly correct assignment' and 'wrong assignment'. The category 'correct assignment' means that the manually generated reference is identical with the result of the automatic system. In the case of 'manual control necessary' the automatic approach leads to the state *possibly flooded* whereas the manual classification assigns the line segments to *flooded* or *trafficable*. The other way around denotes the expression 'possibly correct assignment'. 'wrong assignment' means that one result categorize the segment to *flooded* and the other to *trafficable*. The en-

Tab. 1: Results and evaluation of the assessment system: Evaluation of road data of the Elbe test scenario exploiting different input data.

	t_2	t_2, *DEM*	$t_{1,2}$, *DEM*	$t_{1,2}$, *r*, *DEM*
Correct	68.40 %	68.45 %	69.60 %	87.14 %
Manual	27.88 %	27.77 %	27.48 %	10.96 %
Possibly	2.64 %	2.72 %	2.52 %	1.79 %
Wrong	1.08 %	1.06 %	0.40 %	0.11 %

Fig. 9: Detail result of the assessment system using all available input data: image t_1, image t_2, DEM and manual generated reference at time t_1; green = trafficable, yellow = possibly flooded, red = flooded, dark blue = trafficable (changed from flooded at time point t_1 to trafficable at time point t_2).

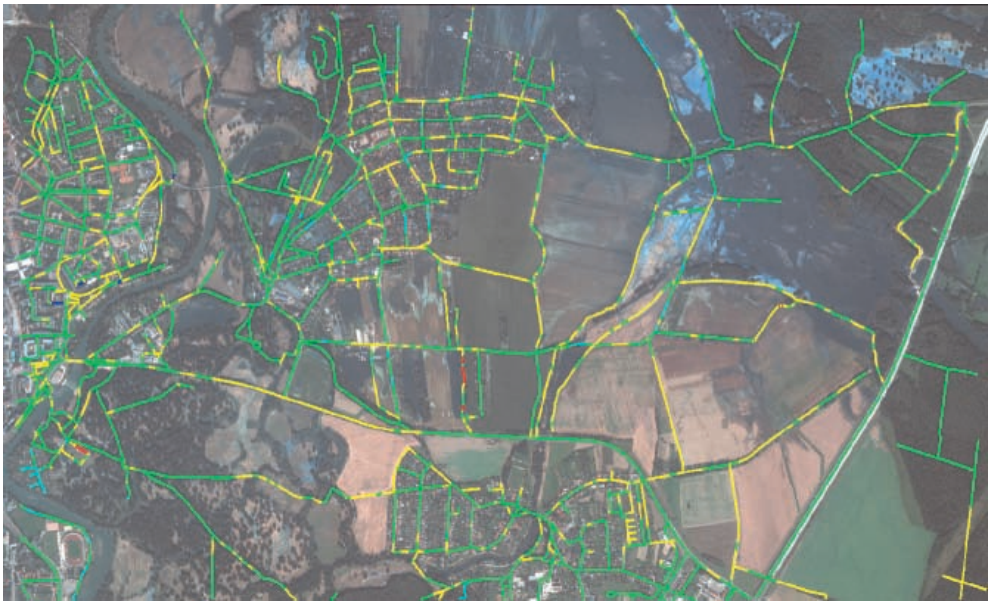

Fig. 10: Evaluation of the assessment system using image t_2, image t_1 and DEM; green = 'correct assignment', yellow = 'manual control necessary', cyan = 'possibly correct assignment', red = 'wrong assignment' [system = trafficable, reference = flooded], dark blue = 'wrong assignment' [system = flooded, reference = trafficable].

hancement of the automatic system by the combined interpretation is shown in Tab. 1.

The first column in Tab. 1 represents the result using only the image t_2 without any further information. The result with about 1% of 'wrong assignments' and about 68% 'correct assignment' is almost identical if an additional DEM as input data is used (cf. Tab. 1: t_2, *DEM*).

In Fig. 10 the result of the third column from Tab. 1 is visualized which includes the additional scene at time point t_1 as input data. Green road segments correspond to 'correct assignment', yellow to 'manual control necessary', cyan to 'possibly correct assignment' and red or blue belongs to 'wrong assignment'. If the system assigns a road segment to the category *trafficable* but the reference is *flooded* the road segment is colored in red. Dark blue road segments are assigned to *flooded* by the system and *trafficable* by the reference.

The forth column (cf. Tab. 1: $t_{1,2}$, *r*, *DEM*) shows the results exploiting an additional manually generated reference at time point *t1*. The results are by far better then the previous obtained results. The major reason for the improvement follows from the assumption that trafficable roads at time point t_1 are also trafficable at time point t_2. The assumption can be made since the flood was receding. The 'correct assignments' arise from 69% to 87% and the 'wrong assignments' decrease from 0.4% to 0.1%. But it is important to point out, that a correct reference at the time point t_1 has to be generated. Nevertheless, it has no influence of the fact that the system is near-realtime since the time consuming generation of the reference can be done at time point t_1.

4 Conclusions

In this paper three modules dealing with the automatic extraction and updating, the refinement and the assessment of roads are presented. The different modules are investigated regarding their usability in case of natural disasters. The automatic extraction of roads based only on the image information cannot deliver reliable information which is needed in case of natural disasters. However, the automatic extraction can speed up the semiautomatic extraction of accessible roads. Furthermore the updating and refinement of existing GIS road data are crucial methods in order to get a complete, up-to-date and geometric correct road network which is a prerequisite for the final damage assessment.

In future work the damage assessment system will be improved using a consistent statistical framework. Up to now, the combination of the derived probabilities is embedded into a rule-based framework. This framework will be substituted using the statistical theory of Dynamic Bayesian Networks. A special Dynamic Bayesian Network and promising graphical model are Hidden Markov Models.

References

Baltsavias, E., Grün, A. & van Gool, L. (Eds.), 2001: Automatic Extraction of Man-Made Objects from Aerial and Space Images (III). – Balkema Publishers, Lisse: 415 p.

Baumgartner, A., Hinz, S. & Wiedemann, C., 2002: Efficient Methods and Interfaces for Road Tracking. – International Archives of Photogrammetry, Remote Sensing and Spatial Information Sciences **34** (3B): 28–31.

Baumgartner, A., Steger, C., Mayer, H., Eckstein, W. & Ebner, H., 1999: Automatic Road Extraction Based on Multi-Scale, Grouping, and Context. – Photogrammetric Engineering & Remote Sensing **65** (7): 777–785.

Blake, A. & Isard, M., 1998: Active Contours. Springer, Berlin Heidelberg New York, 351 p.

Butenuth, M., 2007: Segmentation of Imagery Using Network Snakes. – Photogrammetrie – Fernerkundung – Geoinformation **1/07:** 7–16.

Butenuth, M. & Heipke, C., 2010: Network Snakes: Graph-based Object Delineation with Active Contour Models. – Machine Vision and Applications, DOI: 10.1007/s00138-010-0294-8, in print.

Frey, D. & Butenuth, M., 2009: Classification system of GIS-objects using multi-sensorial imagery for near-realtime disaster management. – International Archives of Photogrammetry, Remote Sensing and Spatial Information Sciences **33** (3/W4): 103–108.

Frey, D. & Butenuth, M., 2010: Classification system of GIS-objects using multi-temporal imagery for near-realtime disaster management. – International Archives of Photogrammetry, Remote Sensing and Spatial Information Sciences **33** (7A): 43–48.

Gamba, P., Hellwich, O. & Lombardo, P. (Eds.), 2003: ISPRS Journal of Photogrammetry and Remote Sensing, **58** (1–2), Theme issue on Algorithms and Techniques for Multi-Source Data Fusion in Urban Areas: 125 p.

Gerke, M. & Heipke, C., 2008: Image-based quality assessment of road databases. – International Journal of Geographical Information Science **22** (8): 871–894.

Gerke, M., Butenuth, M., Heipke, C. & Willrich, F., 2004: Graph-supported verification of road databases. – ISPRS Journal of Photogrammetry and Remote Sensing **58** (3–4): 152–165.

Grün, A., Baltsavias, E. & Henricsson, O. (Eds.), 1997: Automatic Extraction of Man-Made Objects from Aerial and Space Images (II). – Birkhäuser Verlag, Basel.

Hedman, K., Hinz, S. & Stilla, U., 2006: A Probabilistic Fusion Strategy Applied to Road Extraction from Multi-Aspect Sar Data. – International Archives of Photogrammetry, Remote Sensing, and Spatial Information Sciences **36** (3): 55–60.

Hinz, S. & Wiedemann, C., 2004: Increasing Efficiency of Road Extraction by Self-Diagnosis. – Photogrammetric Engineering and Remote Sensing **70** (12): 1457–1466.

Huadong, G., 2009: Natural Disaster Mitigation: A scientific and Practical Approach. InterAcademy Panel on International Issues. – Science Press Beijing, China.

Kass, M., Witkin, A. & Terzpopoulos, D., 1988: Snakes: Active Contour Models. – International Journal of Computer Vision **1** (4): 321–33.

McLachlan, G. & Peel, D., 2000: Finite mixture models. – Wiley-Interscience.

Mayer, H., 1999: Automatic Object Extraction from Aerial Imagery – A Survey Focusing on Buildings. – Computer Vision and Image Understanding **74** (2): 138–149.

Nielsen, A., Conradsen, K. & Simpson, J., 1998: Alteration detection (MAD) and MAF postprocessing sing in multi-spectral, bitemporal image data: New approaches to change detection studies. – Remote Sensing of Environment **64** (1): 1–19

Soergel, U., Thoennessen, U., Brenner, A. & Stilla, U., 2006: High-resolution SAR data: new opportunities and challenges for the analysis of urban areas. – IEEE Radar, Sonar & Navigation **153** (3): 294–300.

Wessel, B. & Hinz, S., 2004: Context-supported Road Extraction from SAR-Imagery: Transition from Rural to Built-up Areas. – EUSAR 04, 399–403.

Wiedemann, C. & Hinz, S., 1999: Automatic Extraction and Evaluation of Road Networks from Satellite Imagery. – International Archives of Photogrammetry and Remote Sensing **32** (3-2W5): 95–100.

Addresses of the Authors:

Dipl.-Ing. Daniel Frey, Dr.-Ing. Matthias Butenuth, Technische Universität München, Lehrstuhl für Methodik der Fernerkundung, D-80333 München, Tel.: +49-(0)89-28922671, Fax: -2809573, e-mail: daniel.frey@bv.tum.de, matthias.butenuth@bv.tum.de

Prof. Dr.-Ing. Stefan Hinz, Karlsruher Institut für Technologie (KIT), Institut für Photogrammetrie und Fernerkundung, D-76128 Karlsruhe, Tel.: +49-(0)721-608-2314, Fax: -8450, e-mail: stefan.hinz@kit.edu

Manuskript eingereicht: Juni 2010
Angenommen: September 2010

PFG 2010 / 6, 463 – 474
Stuttgart, Dezember 2010

Article

Curvelet-based Change Detection on SAR Images for Natural Disaster Mapping

Andreas Schmitt, Birgit Wessel & Achim Roth, Oberpfaffenhofen

Keywords: SAR, Change Detection, Alternative Image Representation, Curvelets

Summary: This paper focuses on the use of SAR data in the context of natural disasters. A Curvelet-based change detection algorithm is presented that automatically extracts changes in the radar backscattering from two TerraSAR-X acquisitions – pre-disaster and post-disaster – of the same area. After a logarithmic scaling of the geocoded amplitude images the Curvelet-transform is applied. The differentiation is then done in the Curvelet-coefficient domain where each coefficient represents the strength of a linear structure apparent in the original image. In order to reduce noise the resulting coefficient differences are weighted by a special function that suppresses minor, noise-like structures. The resulting enhanced coefficients are transformed back to the image domain and brought to the original scaling, so that the values in the difference image describe the increase and the decrease with respect to the amplitude value in the initial image. This approach is applied on three crisis scenarios: flood, forest fire, and earthquake. For all scenarios including natural landscapes and urban environments as well areas with changes in the radar amplitude are clearly delineated. The interpretation of the changes detected in the radar images needs additional knowledge, e. g., pre-disaster maps. The combination of both could possibly deliver a robust and reliable database for the coordination of rescue teams after large-scale natural disasters.

Zusammenfassung: *Auf Curvelets basierende Änderungserkennung in SAR-Bildern für die Kartierung von Naturkatastrophen.* Fernerkundung im Krisenkontext basiert auf einer schnellen und zuverlässigen Datenakquisition. Radarsysteme sind für diesen Zweck aufgrund ihrer i. A. wetter- und beleuchtungsunabhängigen Aufnahme besonders geeignet. In diesem Artikel wird eine Methode vorgestellt, aus zeitlich versetzten Aufnahmen des deutschen Radarsatelliten TerraSAR-X vollautomatisch Veränderungen abzuleiten. Die geokodierten Radaramplitudenbilder werden dazu logarithmisch skaliert und mithilfe der Curvelet-Transformation in den Curvelet-Koeffizientenraum überführt. Jeder Koeffizient entspricht hier der Stärke einer bestimmten linearen Struktur im Bild. Aus den Koeffizienten zweier Bilder kann nun ein Differenz-Koeffizientenbild berechnet und anschließend durch eine spezielle Gewichtungsfunktion verbessert werden. Während starke Strukturen unverändert übernommen werden, erfolgt für Strukturen mittlerer Stärke eine kontinuierliche Herabgewichtung bis zum kompletten Entfernen zu schwacher Strukturen. Auf diese Weise wird nicht nur die Anzahl der Koeffizienten, sondern auch das Rauschen im Bild deutlich verringert und der Bildinhalt auf die wichtigsten Strukturen beschränkt. Nach der Rücktransformation in den Bildraum und die ursprüngliche Skalierung kann die Änderung anteilig in Bezug auf die Ausgangsamplitude als Zu- und Abnahme dargestellt werden. Zur Demonstration des Potentials der Curvelet basierten Änderungserkennung werden drei Anwendungsfälle aus dem Krisenkontext vorgestellt: Überflutung, Waldbrand, Erdbeben. In allen drei Fällen lässt sich die von der Katastrophe betroffene Fläche eindeutig von Flächen ohne Änderung abgrenzen. Die Interpretation dieser Änderungen ist jedoch ohne Zusatzwissen nicht möglich. Eine Verschneidung der Ergebnisse der Änderungserkennung mit bestehenden Geoinformationen hingegen liefert eine verlässliche Datengrundlage für die Organisation von Rettungskräften nach Naturkatastrophen.

© 2010 E. Schweizerbart'sche Verlagsbuchhandlung, Stuttgart, Germany
www.schweizerbart.de
DOI: 10.1127/1432-8364/2010/0068
1432-8364/10/0068 $ 3.00

1 Introduction

Remote sensing products for disaster monitoring have to be fast and reliable. In most cases the coordinators do not have the time to wait for the next sunny day to acquire cloudless optical satellite images of the catastrophe. Radar sensors share the advantage to operate almost independently of weather and illumination, so that SAR images can be acquired in spite of a cloudy sky and even by night. Each illuminated object produces a certain SAR signature in the image. As the signatures of several objects overlay and interfere in fine-structured areas, a classification on SAR images is very complicated. Hence, the idea is not to classify single SAR images, but to identify changes between two image acquisitions before and after a natural disaster. In regions not affected by the impact, the radar signatures remain constant. Changes on the real objects mostly cause changes in the corresponding signatures, so that the affected regions can clearly be delineated. If the geometric properties of the images are held constant by using repeat orbit acquisitions, the only problem is the handling of the SAR inherent radiometry with its deterministic multiplicative noise-like component: speckle. Speckle is caused by the coherent sum of many distributed scatterers in one resolution cell (pixel). Hence, only individual pixels are affected whereas the structures of a scene joining an arbitrary number of individual pixels to geometric primitives e. g., lines, remain unchanged. Therefore, the comparison of two SAR amplitude images can be greatly simplified – because the false alarm rate is reduced – by comparing structures instead of single pixels. For this task a structure-based image description, called Curvelets, is utilized. The complex Curvelet coefficients, standing each for the strength of a linear feature in the image, allow us to compare and to manipulate structures in order to enhance a single as well as the difference between two SAR images. The developed change detection method runs automatically and delivers very robust results in a relatively short computation time. In contrast to the previous publications – reported in the following section – this article presents the theoretical background of the Curvelet-based change detection for the first time. Afterwards, the potential of the developed algorithm is validated for rapid mapping applications in the context of natural hazards. Three different disaster scenarios are considered: (1) The annual flood in the Caprivi stripe in Namibia (April 2009), which was the common test site for the DeSecure project; (2) Forest Fires on La Palma, Canary Islands (August 2009), where the Centre for Satellite Based Crisis Information (ZKI) of the German Aerospace Center has mapped the burned areas; (3) Damage on buildings in the city of Padang, Indonesia, after the earth quake of October 2009. For this test site reference information extracted visually from optical satellite images as well as some ground truth information, collected by several teams is available. Unfortunately, the ground truth data only covers single streets or building blocks.

The results of our change detection approach for SAR images are compared to the results of ZKI and the ground truth data respectively. In terms of the validation it is important to remember that the change detection on SAR data and the reference data – mainly extracted from optical satellite images – often show different results because of the different geometrical and radiometrical properties. Though, this study underlines the usefulness of SAR sensors as complementary data source in the context of satellite-based disaster management.

2 Related Work

Due to the geometric and radiometric properties of SAR images change detection gets more complicated – compared to optical data. Some basics of SAR change detection, advantages and constraints can be found in (Polidori et al. 1995), which reviews the fundamental approaches. (Scheuchl et al. 2009) distinguishes two different types of change detection: amplitude change detection and coherent change detection, exploiting the phase information. The latter one has been examined by (Wright et al. 2005). The method presumes a stable phase measurement, so that each incoherent region can be classified as changed. Regarding shorter wave lengths, even a repeat pass acquisition with a very short repetition

time (11 days in the case of TerraSAR-X) cannot assure coherence over natural cover. In the case of natural disaster monitoring, where reference images often date from several years ago coherence-based methods are not applicable because too much disturbing incoherence is caused by natural surfaces.

The amplitude-based change detection is better suited for the monitoring of diverse landscapes over a long period of time. (Derrode et al. 2003) and (Bouyahia et al. 2008) adopt a hidden and a sliding hidden Markov chain model respectively to select areas with changes in reflectivity even from images with different incidence angles. Although this method allows to process very large images and does not need additional parameter tuning, except the window size, according to the authors still a lot of research work has to be done to improve the preliminary results. Another idea starting with the fusion of several SAR images of different incidence angles and a coarse digital elevation model to a „superresolution" image is presented by (Marcos et al. 2006) and (Romero et al. 2006). Man-made objects, i. e., geometrical particularities that are not captured by the digital terrain model used for the orthorectification, are classified by their diverse appearance in the single orthorectified images due to the different acquisition geometries. So, seasonal changes in natural surroundings can easily be distinguished from changes in built-up areas. One disadvantage is the large number of different SAR images of the same area needed to generate the „superresolution" image.

In contrast to the precedent approach, (Balz 2004) needs a high resolution elevation model (e. g., acquired by airborne laser scanning) to simulate a SAR image with respect to the geometric appearance of the illuminated area. This simulated SAR image is subsequently compared to the real SAR data. The quality of the results is naturally highly dependent on the resolution of the digital elevation model and its co-registration to the SAR image. The influence of different surface materials is ignored so far. Although this method seems to be very promising, its application is still restricted to small-sized sample data. Another approach – based on radar measurements – has been published by (Molinier et al. 2007). This study focuses on the use of different polarimetric decompositions for the retrieval of several "polarimetric" features. The change detection consists in comparing the features extracted from the first image to the features extracted from the second image. As the feature extraction algorithm has to be trained in advance, this method is not suited for fully automatic data processing, e. g., in process chains. (Gamba et al. 2006) proposes a combined approach based on pixel values and geometrical features as well which are assumed to provide two uncorrelated sources of information. The goal is to utilize standard methods – implemented in all available SAR software products – to produce a rough pixel based change detection map and to extract edges of both amplitude images. The extracted features are subsequently compared to discriminate areas with changes from areas without changes and hence to stabilize the results of the pixel-based change map.

A very interesting approach using the Wavelet representation of a logarithmically scaled ratio image is given in (Bovolo & Bruzzone 2005). For the first time the influence of the speckle effect and several speckle reduction techniques on the change detection results is addressed. The originally one-dimensional Wavelet transform is extended to two dimensions in order to represent an image at different scales. The change detection results from coarser to finer scales are recombined to the final change map. Unfortunately, the procedure still is characterized by a high amount of manual interactions, e. g., trial-and-error threshold determination. Although the results are very promising, Wavelets do not seem to be the best representation for SAR images of urban areas (Schmitt et al. 2010b). Four different representations have been introduced into the same change detection procedure: Laplacian pyramid, Wavelets, Curvelets, and Surfacelets. While the Laplacian pyramid only distinguishes scales, Wavelets can distinguish horizontally and vertically aligned features. But, as most SAR signatures of urban areas are composed of linear elements of an arbitrary orientation, the Curvelet decomposition turns out to be the most effective way to describe urban scenes in SAR images (Schmitt et al. 2010b). Surfacelets are more suitable to

describe small-sized ellipse-like features, e. g., for car tracking purposes.

Curvelets for SAR image enhancement, structure extraction and change detection are considered for the first time in (Schmitt et al. 2009a). The core of this method is a special weighting function that is applied to the complex Curvelet coefficients of an image. Depending on the application different weighting functions are utilized. While the precedent publication mainly shows the potential of the Curvelet-based image understanding, (Schmitt et al. 2009b) focuses on change detection and its application to real SAR data over construction sites and mining areas. Since then, the weighting function as well as the scaling of the results has been improved several times in order to develop a fully automatic change detection approach independent of the image content. As the interpretation of the changes still is a very challenging task, multi-polarized SAR data is introduced as input data in (Schmitt et al. 2010a). By the help of the dual polarized High Resolution Spotlight mode of TerraSAR-X, the authors try to attach a physical meaning to the detected changes and to relate the derived changes in the scattering type to changes on real objects.

3 Change Detection with Curvelets

The Curvelet transform is designed to describe an image with singularities across straight lines, by a minimum number of coefficients (Candès & Donoho 1999). This fact shows the original purpose of the Curvelet transform: image compression. The basic element of the Curvelet theory is a linear feature, called Ridgelet, that is composed of a sine and a cosine component (see Figs. 1 & 2) represented by the real and the imaginary part of the corresponding coefficient. To describe an image effectively this basic element is transported to a wide range of scales, orientations and positions (Candès et al. 2005) and from now on called "Curvelet". In other words, each complex coefficient belongs to a certain Curvelet with a defined length, in a certain orientation and on a special position. The amplitude of the coefficient shows the strength of this linear

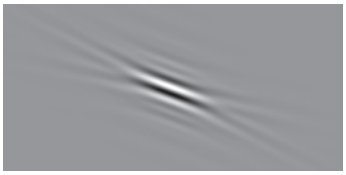

Fig. 1: Sine component.

Fig. 2: Cosine component.

feature in the original image. The value of one single pixel is thus calculated as sum of the contributions of all Curvelets in the image.

Transporting this theory to SAR images, clear structures in the image are always characterized by high coefficient amplitudes. In other words, the lower coefficients can be omitted without loss of structures. Former studies examine several types of weighting functions and different methods to adapt the function parameters to the image content. The results have already been submitted for publication. In short, the described image enhancement algorithm is based on a weighting function that is automatically adapted to the image content and then applied to the Curvelet coefficients of a SAR image. In terms of describing multiplicative speckle noise by an additive image representation, the SAR amplitudes have to be scaled logarithmically before the Curvelet transform is done. After weighting the coefficients and the inverse transform, the image is brought back to the original scaling by an exponential function.

The Curvelet-based change detection algorithm for already co-registered images exploits the following mathematical relations:

$$L_{x,y} = \sum_{i=1}^{n} C_i \cdot k_i \qquad (1)$$

The logarithmized SAR amplitude $L_{x,y}$ found at position x, y in the image forms out of the sum over all Curvelets C_i multiplied with

the corresponding complex coefficients k_i. To detect changes in the radar amplitude the amplitude difference $D_{x,y}$ is calculated.

$$D_{x,y} = L_{2_{x,y}} - L_{1_{x,y}} \tag{2}$$

To express this relation via the Curvelet Coefficients, Eq. (1) is inserted into Eq. (2). As the input images share the same size, they share also the same number n of Curvelets. Therefore, the decomposition in scales, orientations and positions of the first image is consistent with the decomposition of the second image, i. e., the variable C_i stays constant while k_i varies depending on the image content.

$$D_{x,y} = \sum_{i=1}^{n} C_i \cdot k_{2i} - \sum_{i=1}^{n} C_i \cdot k_{1i} = \sum_{i=1}^{n} C_i \cdot (k_{2i} - k_{1i}) \tag{3}$$

In a nutshell, the images are compared by differentiating the corresponding Curvelet coefficients. An overview to the method is given in the flow chart in Fig. 3. The input images have to be co-registered in advance. In the case of TerraSAR-X data, the geocoding based on the science orbit information is sufficient. For practical use, the input images should be *Enhanced Ellipsoid Corrected* (*EEC*) products. Then, no further pre-processing is necessary. After the logarithmic scaling the Curvelet transform is performed. The differentiation of the Curvelet coefficients follows. To suppress clutter the image enhancement algorithm is applied to the coefficient differences before the difference image is transformed back to the spatial domain and scaled exponentially. The pixel values of the resulting difference image correspond to the relative changes $R_{x,y}$ in the SAR amplitudes, i. e., a relative increase by a certain percentage, see Eq. (4).

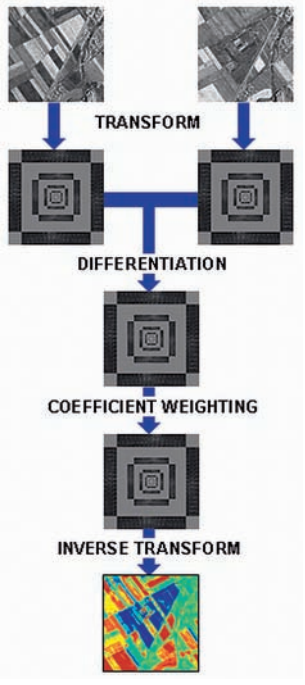

Fig. 3: Flowchart of the Curvelet-based change detection approach.

$$R_{x,y} = \left(e^{|Dx,y|} - 1\right) \cdot sign(D_{x,y}) \tag{4}$$

The sign of the differences gives the direction of the increase. While positive difference indicate an increase from the first to the second image, negative differences stand for an increase from the second to the first image. The exponential function is subsequently applied to the absolute value of the differences, which implies that every difference is seen as increase either from the first to the second image or the other way round. That's the reason why both increases and "decreases" of more than 100% can appear in both directions. At least the results of the exponential function are reduced by their minimum value, i. e., 1, so that the $R_{x,y}$ directly refers to the relative increase in the radar amplitude. The adoption of relative changes again accommodates the multiplicative nature of SAR images.

Mapping the increase and the decrease in the SAR amplitudes of single polarized images, allows to delineate regions that are characterized by this behavior, but it does not allow any interpretation of the mapped change. To explain what happened to the illuminated objects it is necessary to consult further data sources, e. g., a land cover classification or a building mask etc. One essential problem in the fusion of different data sources is still the coregistration of images having varying acquisition geometries, e. g., SAR data and optical data. Hence, our future work primarily will concentrate on the inclusion of polarimetric SAR data as purely SAR-based approach,

in order to attach the changes to certain scattering types. The knowledge about the change in the scattering geometry might help to interpret the change on the illuminated object and bear unknown potentials of SAR sensors.

4 Flood in Namibia

As common test site for the DeSecure project the Caprivi basin in the Caprivi stripe belonging to Namibia (Africa) was chosen. The annual flood reached very high water levels in the year 2009. the first SAR image has been taken during the flood in April (Fig. 4). The second image – seen as the pre-disaster acquisition – has been acquired in September after the flood (Fig. 5). Dark regions show very smooth surfaces where the incoming microwaves are scattered away from the sensor, e. g., calm water or pavement. By comparing the two TerraSAR-X Spotlight images with a ground pixel spacing of 1.75 m visually, we perceive large black regions in Fig. 4, showing the flooded areas, whereas in Fig. 5 the black pixels are restricted to the river and some roads. Flooded vegetation, i. e., flooded forests causes a higher backscattering. The trunks of trees enclosing a perpendicular angle with the water surface form a diplane scatterer that increases the backscattering of the whole area. In Fig. 4 the forested region on the top right – presumably flooded – appears brighter than in Fig. 5. Considering the Curvelet-based change detection, we have to take into account that the result is a change map instead of a water mask. Therefore, areas that are flooded in both images, e. g., the river, are not reported as change. As input for the change detection algorithm we use the enhanced ellipsoid corrected products in the radiometrically enhanced type.

Fig. 7 depicts the detected changes from the "pre-disaster" image to the image acquisition during the flood. The changes are colored according to the legend on the right. Changes of more than one hundred percent are not further distinguished. Green regions mark areas with no or only minor changes. Red colors mark an increase in the backscattering. In the imaged region this effect is mainly caused by flooded vegetation showing a high diplane scattering. Blue refers to a decrease in the backscattering amplitude which corresponds to recently flooded regions. As expected, only minor changes are indicated over the river and the road crossing the river. In comparison to the reference water mask, derived by the DeSecure project using thresholding methods on the backscattered intensity, the blue regions of the Curvelet-based change detection fit the flooded regions in Fig. 6. One larger region left in the middle that is reported flooded in Fig. 6 is marked in red in Fig. 7 because we find flooded vegetation there that causes an increase in backscattering. Having a closer look

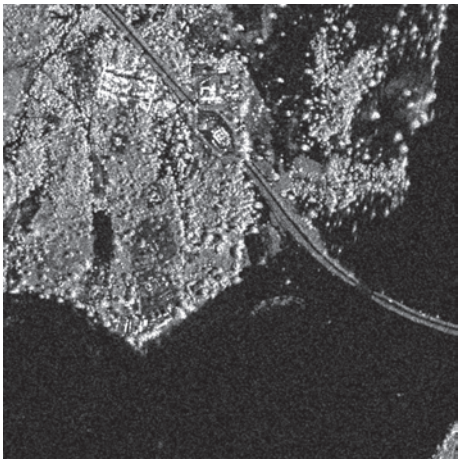

Fig. 4: Subset of TerraSAR-X Spotlight acquisition during the flood (06.04.2009).

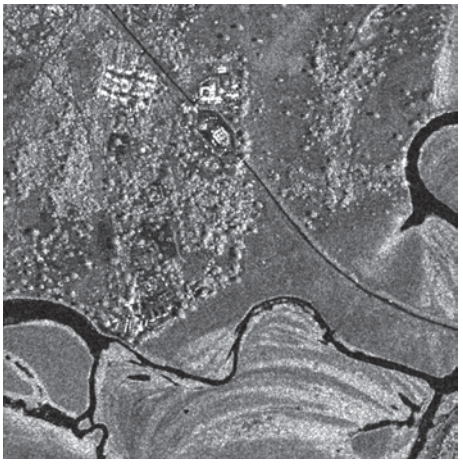

Fig. 5: Subset of TerraSAR-X Spotlight acquisition after the flood (07.09.2009).

Fig. 6: Reference data: roads and buildings from Quickbird imagery, watermask from TerraSAR-X ScanSAR (11.04.2009).

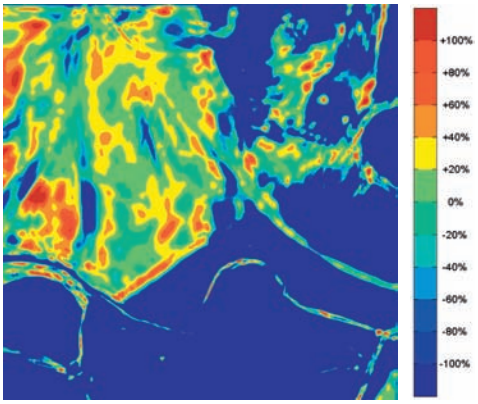

Fig. 7: Relative change of radar amplitude from 07.09.2009 (after the flood) to 06.04.2009 (during the flood), colored according to the colorbar on the right.

on both Figs. 6 and 7 we see many details that differ on the top left of the subset whereas the results near the river coincide very well. There are two simple reasons for this behavior. Firstly, the reference data is not ground truth data. As it is derived by simple amplitude thresholding of a TerraSAR-X ScanSAR scene and subsequently manually corrected, it only covers open water surfaces, i. e., flooded vegetation cannot be identified. Secondly, the ScanSAR image has been acquired five days later than the Spotlight images. Due to the very flat landscape, even a small deviation in water level causes large laminar changes in the flooded areas.

5 Forest Fires on La Palma

The second application of the Curvelet-based change detection approach is the mapping of burnt forest areas. The situation has been de-

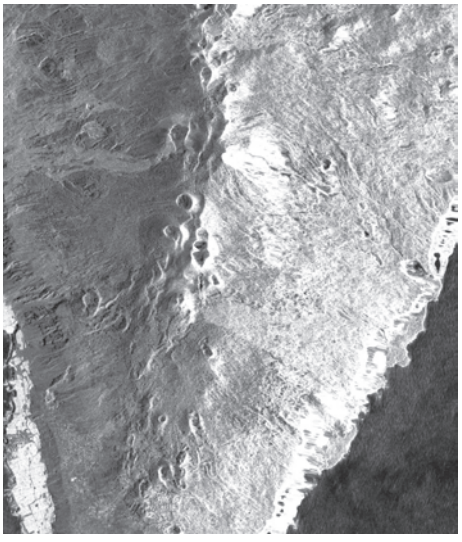

Fig. 8: Subset of TerraSAR-X Stripmap image before the forest fires (13.12.2007).

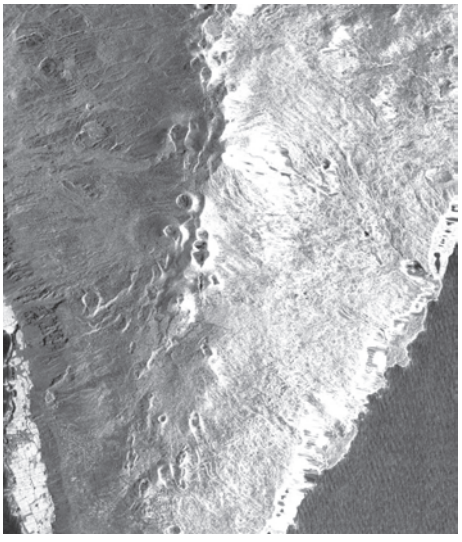

Fig. 9: Subset of TerraSAR-X Stripmap image after the forest fires (09.08.2009).

scribed by ZKI as follows: "Several forest fires occurred between July 31, 2009 and August 3, 2009 on the Canary Island of La Palma, Spain. 30 houses and several vineyards were destroyed. More than 4000 residents were evacuated from the area on August 1, 2009 (ZKI 2009a). As input for the Curvelet-based change detection we use TerraSAR-X radiometrically enhanced Stripmap products with a pixel spacing on ground of 2.75 m (EEC). The image in Fig. 8 shows the pre-disaster landscape on 13.12.2007. In Fig. 9 the post-disaster image dating from 9.8.2009 is depicted. The visual comparison delivers almost no changes, except on the ocean's surface on the bottom right.

In contrast to that the Curvelet-based change detection clearly delineates the burnt regions via the relative change in the backscattering amplitude (see Fig. 11). The reference map by ZKI is depicted in Fig. 10 and explained as follows: "The map shows the burnt areas as well as the locations of active fires between July 31, 2009 and August 3, 2009. The burnt areas were derived through the analysis of two Spot 5 scenes (pre disaster: 30/07/2007, post disaster: 07/08/2009). The locations of active fires were automatically derived from MODIS data" (ZKI 2009a). Although the reference again shows the situation at another time than the TerraSAR-X acquisition the burnt areas from Fig. 10 coincide very well with the regions showing an increase in backscattering in Fig. 11. The reason for this increase lies in the change of the scattering mechanism. While the leafy crowns of trees cause a high volume scattering – high values in the HV polarization and low values in both the HH and the VV polarization – the bare soil and the nude trunks respectively show high surface and diplane scattering, that means higher values in HH and VV. The TerraSAR-X images acquired in the HH polarization subsequently should report an increase in backscattering over burnt areas. Why the large area in the middle right that is marked as burnt in the reference map only is reported as minor change in Fig. 11, cannot be explained on the actual information basis. The effect on radar images highly depends on the change of the surface roughness of the illuminated areas caused by the fire. The use of multi-polarized radar data would help to identify the underlying scattering mechanisms instead of taking assumptions as hitherto. This could give a deeper insight to the type of forest before the fires and the degree of destruction after the fires.

6 Earthquake in Padang

The third example concerns the detection of damaged buildings in dense city centers. "On September 30, 2009, a severe earthquake took

Fig. 10: Reference data, visually digitized out of optical satellite image (ZKI 2009a).

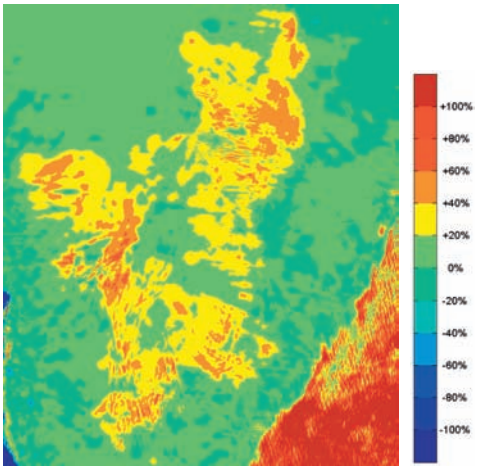

Fig. 11: Relative change of radar amplitude 13. 12. 2007 – 09. 08. 2009, according to colorbar.

place in the Indian Ocean with a magnitude of 7.9 and several aftershocks. The epicentre was registered about 50 km north-eastern of Padang in a depth of 85 km. Heavy shocks caused the collapse of many buildings and bridges, fires broke out and major parts of the technical infrastructure failed. More than 770 people died, much more than 2100 are injured (information of October 2, 2009). The International Charter on Space and Major Disasters was triggered to provide post-disaster satellite imagery for damage mapping and to support the aid response" (ZKI 2009b). A pre-disaster acquisition in the standard high resolution Spotlight mode dating from 21.11.2007 was available. The post-disaster image has been acquired in an experimental mode with the double pulse repetition frequency (PRF) and therefore possesses an increased azimuth resolution. In order to achieve equally-sized pixels on ground (1.25 m × 1.25 m) two different processing types in the geocoding step are utilized for image comparison. The first image (Fig. 12) with a minor azimuth resolution is processed as spatially enhanced product with a reduced accuracy in the radiometry, whereas the second image (Fig. 13) with a higher azimuth resolution is processed as radiometrically enhanced product with a reduced spatial resolution. The effects of the different acquisition modes and pre-processing steps are a higher noise level in Fig. 12 and a higher level of detail in Fig. 13. Despite these discrepancies in the input images, the automatic change detection delivers respectable results, see Fig. 15.

In order to enable the operator to attach single small-sized changes to objects, it is overlaid with the building mask that has been extracted from optical satellite imagery of IKONOS by (Taubenböck et al. 2009). Many changes – visible near the river – presumably refer to boats or pontoons. Presuming that all other mapped changes belong to buildings, we perceive striking deviations that result from the different image acquisition geometries of radar and optical data. The images should have been coregistered using the same high resolution surface model to avoid these effects. Although this inconsistence is negligible for our coarse validation, it has to be taken into account for real disaster applications. As reference information we use the damage assessment produced by (ZKI 2009b) which is described as follows: "Destroyed and damaged structures were derived by analyzing information provided by the Indonesian Disaster Management Authority (BNPB), from post-disaster Quickbird imagery acquired on October 3, 2009 (ground resolution 0.6 m) and from field data. The damage assessment is incomplete and in some cases inaccurate due to cloud cover and the difficulty to identify partly damaged buildings from bird's perspective"

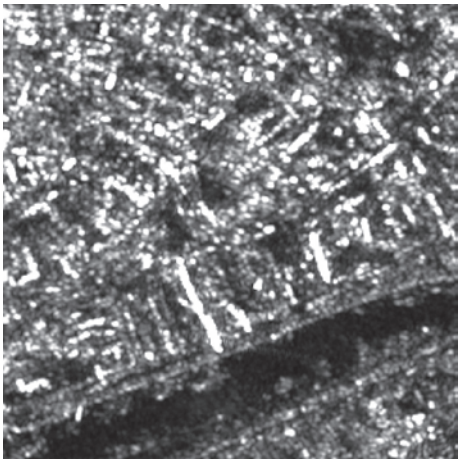

Fig. 12: Subset of TerraSAR-X Spotlight image, PRF 150 Mhz, spatially enhanced, pixel spacing 1.25 m (21. 11. 2007).

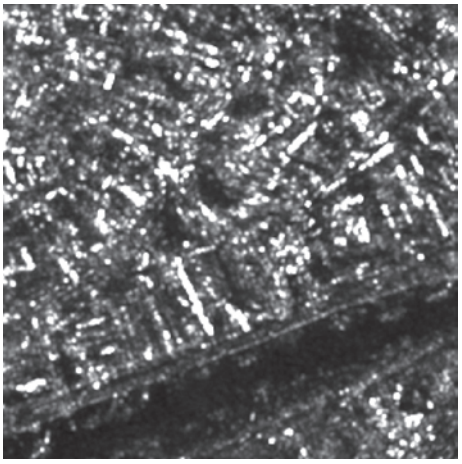

Fig. 13: Subset of TerraSAR-X Spotlight image, PRF 300 Mhz, radiometrically enhanced, pixel spacing 1.25 m (03. 10. 2009).

Fig. 14: Reference data, including streets and potentially damaged buildings: red (according to building structure survey) and yellow (on building characteristics derived from satellite imagery).

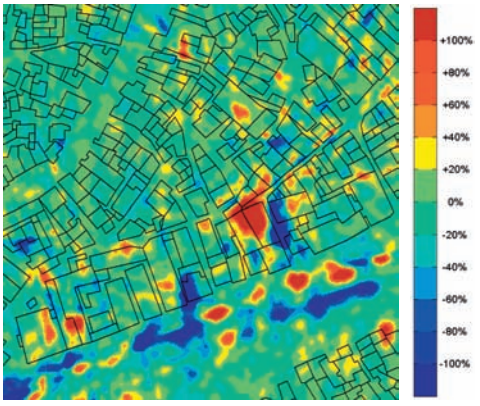

Fig. 15: Relative change of radar amplitude 07. 09. 2009 – 06. 04. 2009 and building mask from IKONOS imagery (Taubenböck et al. 2009).

(ZKI 2009b). Comparing the change detection results in Fig. 15 to the damage map in Fig. 14, only few sure coincidences are visible. Beside the incompleteness of the reference map, again the image acquisition geometry plays an important role. As the parallel projection in the case of optical scanning sensors is very similar to an orthogonal projection due to the large distance to the imaged objects, mostly roofs and nearly no facades are visible. In contrast the range projection of radar sensors reproduces roofs and facades as well. Hence, while optical sensors only reveal changes on nearly horizontal planes, i. e., ground or roofs, radar sensors show a high capability to map even changes on the buildings facades. Unfortunately, without any prior information the radar change detection results are only of limited value, because changes on natural surfaces cannot be distinguished from changes on man-made objects. But, this new technique enables to delineate areas with distinct changes to support the decision if a building that has been classified "potentially damaged" from pre-disaster analysis or optical satellite data is actually damaged or not. To conclude this example, radar information might not replace optical sensors and in-situ surveys, but it is a complementary tool to get reliable change information over large areas in a very short period of time and independent of weather, daylight or the accessibility of the injured city.

7 Conclusion

In this article we present a new change detection technique based on the Curvelet transform. This approach requires two or more coregistered SAR amplitude images. Changes in the SAR amplitudes over a certain period of time are captured as increase or decrease relative to the preceding amplitude values. Of course, the change detection approach can only detect changes present in the SAR amplitude data. Additionally, the size of the changes to be mapped must be superior to the pixel size, which was true for the chosen examples: flooded regions, burnt areas after forest fires, damaged buildings after an earthquake. The approach delivers robust and quasi noise-free results over natural landscapes as well as over urban environments. Validating urban scenes we have to consider the reference data source. Changes in the SAR image are always caused by changes on the imaged objects, but those are not always captured by other data sources used as reference, e. g., optical satellite data. And though the quantitative validation for large area applications is nearly impossible due to the lack of suitable reference data, the qualitative validation proved the reliability of the detected changes. The interpretation of the mapped changes is still topic to our research. The future focus lies on the exploitation of multi-polarized SAR data in terms of inter-

preting changes to objects by changes to the scattering mechanism. Another aim will be the fusion with pre-disaster optical image information in order to support human operators in interpreting the results of the SAR change detection, e. g., by the help of vulnerability maps or buildings masks.

References

Balz, T., 2004: SAR simulation based change detection with high-resolution SAR images in urban environments. – International Archives of Photogrammetry, Remote Sensing and Spatial Information Sciences **35** (B7): 472–477.

Bouyahia, Z., Benyoussef, L. & Derrode, S., 2008: Change detection in synthetic aperture radar images with a sliding hidden Markov chain model. – Journal of Applied Remote Sensing **2** (1).

Bovolo, F. & Bruzzone, L., 2005: A Detail-Preserving Scale-Driven Approach to Change Detection in Multitemporal SAR Images. – IEEE Transactions on Geoscience and Remote sensing **43** (12): 2963–2971.

Candès, E.J. & Donoho, D.L., 1999: Curvelets – a surprisingly effective nonadaptive representation for objects with edges. – Curve and Surface Fitting. Innovations in Applied Mathematics, Vanderbilt University Press, Saint-Malo (France): 105–120.

Candès, E.J., Demanet, L., Donoho, D.L. & Ying, L., 2005: Fast Discrete Curvelet Transforms. – Multiscale Modeling and Simulation **5:** 861–899.

Derrode, S., Mercier, G. & Pieczynski, W., 2003: Unsupervised Change Detection in SAR Images Using a Multicomponent HMC model. – Analysis of multitemporal remote sensing images. World Scientific Publishing Corporation: 16–18.

Gamba, P., Dell'Acqua, F. & Gianni Lisini, G., 2006: Change Detection of Multitemporal SAR Data in Urban Areas Combining Feature-Based and Pixel-Based Techniques. – IEEE Transactions on Geoscience and Remote Sensing **44** (10): 2820–2827.

Marcos, J.-S., Romero, R., Carrasco, D., Moreno, V., Valero, J.L. & Lafitte, M., 2003: Implementation of new SAR change detection methods: superresolution SAR change detector. – Journal for Photogrammetry and Remote Sensing **57:** 327–345.

Molinier, M., Laaksonen, J., Rauste, Y. & Hame, T., 2007: Detecting changes in polarimetric SAR data with content-based image retrieval. – IEEE Geoscience and Remote Sensing Symposium.

Polidori, L., Caillault, S. & Canaud, J.-L., 1995: Change detection in radar images: methods and operational constraints. – IEEE Geoscience and Remote Sensing Symposium: 1529–1531.

Romero, R., Marcos, J.-S., Carrasco, D., Moreno, V., Valero, J.L. & Lafitte, M., 2006: SAR Superresolution Change Detection for Security Applications. – ESA-EUSC Image Information Mining for Security and Intelligence, Torrejon air base, Madrid, Spain: on CD.

Scheuchl, B., Ullmann, T. & Koudogbo, F., 2009: Change Detection using High Resolution TERRASAR-X Data: Preliminary Results. – International Archives of Photogrammetry, Remote Sensing and Spatial Information Sciences **38** (1-4-7/W5): on CD.

Schmitt, A., Wessel, B. & Roth, A., 2009a: Curvelet Approach for SAR Image Denoising, Structure Enhancement, and Change Detection. – International Achives of Photogrammetry, Remote Sensing and Spatial Information Sciences **38** (3/W4): 151–156.

Schmitt, A., Wessel, B. & Roth, A., 2009b: Curvelet-based change Detection for man-made Objects from SAR Images. – IEEE Geoscience and Remote Sensing Symposium: 1059–1062.

Schmitt, A., Wessel, B. & Roth, A., 2010a: Introducing Partial Polarimetric Layers into a Curvelet-based Change Detection. – 8th European Conference on Synthetic Aperture Radar: 1018–1021.

Schmitt, A., Wendleder, A., Wessel, B. & Roth, A., 2010b: Comparison of Alternative Image Representations in the Context of SAR Change Detection. – IEEE Geoscience and Remote Sensing Symposium: on CD.

Taubenböck, H., Goseberg, N., Setiadi, N., Lämmel, G., Moder, F., Oczipka, M., Klüpfel, H., Wahl, R., Schlurmann, T., Strunz, G., Birkmann, J., Nagel, K., Siegert, F., Lehmann, F., Dech, S., Gress, A. & Klein, R. (2009): Last-Mile preparation for a potential disaster – Interdisciplinary approach towards tsunami early warning and an evacuation information system for the coastal city of Padang, Indonesia. – Natural Hazards and Earth System Sciences **9:** 1509–1528.

Wright, P., Macklin, T., Willis, C. & Rye, T., 2005: Coherent Change Detection with SAR. –European Radar Conference: 17–20.

ZKI, 2009a: Center for Satellite Based Crisis Information (ZKI) – Emergency mapping & Disaster Monitoring, a service of German Remote Sensing Data Center (DFD), 8.8.2009 www.zki.dlr.de/applications/2009/canaryislands/176_en.html (30.8.2010).

ZKI, 2009b: Center for Satellite Based Crisis Information (ZKI) – Emergency mapping & Disaster Monitoring, a service of German Remote Sensing Data Center (DFD), 1.10.2009 www.zki.dlr.de/applications/2009/indonesia/179_en.html (30.8.2010).

Address of the Authors:

Dipl.-Ing. Andreas Schmitt, Dr.-Ing. Birgit Wessel, Dipl.-Ing. Achim Roth, Deutsches Zentrum für Luft- und Raumfahrt (DLR), Deutsches Fernerkundungsdatenzentrum (DFD), Oberpfaffenhofen, Münchner Straße 20, D-82234 Weßling, Tel.: +49-8153-28-3341, -3307, -2706, Fax: -1445, e-mail: andreas.schmitt@dlr.de, birgit.wessel@dlr.de, achim.roth@dlr.de

Manuskript eingereicht: Juni 2010
Angenommen: September 2010

PFG 2010 / 6, 475 – 488
Stuttgart, Dezember 2010

Article

Flood Extent Mapping Based on TerraSAR-X Data

Virginia Herrera Cruz, Marc Müller, Friedrichshafen & Christian Weise, München

Keywords: TerraSAR-X, radar, flood mapping, classification, object-based, pixel-based

Summary: The use of Earth observation data and techniques in the context of disaster management support has received growing importance in recent years. Due to global climate change the scientific community foresees an increase in both the intensity and frequency of extreme weather events. The high resolution, multi-polarization and multi-incidence angle capabilities of the radar satellite TerraSAR-X, its quick site access and receiving times open interesting perspectives for flood mapping and subsequent assessment of damages. Furthermore, the nearly all-weather capacity of SAR data constitutes its main advantage above optical systems for mapping of flood events. The work presented in this paper focuses on the development of an object-based classification approach for operational flood extent mapping in near-real time conditions using TerraSAR-X data. The object-based methodology is assisted by pixel-based operations and both are implemented in a solution within the eCognition software environment. The final objective is to develop a tool which can be easily used by an interpreter without the need of a profound knowledge of image processing. For this purpose an eCognition based semi-automated solution – a *Graphical User Interface* with a rule set behind – is set up. This application is tested in various scenarios and is further developed in parallel to these tests. The overall study clearly demonstrates the potential of TerraSAR-X data and object oriented methods for a rapid delineation of flood extent in an operational environment.

Zusammenfassung: *Verwendung von TerraSAR-X-Daten zur Kartierung überschwemmter Bereiche*. In den letzten Jahren hat die Anwendung von Fernerkundungstechniken sowie der Einsatz von Erdbeobachtungsdaten im Zusammenhang mit Katastrophenmanagement an Bedeutung gewonnen. Bedingt durch den globalen Klimawandel erwartet die Wissenschaftsgemeinde eine Zunahme an extremen Wetterereignissen sowohl bezüglich Ausmaß als auch Häufigkeit. Die Fähigkeit des TerraSAR-X-Satelliten, hochauflösende und multi-polarisierte Satellitenbilder unter verschiedenen Einfallswinkeln aufzunehmen sowie seine Tasking-Flexibilität und der schnelle Datenerhalt bieten erweiterte Perspektiven für die Hochwasserkartierung bzw. die Schadenabschätzung. Außerdem stellt das nahezu allwettertaugliche Aufnahmeverfahren von SAR-Daten einen bedeutenden Vorteil gegenüber optischen Daten für die Kartierung von Hochwasserereignissen dar. Die hier vorgestellten Arbeiten konzentrieren sich auf die Entwicklung eines objektbasierten Klassifikationsansatzes für das operationelle Kartieren von Hochwasser unter nahe Echtzeit-Bedingung und unter Verwendung von TerraSAR-X-Daten. Die objektbasierte Methode wird unterstützt durch eine pixelbasierte Methode, beide Ansätze sind in einer eCognition-Softwareumgebung implementiert. Ziel ist die Erstellung eines Software-Werkzeuges, das relativ einfach und ohne fundierte Kenntnisse der Bildbearbeitung eingesetzt werden kann. Zu diesem Zwecke wurde eine auf eCognition basierende semi-automatische Lösung entwickelt, die eine graphische Benutzeroberfläche inklusive Regelsatz im Hintergrund als wesentlichen Bestandteil hat. Diese Lösung wurde in verschiedenen Szenarien getestet und parallel dazu weiterentwickelt. Insgesamt zeigen die Ergebnisse deutlich das Potential von TerraSAR-X-Daten und objektorientierten Methoden für eine schnelle Kartierung der Hochwasserausdehnung unter operationellen Bedingungen.

© 2010 E. Schweizerbart'sche Verlagsbuchhandlung, Stuttgart, Germany
www.schweizerbart.de
DOI: 10.1127/1432-8364/2010/0069
1432-8364/10/0069 $ 3.50

1 Introduction

Flood is one of the most widespread natural disasters and the one which affects the highest number of people in average (CRED 2009). It regularly causes large numbers of casualties with increasing economic loss. Annually flood events result in estimates of up to 25,000 deaths worldwide, extensive homelessness, disaster-induced disease, crop and livestock damage and other serious harm (UNU 2010). Even the most advanced nations are severely affected: The seasonal floods of the Mississippi River have averaged 25 deaths annually since the 1980s (ibid.). In Europe, the 2002 floods killed roughly 100 people, affected 450,000 people and left $ 20 billion in damages (ibid.). Already in the first half of 2010, floods caused by the storm Xynthia have affected all Atlantic countries from Portugal to Germany, hitting especially France. Also, in March 2010 the continuing rain was inundating the South of Spain, leaving hundreds of people homeless. Only two to three month later heavy rains caused floods in Poland, Hungary, Slovakia and the Czech Republic – let alone the devastating flood events in China and above all in Pakistan in August of 2010. The latter affected almost 14.5 million people with an official death toll risen to 1,384 and with 1,680 people reported as injured. Over 722,000 houses have been either damaged or destroyed (UN-SPIDER 2010). Consequently, disaster management is of particular humanitarian, social, economic, and political interest. It involves assessments of vulnerability and risk, the monitoring of hazard prone zones, the planning and management of rescue operations and post disaster damage assessment to be finally better prepared for the next time of a disastrous event.

Using remote sensing data allows for mapping inundated areas for a more accurate assessment of the disaster extent – especially for areas difficult to access – and for a more large-scale and cost-effective way than ground observation (Waisurasingha et al. 2008, Okamoto et al. 1998). Remote sensing is also an important information source for the calibration of hydrological models which are used, e. g., in forecasting (Zwenzner & Voigt 2009). Optical data as well as radar data – both airborne (e. g., Ramesh et al. 2010) and space-borne – has been used for this purpose. Using optical data (especially its red to SWIR spectrum) is often referred to as a most straightforward way to extract flood extent from Earth observation data (Ji et al. 2009). Huang et al. (2009) – analysing Spot-5 data – and Irimescu et al. (2010) – using MODIS TERRA and AQUA data – are among the related works. Other satellites used are, e. g., Landsat and the Advanced Very High Resolution Radiometer (Ji et al. 2009). Irimescu et al. (2010) propose the use of Normalised Difference Vegetation Index (NDVI) for water detection while Ji et al. (2009) defends when possible the use of NDWI calculated from green-SWIR / green+SWIR. Nevertheless, as flooding is often associated with extreme weather events, optical data acquisition encounters limitations due to cloud coverage. Contrarily, radar data presents the advantage of its near all weather operating capability allowing to acquire imagery of affected areas also during night time. Therefore radar is seen as the only secure alternative for mapping flood events in its peak (Schumann et al. 2009). For a long time its limited resolution has been seen as a hinder for its use in mapping of flood events. In 2006 Schumann et al. (2006) reported SAR data as having medium spatial resolution, often limited to single frequency, difficult to georectify accurately and geometrically and radiometrically distorted. But the new SAR satellites generation overcome these limitations by providing a wide catalogue of resolutions (down to 1 meter) and swaths with a very appropriate relation for flood evaluation. Discussion about the appropriate spatial resolution for flood mapping can be found in Schumann et al. (2009). Furthermore, today's SAR data – and especially TerraSAR-X data – is highly precise in terms of geocoding, positional accuracy and absolute radiometric calibration (Ager & Bresnahan 2009).

The examples presented here focus on three flood events of high intensities that occurred in June 2008 in a highly populated area of the USA and in February 2009 and April 2009 in two savannah areas of Australia and Namibia, respectively.

The first area of interest is located close to the St. Louis County (Missouri). The flood

event that occurred from May to August 2008 was caused by heavy rains. It affected high populated areas of the States of Illinois, Indiana, Iowa, Michigan, Minnesota, Missouri, and Wisconsin.

The second area is the Gulf Country region in North Queensland. It is a large savannah area with a monsoonal climate characterised by the alteration of dry winters and wet summers. It has a well known dynamic of flood events. Populations in the area are used to have three to four weeks of isolation during the wet season. Nevertheless, at the beginning of 2009, the unexpected volume of water kept the two towns of the area much longer isolated.

Finally, the Caprivi region is a narrow strip of land compressed between the arms of the Zambezi and the Kwando rivers and bordering with the countries Zambia, Botswana and Zimbabwe. The area is the wettest of Namibia, with a seasonal tropical climate with the rainy season lasting from December to March.

2 SAR Based Flood Extent Mapping

In this paper main emphasis is put on the development of a SAR-based flood mapping workflow suited for an operational implementation. In this domain quite a lot of research has been done in recent years (Martinis et al. 2009). Often used is the thresholding of the image histogram (Martinis et al. 2009, Gebhardt et al. 2008, Henry et al. 2006, Schumann et al. 2006) or of an arithmetic image (ratio or difference usually, Brakenridge et al. 2003) with different methods of interactive or automatic detection of the threshold values. Thresholding is a simple and resources economical method, but when applying it to pixels it requires a previous speckle filtering and again post-processing filtering and it is only effective in well contrasted images (Martinis et al. 2009).

Segmentation approaches play then an important role. The mapping process benefits, this way, not only from the absence of the salt and pepper effect, but also from the textural and contextual information contained in the objects. Sophisticated methods as Artificial Neural Networks (Kussul et al. 2008) or Active Contour Models – in its statistical variation (Horritt et al. 2001, Mason et al. 2010) or in its geometric variant (Huang et al. 2005) so called level-sets – have been applied to segment SAR data in the context of flood mapping both for whole scenes and region-based (Silveira & Heleno 2009). But Active Contour Models require enormous data preparation which today prevents their application for near real time mapping. A common approach for segmentation, more simple to apply are algorithms using the *Fractal Net Evolution Approach* (FNEA), commercially introduced by Baatz & Schäpe (1999) and implemented in the eCognition software. Neubert et al. (2008) and Meinel & Neubert (2004) show in an extensive review and comparison of segmentation methods best performances for the FNEA.

To profit from the simplicity of thresholding and the additional information saved in the pixel objects and the description power of the decision trees, different combined approaches could be considered. Martinis et al. (2009) for example combine a histogram thresholding approach and a segmentation based classification for flood detection in high resolution TerraSAR-X data. The threshold is automatically calculated based in local thresholding analysis of selected areas or splits. The threshold is afterwards integrated into a multi-scale segmentation process. They proved the better performance of object-based thresholding over pixel-based one. Townsend (2001) and Pierdicca et al. (2009) combine multiple thresholds with decision trees. Another possible combination is the supervised and unsupervised method: For instance, at the Center for Satellite Based Crisis Information of the German Aerospace Center an unsupervised clustering algorithm is applied to images enhanced by local image statistics (minimum / maximum, mean and variance) followed by interactively identification of water clusters (Hahmann et al. 2008).

Considering multi-temporal analysis as superior to single data approaches (Hahmann et al. 2008) change detection methods to detect variations of backscatter or on the coherence among SAR image pairs (Boni et al. 2007, Pierdicca et al. 2008) or by using ratios (An-

DREOLI & YESOU 2007) are also widely investigated. One advantage of those methods is that they profit by comparison possibilities in many cases of uncertainties. The disadvantage is that these methods require much data preparation (ANDREOLI & YESOU 2007) and strongly depend on available pre-event data which is not always at hand in a real emergency situation.

Also, real emergency events require simple tools which can provide a rapid and accurate overview of the situation. Such a tool should be time-effective, reliable, robust and flexible enough to adapt to the circumstances in relation to data and staff available. This kind of a simplified tool also offers the benefit directly to be used by local operators. For all these reasons the creation of a robust rule set and the creation of a user interface for operators having local knowledge but not being remote sensing experts was the guiding idea during the development of the method right from the beginning of the DeSecure project (DESECURE 2010).

The mapping of water with SAR data is based on the specular behaviour of the microwave signal when encountering a smooth surface. For instance, in the case of calm water, the SAR signal is scattered away and the surface appears dark in the satellite image. However, in case of a flood event, when extreme winds and rain occur at the time of image acquisition, the induced changes in the smooth surface of the water can increase the intensity of the response signal and produce artefacts which will complicate a straightforward classification of the flooded surface (KUSSUL et al. 2008). Further difficulties are flooded vegetation and / or man-made structures. Different structures poking out of the water can produce a enhancement of the signal due to a double bounce effect in the different SAR bands. This effect depends on the relation between the size and spacing of the structures and the chosen wavelength. As an example, changes from flood to not flooded in forested areas can be observed in C-band (HAHMANN et al. 2008) and with L-band (TOWNSEND 2001), because the signal is able to penetrate the forest canopy. Concerning X-band the shorter wavelength does not allow the penetration of the forest canopy (HAHMANN et al. 2008). For further details on the different SAR signal interactions with the Earth's surface it is referred to Raney in HENDERSON & LEWIS (1998).

The work presented here focuses on the development of a semi-automated procedure for flood extent mapping under near-real time (NRT) conditions. NRT is here understood as a combination of delivering TerraSAR-X images to the operator within 2 hours after image acquisition plus producing and delivering the flood extent map to the user within 2 hours on top.

The whole flood mapping procedure is implemented within the eCognition software suite and developed in the Cognition Network Language (CNL). CNL is an object-based procedural computer language which is specially designed to enable the analysis of complex, interactive, context-dependent image analysis tasks, like flood mapping. Each language element representing the dynamic of the analysis is called "process" and organized in a process tree hierarchy (rule set). Especially interactive processes allow interactions with users in an image analysis workflow. The execution environment of the software suite uses a workspace concept in which the user of a workflow may process many images offline and – if needed – in parallel on a computer cluster. It is thus possible to give a step-wise structure to the flood mapping analysis, to separate modules with different degrees of automation in the overall workflow and to analyze images in a production mode.

The outputs of the tests using eCognition confirmed the potential of TerraSAR-X data and the object-oriented methods for a rapid de-

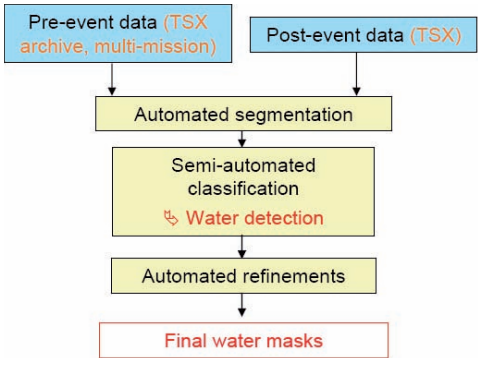

Fig. 1: Flood mapping – general workflow.

lineation of flood extent in an operational environment. The resulting mapping chain is completed by building a Graphical User Interface (GUI). Three modules sequentially activated are distinguished in the developed rules system: Segmentation with automated AoI (Area of Interest) selection, semi-automated extraction of water masks (classification) and automated final refinement (Fig. 1).

After introducing the satellite data used here including a description of the data characteristics and the pre-processing steps (Section 3) each of the three modules is explained separately in the Sections 4–6.

3 Data Set Selection and Preparation

TerraSAR-X is a German radar satellite operating in X-Band (9.65 Gigahertz). In the standard operating mode image data can be acquired in three different imaging modes: ScanSAR, StripMap and SpotLight modes which differ in their spatial coverage and spatial resolution. The ScanSAR mode provides the largest possible coverage with a single scene of 100 km (range) × 150 km (azimuth, extension up to 1,650 km possible) and a corresponding ground resolution of 18 m. StripMap scenes cover a 30 km wide swath with a typical length of 50 km (also extendable to 1,650 km), the ground resolution improves to 3 m. Finally, the SpotLight mode allows the observation of relatively small areas (10 × 10 km²) at up to 1 m resolution.

The high resolution, multi-polarization and multi-incidence angle capabilities of TerraSAR-X data acquisition open very interesting perspectives for flood mapping and damage assessment. Further, the system capabilities of TerraSAR-X render the satellite as a valuable imagery source for disaster management and site monitoring, e. g., due to the satellite's quick site access time of 2.5 days to any point on Earth at 95 % probability.

The programming of TerraSAR-X acquisitions for the affected regions requires a number of decisions regarding acquisition parameters (for a detailed description of products and parameters see Fritz & Eineder 2009). The selection of the best suitable acquisition mode is based on the size of the area affected. StripMap was chosen to cover the area selected for the Mississippi event while ScanSAR scenes were acquired for the Gulf Country and the Caprivi region, respectively. Additionally, SpotLight data of Caprivi were also used for a more detailed mapping. Compared to VV polarization, the HH polarized backscatter coefficient generally presents higher contrast between water and land surfaces (Henry et al. 2006). The use of dual polarization data results in a reduced coverage and resolution, which needs to be traded off against the increased information content. Here, HH polarisation was used for all areas of the study. Shallow incidence angles are preferred for flood mapping as steep incidence angles result in stronger backscatter for open water and reduce the contrast to land surfaces. In an emergency, however, acquiring the first possible scene of the area affected clearly takes priority over considerations on the choice of a proper incidence angle. For mapping the flood extent geocoded data sets are required (EEC products). Concerning the resolution mode, preference is given to RE products (radiometrically enhanced) as they already comprise a speckle reduction and are therefore more suited to segmentation processing.

In parallel to the acquisition planning, an archive search on existing pre-event and auxiliary data is required. TerraSAR-X data are preferred as pre-event data, since scenes acquired by the same sensor can be directly compared to each other. However, if no TerraSAR-X pre-event acquisitions are available, data from any other available source are used (e. g., optical, airborne data). In case of the Mississippi flooding, no TerraSAR-X archive data of the region was available. Thus, a Landsat 7 image was deployed for pre-event information. Additionally, approximately four months after the flood a new TerraSAR-X StripMap scene of the area was acquired and used as pre-event data, to simulate a real scenario for which TerraSAR-X archive data would be available. Also in Namibia, data of the flood recession period had to be used as simulated pre-event data. However, by the time the floods in Queensland occurred, the TerraSAR-X Background Mission was able to supply pre-event data from archive for that

Tab. 1: Mississippi area.

Sensor	Centre (lon/lat)	Imaging Mode	Product	Acquisition date
TerraSAR-X	−90.75° / 38.96°	SM	EEC/RE	23 June 2008
	−90.61° / 39.15°	SM	EEC/RE	17 October 2008
Landsat7	39.3°/ 90.7°	-	-	10 January 2008

Tab. 2: Gulf Country area.

Sensor	Centre (lon/lat)	Imaging Mode	Product	Acquisition date
TerraSAR-X	−17.15°/ 141.00°	SC	EEC/RE	3 June 2008
	−17.25/ 141.23°	SC	EEC/RE	11 February 2009

Tab. 3: Caprivi area.

Sensor	Centre (lon/lat)	Imaging Mode	Product	Acquisition date
TerraSAR-X	24.76°/−17.68°	SC	EEC/RE	11 April 2009
TerraSAR-X	24.72°/−17.59°	SC	EEC/RE	1 September 2009
	24.78°/−17.88°	SL	EEC/RE	6 April 2009
	24.71°/−17.92°	SL	EEC/RE	7 September 2009

area, and therefore a complete ScanSAR data set (pre and post event) could be analysed in that case. Detailed information on the image parameters is shown in Tabs. 1–3.

Auxiliary data sets are also of great importance. Any supplementary information about the test site support and accelerate the event interpretation. It also reduces the effort for the refinement step which is later described. In addition to the image data sets, a visual interpretation of the environmental conditions was performed for the Australian flood event. This interpretation map, chiefly based on manual work, was used as reference.

4 Automated Segmentation

Segmentation is the process of completely partitioning a scene (e. g., a remote sensing image) into non-overlapping regions (segments) in scene space (e. g., image space Schiewe 2002), based on homogeneity and heterogeneity criteria, respectively (Haralick & Shapiro 1985 in Neubert et al. 2006). In the object-oriented classification, the final aim of the segmentation is to delineate the meaningful regions which represent the objects that need to be classified. Despite the popularity of segmentation processes for remote sensing images in the last years, segmentation is by no means a new field of research. On the contrary, segmentation was already in the 1970's a topic of interest (cf. Kettig & Landgrebe 1976). And so far, about one thousand kinds of segmentation approaches have already been developed (Chen & Luo 2003) within disciplines like artificial intelligence, signal processing, computer vision etc. with successful applications in medicine, telecommunications, engineering or neuro-informatics (Schiewe et al. 2001). There is a high variety of segmentation algorithms already available for remote sensing images. A good review and comparison can be found in Neubert et al. (2008) and Meinel & Neubert (2004).

Referring back to Section 2, *FNEA* is one of the most commonly used approaches. It is a bottom-up region-growing technique starting with one-pixel objects. In many subsequent steps smaller image objects are merged into

larger ones. The growing decision is based on local homogeneity criteria describing the similarity of adjacent image objects in terms of size, distance, texture, spectral similarity and form. The scale at which this segmentation is done can and has to be chosen in relation to the characteristics of the data set and the objective of the work. The aim of the segmentation is to delineate the meaningful regions which represent the objects that will be classified. For this reason it is mandatory for the quality of the further classification step that the borders of the water bodies (permanent or not) are clearly highlighted.

The segmentation module of the process developed here is a rule set for automated analysis which basically combines cycles of MRS and classification and is assisted by other more simple segmentations not based on the image content (chessboard segmentation). To allow the processing of large data sets the rule set included the tiling, parallel processing and final stitching of the region. In order to accelerate the segmentation, which is the most time consuming process of the overall flood mapping processing chain, only regions potentially containing water are automatically selected and segmented. Thus, the amount of segments (objects) and the respective processing time is drastically reduced. The result is an automated and target-centred segmentation "image" in which the information of both dates, pre and post event is taken into account. The process can be batched to analyse as many images as necessary.

The activation of the automated segmentation step is initiated with an automated revision of the project parameters for the number of layers and the calculation of scene statistics (mean, standard deviation and extreme pixel values). Then – after tiling the image – the parallel processing begins for each tile with a chessboard segmentation. By this means the whole tile is segmented into squares of 60×60 pixels. Based on the scene statistics previously calculated and on empirical analysis of a large collection of SAR data, different threshold values are identified for units not containing water. Those values will be included as previous condition for the segmentation. If the square object in question is within this threshold or in contact to an object which is in it, it will be segmented.

The segmentation of the units containing water is then made using the MRS algorithm. Considering objects not as a static unit, but as a dynamic concept in which objects grow, shrink, and become re-segmented and smoothed etc., there exists a wide range of scale parameters which could fit the segmentation purposes here. Hence, an ideal parameter set for a perfect segmentation can never be selected.

Pragmatically, the necessary parameter adjustments depend on the size, shape and backscatter of the expected objects and the speci-

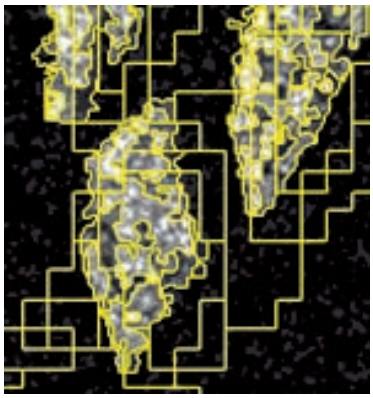

Fig. 2: MRS result using Landsat 7 and TerraSAR-X data – Overlaid on **TerraSAR-X** post-event scene.

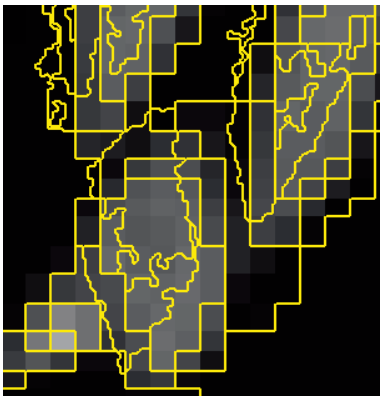

Fig. 3: MRS result using Landsat 7 and TerraSAR-X data – Overlaid on **Landsat 7** pre-event scene.

fied Minimum Mapping Unit (MMU). In this study – depending on the availability of one or two scenes as input data – a mono-temporal segmentation or a bi-temporal segmentation, respectively, has been automatically performed. Both processes will produce only one segmentation layer, but for the bi-temporal segmentation a segmentation of the pre-event dataset is produced inside the segments of the post-event data set. Finally, all tiles are stitched together. A re-segmentation of the tile borders is then conducted to harmonize the segments in the whole scene and to avoid false objects created by the tiles' borders.

Figs. 2 and 3 display an example of the segments obtained using a combination of TerraSAR-X and Landsat data for the Mississippi scenario. The same segments are displayed once over the TerraSAR-X post-event scene and once over the Landsat 7 scene. As it can be seen the automated segmentation process uses information of both scenes. When comparing these segmentation results to those obtained using only TerraSAR-X data the object shapes differ between the two scenarios due to the different resolution of the two pre-event layers (3 m, TerraSAR-X image vs. 30 m [resampled to 3 m], Landsat 7 image) and the different nature of radar and optical imaging techniques. Specifically, the speckle of the SAR data strongly influences the object shapes and sizes.

5 Semi-automated Extraction of Water Mask (Classification)

Unlike pixel-based techniques which only use the pixel values, the object-based techniques can also use texture, shape and context information of a scene. The optimal features, i. e., measurable properties of the segments, for water detection are identified and constitute the basis for the "water" / "non water" classification of the pre-event and post-event scenes.

The similar spatial behaviour of water in SAR images and in the NIR channel of optical data is used here as common ground for a flood mapping workflow considering not only TerraSAR-X data, but also optical archive data: In optical images, water absorbs most of the incident radiation and therefore appears dark in colour-infrared images. The characteristic spectral reflectance curve shows a reduction of intensity with increasing wavelength. In the near infrared the reflectance of deep, clear water is virtually zero, for this reason the channel 4 of Landsat 7 is used for the discrimination of water / non-water; in case of SAR X-band, under low to moderate wind conditions, backscatter from water surfaces is low. Thus, a water body appears dark compared to the backscatter of other land cover features; based on this water surface behaviour, a rule-based classification system with tuneable variables and a user-friendly interface is constructed for the effective extraction of the water extent.

The first classification step is based on an object-based thresholding of the intensity values, controlled by texture, shape and context features. A tool supports the operator allowing him to manipulate the different features so that the water mask extent can be changed online. However, the resulting water cover is not always perfect, as can be seen in Fig. 4, which shows the permanent water body extracted using channel 4 of the Landsat scene (a) and the TerraSAR-X scene (b), respectively. Main discrepancies in these two water masks result from the diverse image resolutions and from the different acquisition dates. It can be noticed that in the two cases areas affected by shadows are classified as water since they present a low reflectivity. These errors that appear in more in the Landsat classification are corrected with further widgets that can be optionally used. Two types of corrections or interactive refinements are implemented with those widgets. The first one is an objects-based reclassification of the "water" segments, based on the previously defined water class. The second one is the pixel-based thresholding of the water borders and neighbouring objects. As in some occasions a certain water course is interrupted because few water pixels dropped in a mainly non-water polygon. Subsequent to the pixel-based correction the water course will be connected again.

For the post-event data the semi-automated extraction of the water mask is based on the same methodology. The obtained results are shown again in Fig. 4 for the Mississippi River case (c and d). The water masks look similar

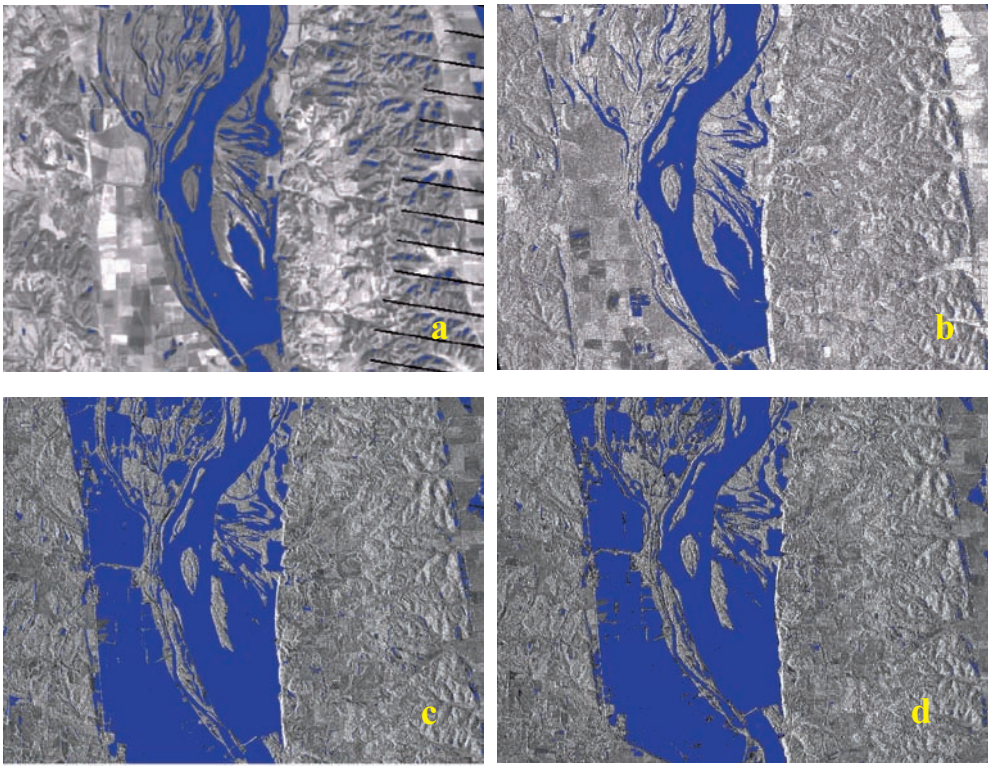

Fig. 4: a) Landsat 7-based *pre-event* water mask b) TerraSAR-X-based *pre-event* water mask c) TerraSAR-X-based *post-event* water mask d) Permanent water / flood mask derived from the combination of Landsat 7 and TerraSAR-X data.

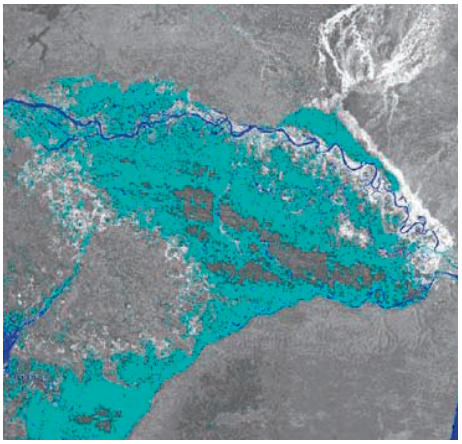

Fig. 5: Intermediate step – result of the semi-automated classification (blue: permanent water body, cyan: flooded area).

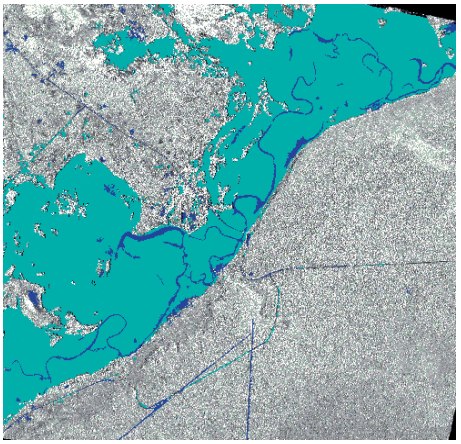

Fig. 6: Intermediate step – result of the semi-automated classification (colours: see left).

despite the fact that two different layers were used as pre-event data for the original segmentation. It is worth mentioning that the selection of the pre-event layer had a direct impact on the shape and size of the objects and on the specific value needed for the features to be selected within the classification process.

The need for refinements of the water masks typically depends on the relief and on the environmental conditions. For example, wind has a particular influence on SAR-based classification results as higher wind speeds could result in larger errors. In the Caprivi scenario, the strong winds affecting the ScanSAR scene prevented the detection of the whole mass of water (Fig. 5). In comparison, the SpotLight scene (Fig. 6), recorded at a different date and with a shallower angle shows a very clear distinction of water and therefore needs nearly no refinement steps. Worth mentioning are also the double-bounce effect that can be observed to the sides of the rivers (Fig. 5).

6 Automated Refinements

The final step in the flood mask production is the generation of two water masks in order to separate the flooded areas from the permanent water bodies such as rivers, lakes and ponds.

The automated refinement step consists in the improvement of the classifications made on the pre-event and post-event scenes. It includes the automated extraction of the flood and permanent water masks as well as the application of final refinements such as smoothing and minimum mapping filters. A final MMU is also defined depending on the quantity of detail desired in the final water mask and the precision of the final map, respectively. Finally, the borders of the polygons are smoothed using growing and shrinking pixel based algorithms.

The results obtained for the Australia case are very satisfying. Fig. 7 shows a detail of the area considered for the analysis. A reference map (Fig. 8) was manually delineated for part

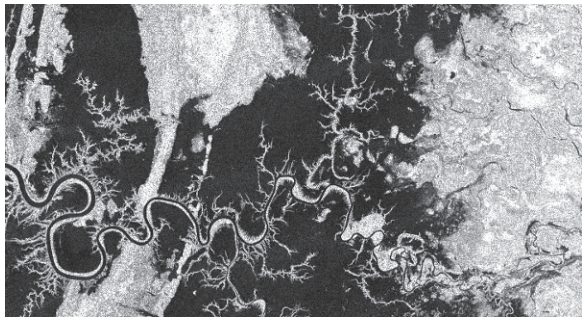

Fig. 7: Detail of ScanSAR post-event scene over the Gulf Country affected area. Low backscattering of the radar signal (dark) indicates permanent water and flooded areas, respectively.

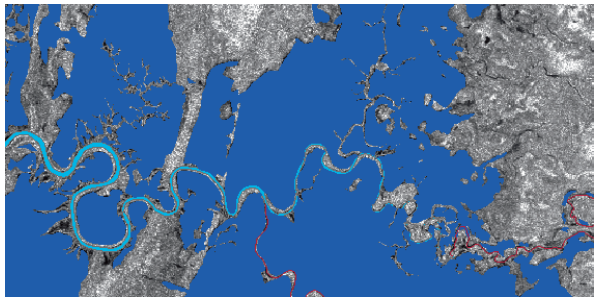

Fig. 8: Manually delineated water extent map (reference), Gulf Country (cyan: permanent water body, blue: flooded area), superimposed on ScanSAR post-event scene (colours in the background due to display).

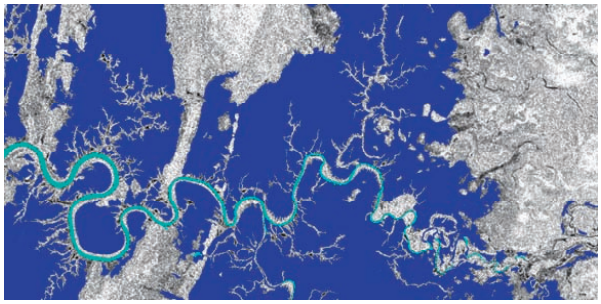

Fig. 9: Final flood mask product from the semi-automated procedure, Gulf Country (colours and background as above).

of the ScanSAR image. This map allowed a preliminary qualitative evaluation of the results (Fig.9) of the developed flood mapping processing chain. Further qualitative and quantitative evaluations are currently under way.

It is worth mentioning that the manual delineation required more time for a third of the total scene than time needed by the semi-automated process for the whole scene. This means that even if no further process was implemented for the correction of the shadows in flood plain areas, it could be assumed that deselecting areas of shadows by manual editing tools might be still more time-effective than visual interpretation.

7 Conclusion and Outlook

This paper gives an overview of the development and implementation of a TerraSAR-X based semi-automated workflow for flood extent mapping performed in the framework of the DeSecure project.

For this purpose we combined a series of existing techniques for pixel- and object-based analysis to produce a user friendly tool for flood mapping. The developed semi-automated workflow was tested in a variety of scenarios and a preliminary validation of the results has been made confronting them with flood extent maps generated manually by visual interpretation. Finally, the workflow was implemented into a pre-operational test using two different TerraSAR-X products: A bi-temporal ScanSAR data set and a bi-temporal SpotLight data set.

Altogether, TerraSAR data demonstrated its high capacity for the mapping of flood events. Furthermore, the high resolution, the multi-polarization and multi-incidence angle capability of TerraSAR-X, its quick site access and receiving times open very interesting perspectives for flood mapping and the assessment of damages after a natural disaster. Concerning an automation of mapping processes, the degree to which it can be applied is directly related to the quality of the received SAR signal in the available TerraSAR-X images for the respective flood events. Strong wind or rain and some landscape conditions might lead to certain noise or other effects which produce an atypical backscatter signal of water. This effect is intensified by a shallow incidence angle of the acquired scene. As near-real time conditions for flood mapping are also addressed, it is not possible to change the environmental condition if they are not favourable. However, the image acquisition capabilities (e. g., combining descending and ascending orbits) and the quick tasking of the satellite can provide within relatively short time more images to counteract such disturbances.

Nevertheless, object-based methods – which allow the use of context information – and the stepwise approach with its different levels of automation and possibility for parameter tuning showed to be rather adjustable to these circumstances.

The ScanSAR post event scene for the Namibia scenario was a good example of unfavourable conditions: On the one hand low incidence angle and wind, on the other hand water covered areas under vegetation provoking double-bounce effects changing the typi-

cal low backscattering characteristic of water. As a consequence for the mapping the ScanSAR-based map required more post-processing than the SpotLight-based one, which only required minor corrections.

In terms of workflow the main findings and framework conditions to be put here can be summarised as follows:

Large images were successfully processed ($30 \times 50\,km^2$ [StripMap], $100 \times 150\,km^2$ [ScanSAR]) and the TerraSAR-X RE products could be used without previous pre-processing or need of speckle filtering:

The adaptability and flexibility of the workflow was demonstrated applying it to satellite scenes representing different environmental conditions. Concerning the mapping chain's robustness it has been tested using different TerraSAR-X imaging modes and, as in case of the Mississippi River flooding, different sensors (TerraSAR-X data [3 m res], Landsat 7 ETM+ [30 m res]). Nevertheless, to draw conclusions about the rule set's performance using optical data, further tests are required. Regarding the result's uncertainties caused by strong winds and / or rain during image acquisition, additional manual editing may be required while in some special cases the meteorological conditions may not allow the application of the rule set in all. However, in order to minimise wind and rain effects in the satellite image, the incidence angle of the TerraSAR-X data acquisition should be as shallow as possible. As to the homogeneity level of the segments this can be adjusted by the operator, reflecting the system's adaptation possibilities, especially when the environmental conditions during image acquisition are not favourable (inundations in densely wooded areas are unfavourable but have not yet been analysed). Under favourable conditions though, the manual editing is minimised but cannot be eliminated completely.

The enhancements of the semi-automated system as presented here towards a multi-mission suited system, has several advantages for a NRT damage assessment: Highly accurate flood extents could be delineated even if no TerraSAR-X pre-event data are available. And, the revisit time over the affected region is increased by the use of multi source remote sensing data which is an important factor when processes such as rising or declining water levels should be monitored. Nevertheless, one should not forget the additional effort required for co-registration when working with different sensors.

Regarding the validation of the flood mapping for the Australian Gulf Country test site it has been noticed that, first of all, the processing of the whole scene with the developed procedure required approximately less than 5 % of the working time than the manual delineation of the flood extent. Secondly, the flood delineation results of either method were identical. Finally, this comparison has also demonstrated the effectiveness of the workflow: The mask generated with the semi-automated process shows a level of detail that an interpreter by means of digitising is not able to reach in reasonable time. Concerning further qualitative and quantitative evaluations of the results the analysis has only recently been initiated and could not be completed within the term of the DeSecure project. Nor was it possible to perform any field work or to collect field data and / or additional reference data.

Using SpotLight scenes showed to be the ideal condition for an automated mapping of a flood event. It was concluded that within one to two hours after image availability at the operator it is possible to produce a rapid flood extent map (best case scenario for two TerraSAR-X SpotLight acquisitions or subsets in case of larger TerraSAR-X data sets). From this point in time, additional time needs to be considered depending on the need of preprocessing non TerraSAR-X data, the number of pixels to processed, the level of detail required, the level of accuracy and smoothness required for the delineation of the boundary between "water" and "no water" and the level of uncertainty given by the environmental conditions during image acquisitions.

References

Ager, T.P. & Bresnahan, P.C., 2009: Geometric precision in space radar imaging: Results from TerraSAR-X – ASPRS Annual Conference: on CD.

Andreoli, R. & Yesou, H., 2007: Change detection analysis dedicated to flood monitoring using Envisat wide swath mode data. – Envisat symposium: on CD.

Baatz, M. & Schäpe, A., 1999: Multiresolution segmentation – an optimization approach for high quality multiscale image segmentation. – Angewandte Geographische Informationsverarbeitung.

Boni, G., Castelli, F., Ferraris, L., Pierdicca, N., Serpico, S. & Siccardi, F., 2007: High resolution COSMO/SkyMed SAR data analysis for civil protection from flooding events. – IGARSS: on CD.

Brakenridge, G.R., Anderson, E., Nghiem, S.V., Caquard, S. & Shabaneh, T., 2003: Flood warnings, flood disaster assessments, and flood hazard reduction: the roles of orbital remote sensing. – 30th International Symposium on Remote Sensing of the Environment: on CD.

Chen, Q. & Luo, J., 2003: A geostatistic based segmentation approach for remotely sensed images. – www.definiens.de.

CRED (Centre for Research on the Epidemiology), 2009: Disasters in numbers. – New release. www.unisdr.org/preventionweb/files/12470_2009disasterfigures.pdf (15th June 2010).

DeSecure, 2010: DeSecure project homepage. – www.desecure.info/intro_de.html (15th June 2010).

Gebhardt, S., Künzer, C., Wehrmann, T., Gstaiger, V., Huth, J., Schettler, H. & Schmidt, M., 2008: The WISDOM Project – A water-related Information System for the Mekong Delta, Vietnam: first results of remote sensing. – World water congress: on CD.

Fritz, T. & Eineder, M. (Eds.), 2009: TerraSAR-X Ground Segment, Basic Product Specification Document, Issue **1.6**.

Hahmann, T., Roth, A., Martinis S., Twele, A. & Gruber, A., 2008: Automatic extraction of water bodies from TerraSAR-X data. – IGARSS 2008: 103–106.

Haralick, R. & Shapiro, L., 1985: Image segmentation techniques. – Computer Vision, Graphics, and Image Processing **29:** 100–132.

Henderson, F.M. & Lewis, A.J. (Eds.), 1998: Principles and applications of imaging radar. – Manual of Remote Sensing **2**, John Wiley & Sons, Inc..

Henry, J., Chastanet, P., Fellah, K. & Desnos, Y., 2006: Envisat multipolarized ASAR data for flood mapping. – International Journal of Remote Sensing **27** (10): 1921–1929.

Horritt, M.S., Mason, D.C. & Luckman, A.J., 2001: Flood boundary delineation from Synthetic Aperture Radar imagery using statistical active contour model. – International Journal of Remote Sensing **22** (13): 2489–2507.

Huang, B., Li, H. & Huang, X., 2005: A level set method for oil slick segmentation in SAR images. – International Journal of Remote Sensing **26** (6): 1145–1156.

Huang, M., Gong, J., Shi, Z. & Zhang, L., 2009: River bed identification for check-dam engineering using SPOT-5 image in the HongShiMao watershed of the Loess Plateu, China. – International Journal of Remote Sensing **30** (8): 1853–1865.

Irimescu, A., Craciunescu, V., Stancalie, G. & Nertan, A., 2010: Remote sensing and GIS techniques for flood monitoring and damage assessment. – Study case in Romania, BALWOIDS 2010, Ohrid, Republic of Macedonia: on CD.

Ji, L., Zhang, L. & Wylie, B., 2009: Analysis of dynamic thresholds for the Normalized Difference Water Index. – Photogrammetric Engineering and Remote Sensing **75** (11): 1307–1317.

Kettig, R.L. & Landgrebe, D.A., 1976: Classification of Multispectral Image Data by Extraction and Classification of Homogeneous Objects. – IEEE Transactions on Geoscience Electronics **14** (1): 19–26.

Kussul, N., Shelestov, A. & Skakun, S., 2008: Grid system for flood extraction from satellite images. – Earth Science Informatics **1:** 105–117.

Martinis, S., Twele, A. & Voigt, S., 2009: Towards operational near real-time flood detection using a split-based automatic thresholding procedure on high resolution TerraSAR-X data. – Natural Hazards and Earth System Science **9:** 303–314.

Mason, D.C., Speck, R., Devereux, B., Schumann, G.J.P., Neal, G.C. & Bates, P., 2010: Flood detection in urban areas using TerraSAR-X. – IEEE Transactions on Geoscience and Remote Sensing **48** (2): 882–894.

Meinel, G. & Neubert, M., 2004: A Comparison of segmentation programs for high resolution remote sensing data. – XXth ISPRS Congress: on CD.

Neubert, M., Herold, H. & Meinel, G., 2008: Assessment of remote sensing image segmentation quality. – GEOBIA: on CD.

Okamoto, K., Yamakawa, S. & Kawashiwa, H., 1998: Estimation of flood damage to rice production in North Korea in 1995. – International Journal of Remote Sensing **19:** 365–271.

Pierdicca, N., Chini, M., Pulvirenti, L. & Macina, F., 2008: Integrating physical and topographic information into a fuzzy scheme to map flooded area by SAR. – Sensors **8:** 4151–4164.

Ramesh, A., Glade, T., Kappes, M. & Malet, J.P., 2010: Delineation of Flood inundated areas using aereal photpinterpretation and GIS-based hydrological modelling – an application in Barcelonnette, France. – Geophysical Research Abstracts **12**, EGU General Assembly 2010: on CD.

Schiewe, J., Tufte, G.L. & Ehlers, M., 2001: Potential and problems of multi-scale segmentation methods in remote sensing. – GIS – Geographische Informationssysteme **6:** 34–39.

Schiewe, J., 2002: Segmentation of High-Resolution Remotely Sensed Data – Concepts, Applications and Problems. – International Archives of Photogrammetry Remote Sensing and Spatial Information Sciences **34** (4): 380–385.

Schumann, G., Bates, P.D., Horritt, M.S. & Matgen, P., 2009: Progress in integration of remote sensing-derived flood extent and stage data and hydraulic models. – Reviews of Geophysics **47**, RG4001.

Schumann, G., Matgen, P., Pappenberger, F., Black, A., Cutler, M., Hoffmann, L. & Pfister, L., 2006: The REFIX model: Remote Sensing based flood modelling". – International Archives of Photogrammetry, Remote Sensing and Spatial Information Sciences **36** (7): on CD.

Silveira, M. & Heleno, S., 2009: Separation between Water and Land using Region Based Level Sets. – IEEE Geoscience and Remote Sensing Letters **6** (3): 471–475.

Townsend, P.A., 2001: Mapping seasonal flooding in forested wetlands using multi-temporal radarsat SAR. – Photogrammetric Engineering and Remote Sensing **67** (7): 857–864.

UNU, 2010: United Nations University. – www.unu.edu/ (15th June 2010).

UN-SPIDER, 2010: United Nations Platform for Space-based Information for Disaster Management and Emergency Response. – www.un-spider.org/disaster/3665/2010-07-22/pakistan/flood-pakistan (6th September 2010).

Waisurasingha, C., Aniya, M., Hirano, A. & Sommut, W., 2008: Use of RADARSAT-1 data and digital elevation model to access flood damage and improve rice production in the lower part of the Chi River Basin, Thailand. – International Journal of Remote Sensing **29** (19–20): 5837–5850.

Zwenzner, H. & Voigt, S., 2009: Improved estimation of flood parameters by combining space based SAR data with very high resolution digital elevation data. – Hydrology and Earth System Sciences **13:** 567–576.

Addresses of the Authors:

Virginia Herrera Cruz & Dr. Marc Müller, Infoterra GmbH, D-88039 Friedrichshafen, Tel.: +49-7545-8-3382, -8439, e-mail: virginia.herrera@infoterra-global.com, marc.mueller@infoterra-global.com

Christian Weise, Definiens AG, D-80339 München, Trappentreustrasse 1, Tel.: +49-89-231180-0, e-mail: cweise@definiens.com

Manuskript eingereicht: Juni 2010
Angenommen: September 2010

PFG 2010 / 6, 489–497
Stuttgart, Dezember 2010

Article

Applying Advanced Techniques to the Dissemination of Satellite Based Crisis Information

T. Andresen, & F. Stracke, Oberpfaffenhofen

Keywords: Satellite based crisis information, DeSecure, interactive 3D environments, web mapping

Summary: Two approaches for the dissemination of satellite based crisis information have been developed within the DeSecure project: dissemination in 2D web clients and interactive 3D near real time scenarios. Compared to printed maps, the advantages of these new approaches are the possibility of interactive exploration as well as near-real-time updates of the information provided. This paper analyzes the potential users, their requirements, the mission scenarios, and describes the solutions developed.

Zusammenfassung: *Neue Ansätze für die Verbreitung satellitenbasierter Kriseninformation*. Im Projekt DeSecure wurden zwei neue Ansätze für die Verbreitung satellitenbasierter Kriseninformation entwickelt: Die Verbreitung unter Nutzung von interaktiven 2D Kartenanwendungen sowie über Nah-Echtzeit 3D Szenarien. Diese neuen Ansätze haben gegenüber der bereits etablierten Veröffentlichung über gedruckte Karten einige deutliche Vorteile. So kann u. a. die Information einerseits interaktiv exploriert werden und andererseits besteht die Möglichkeit der Aktualisierung in Nah-Echtzeit. In diesem Artikel werden die potentiellen Nutzer und deren Anforderungen sowie entsprechende Einsatzszenarien analysiert und die entwickelten Lösungen beschrieben.

1 Introduction

Today, the dissemination of satellite based crisis information using printed maps is well established by most of the leading organizations involved in emergency mapping (e. g., Centre for Satellite Based Crisis Information (ZKI), SERTIT, MapAction). DeSecure is a joint research project with the objective of improving satellite based crisis information (SBCI) workflows. The entire production cycle of e. g., data access, information extraction and dissemination was analysed during the project duration from 2007–2010.

This paper describes two approaches for disseminating crisis information to the user. The first approach addresses the application of recent web mapping technologies to satellite based crisis information (SBCI) to ensure that continuously updated data are delivered to the user. In the second one, modern interactive 3D visualization software is applied for communicating information during a crisis. Combining the advantages of web mapping technologies with the intuitive understanding of 3D virtual worlds, the focus of our research was on developing a concept for implementing earth observation and GIS data in virtual environments and improving the user interfaces to allow for fast and easy information access.

Since 2003, the ZKI of the German Aerospace Center (DLR), the leading German provider of satellite based crisis information (SBCI), has delivered such SBCI maps to customers engaged in emergency response and/or relief activities. These maps provide detailed and highly valuable information. A printed map has specific advantages. The information they contain is distinctly arranged and focuses on a specific topic. Printed maps allow orientation as well as measurement. They are high-

© 2010 E. Schweizerbart'sche Verlagsbuchhandlung, Stuttgart, Germany
www.schweizerbart.de
DOI: 10.1127/1432-8364/2010/0070
1432-8364/10/0070 $ 2.25

ly suitable for in-field operations, primarily in environments where electronic infrastructure is not available or damaged. Furthermore, a map is a well-known medium familiar to most people. In contrast to these advantages, printed maps have major disadvantages, particularly in the context of the dissemination of satellite based crisis information: Maps are outdated at the time of printing. This lack of timeliness comes along with limited updating options. An update means the creation of a new map, a new print-out and physical delivery to the user. Moreover, a map is static and thus does not support user-driven generation of new information through the interactive exploration, analysis and synthesis of information provided in an interactive environment (MacEachren & Kraak 1997). Furthermore, a user always needs to decode a map for example; the existence of contour lines in a map does not necessarily mean that every user is able to generate the correct idea of the topography of a certain site. Thus, creating a mental map of a certain region by decoding a topographic map might be difficult, because the user needs to first learn/acquire these skills, which would not be necessary using a virtual 3D environment (cf. Häberling 2006). The development and rendering of complex 3D visualizations are normally very time consuming. Recent developments in the real-time 3D sector, e. g., using game engines for visualizations will in the near future allow utilization even in time-critical environments (Fritsch & Kada 2004). In DeSecure Tüngerthal (2009) demonstrated the visualization of a fictive crisis scenario using the CryEngine. Within DeSecure such advanced techniques were applied to disseminate SBCI.

2 Potential User and Mission Scenarios

Maps containing SBCI are mostly used to disseminate information to relief organizations, operational centers, on-site crisis teams and the public. Therefore, potential users of interactive 2D and 3D crisis maps are organizations dealing with crisis situation, the public and the media. These users need precise, up-to-date and easy-to-understand information at hand. Web mapping services and interactive 3D environments deliver permanently updated data to the user in near-real-time, and they offer the possibility to interactively exploit this data to create new information.

Due to the anticipated lack of infrastructure in a crisis region the focus of this work is mostly on supporting teams in operational centers. Some of the possible applications scenarios are

- pre-disaster mission briefing,
- real-time team/crisis management
- common operational picture (COP)
- post-disaster analysis
- training of crisis response teams

During a crisis event such new visualization techniques will help to coordinate different relief organizations and to communicate with on-site teams. Decision making will be supported even in very stressful environments. Interactive 3D real-time scenarios can help to obtain a common operational picture of all the organizations and persons involved, which in turn facilitates crisis operations and the coordination of on-site teams.

3 New Approaches for the Dissemination of Satellite Based Civil Crisis Information

3.1 *Web Mapping Component*

Dissemination of spatial information through interactive web clients is well established (Mitchell et al. 2008), except for the dissemination of SBCI. What are the requirements for this task?

An analysis of SBCI user requirements (DeSecure Consortium 2009) reveals the need for tools that enable the exploration of the information provided (e. g., zoom in/out, pan, layer switch on/off, identify, print). Most of today's web mapping clients (e. g., OpenLayers, Mapbender or ESRI's Sample Flex Viewer) already provide these functions by default. The challenge in providing SBCI through interactive web clients is the configuration of the client and the underlying services in a reliable, fast and easy way. A common development

scenario for a web mapping component, e. g., in the public sector, needs from several days to weeks before a client is made available online. However, a web mapping client for the dissemination of SBCI has to be published within a very short time frame. From the user's point of view, a reference product based on pre-disaster satellite imagery has to be delivered within the first eight hours, and a damage assessment product within 36 hours after the outbreak of the event. (DeSecure Consortium 2009). Due to the general limitations of satellite imagery acquisition (satellite commanding, orbit specifications, weather conditions), these user requirements can often not be met. The ZKI aims to deliver crisis products within eight hours after acquisition of the specific satellite imagery has been completed. In this context knowing the requirements of the specific producers of SBCI is of major importance for building an adequate solution for very fast dissemination of web mapping clients. Analysis of the technical and human resources framework at ZKI (DeSecure Consortium 2010) shows that there is a need for quick and easy web service compilation, smooth performance of the services, and user-specific configuration of web mapping clients using a content management system (DRUPAL).

This analysis leads to a solution mainly based on ESRI technology. In addition, the CMS DRUPAL has been customized. An adapted version of the ESRI Sample Flex Viewer was chosen as web client (see Fig. 1), due to the easy configuration via XML, the functionality, and a widget concept which enables easy and modular customizing and satisfies ergonomic aspects. Furthermore, the CMS DRUPAL was augmented by two user interfaces supporting the process of client configuration (registration of services and configuration of the client). This technical framework enables the dissemination of SBCI via web clients at ZKI in a fast and easy way, as follows (see Fig. 2).

In the first step a copy of the map documents (mxd) from the map production process is configured for the specific service. All settings that are made in the map document are handed over to the service. This includes, e. g., deleting redundant content, setting maximum or minimum extent, as well as adapting symbology, if needed. A structured approach in the creation of the origin map document in the map production process minimizes the effort of this service-specific configuration.

The configured map documents are then published as a web service. Using ArcGIS Server the needed data could be published as services within a few clicks supporting several interfaces (e. g., REST, SOAP, WMS, WFS, WCS, KML). Good performance of the ArcGIS Server services is guaranteed by following the ESRI recommendations for capacity planning (see, e. g., Peters 2007). The URLs to the REST, and if needed to other interfaces of the published services, are registered in the Content Management System (DRUPAL). When service registration is completed, a client could be configured in about three minutes using the implemented client configuration user interface. The CMS also supports the

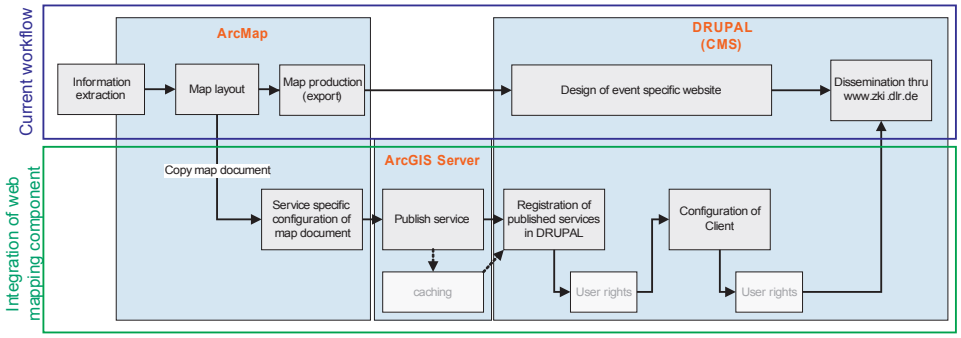

Fig. 1: Workflow of the solution for a web mapping client compilation at ZKI.

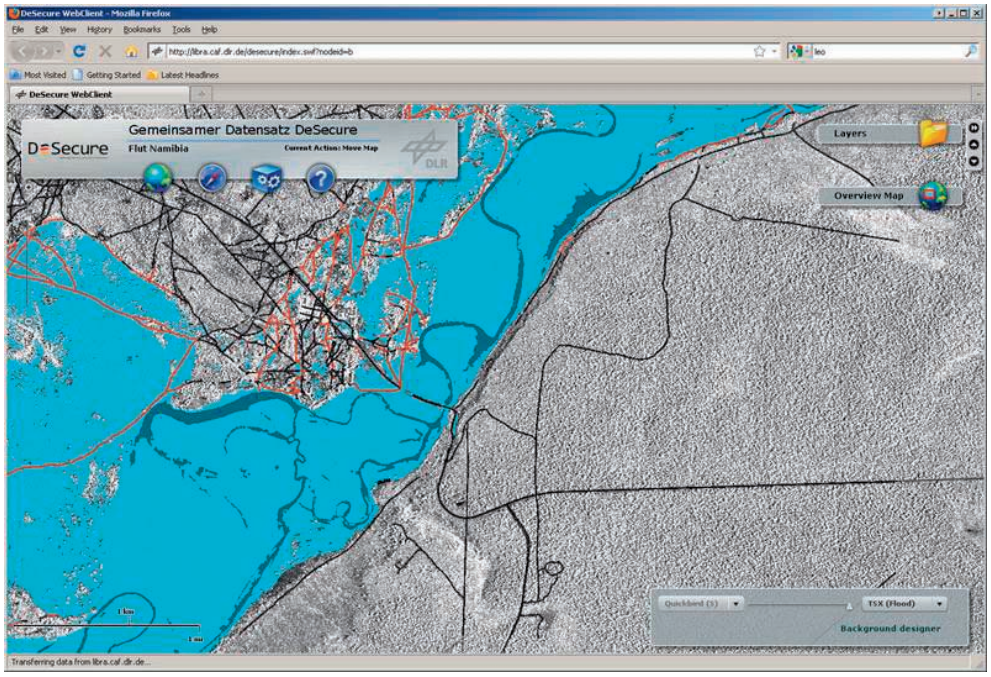

Fig. 2: Screenshot of a ZKI Web Client for the Namibia flood, Caprivi region 2010 (an adapted version of the ESRI Sample Flex Viewer).

definition of access rights for services and client configurations. Thus, after login a user is able to access services and clients via the CMS (ZKI home page), where appropriate access rights have been granted. When a client is activated by a user, a configuration XML is dynamically generated in the background according to the configuration settings and passed over to the Flex client. Updating the client (e. g., adding new services, functions) can also be performed with a few clicks using the implemented configuration interface.

3.2 *Interactive 3D Real-time Scenarios*

3D real-time virtual environments come closer to how we normally see the real world (cf. Slocum et al. 2000) and thus enable even the non-expert (regarding geo-science, cartography, etc.) to navigate easily. Many decisions of stakeholders are based on spatial information (cf. O'Connor 2007). Interactive visualizations in virtual geographic environments (VGE) help people to navigate and understand the information inherent in spatial data sets (cf. O'Coill & Doughty 2004).

Decision making in a distributed team is easier if all work at the same knowledge level, with the same understanding, and roughly the same view of the affected area. According to Lin & Zhu (2006, p. 228) the accessibility of a virtual environment and the ability to share multi-user environments which enable geo-collaboration are key features of virtual geographic environments. Permanently updated geo- and 3D-information assures that the most recent information is available for decision making as soon as possible.

The application of virtual geographic environments or 3D GIS in the civilian crisis management sector is under development, and still not common in operational use in situation rooms. Tiede & Lang (2010) show the value of analytical 3D views also in the context of a simulated crisis exercise. The French joint emergency management operational center (COGIC) uses a 3D visualization system for emergency mapping (see COGIC 2010).

Many of the related initiatives of the European Union like ORCHESTRA (an open service architecture for risk management) and OASIS (open advanced system for disaster and emergency management) are still restricted to 2D (Zlatanova 2008). However, Zlatanova (2008) states that large amounts of 3D data are increasingly available, that disaster management users are prepared to use this data, and that 3D is considered important by the user. The main goal is to support and facilitate the process of decision making.

For a first overall test DLR used the Leica Virtual Explorer to show some basic applications during two real-time exercises in 2006 and 2007 (GNEX'06 and GNEX'07) within the GMOSS (Global Monitoring for Security and Stability) network of excellence (Voigt et al. 2009). Within DeSecure DLR collected user requirements in face-to-face interviews with THW (the German Federal Agency for Technical Relief) staff and at an International Search and Rescue Advisory Group (INSARAG) training session. The interviews revealed that 3D information is needed and already used (e. g., Google Earth) from time to time by crisis teams. Such systems could help in the planning and acquisition phases. But the users also stated that too realistic information could lead to misinterpretation because the user might accept the presented virtual information as true without questioning the reliability of the underlying data (Tüngerthal 2006). The collected user requirements were integrated into a requirements catalogue. Based on the experience gained, a market analysis was conducted and Skyline TerraExplorer was selected as the most appropriate commercial software product at that time. Advantages of the Skyline software are very high 3D performance based on a former game engine, collaboration services, streaming server availability, connectors/importers for various GIS, and the availability of remote sensing data.

Skyline TerraExplorer (see Fig. 3) was used in a client-server installation and tested during several selected crisis scenarios. Firstly, a virtual environment of the Pakistan earthquake in 2005 was created to test the potential of the software. One goal of 3D virtual environments is to guide potential users as well as possible and to avoid their getting lost in a too complicated virtual environment and missing important information (cf. Meng 2003). The built-in user interface of Skyline TerraExplorer could become quite confusing and the user has either to search the data sets in a tree structure or follow a strict guideline on how to structure the various data sets. This is not appropriate for emergency situations. Therefore, several additional tools were developed to facilitate the handling of Skyline TerraExplorer to give even the non-expert an easy-to-use virtual environment which according to Tufte (2007) gives to the observer the greatest number of ideas in the shortest time. In order to guide the user through the virtual environment, two extensions were created, a "visibility manager" for a clear overview of information layers and a "location manager" for fast and easy navigation to selected places. In addition, a connec-

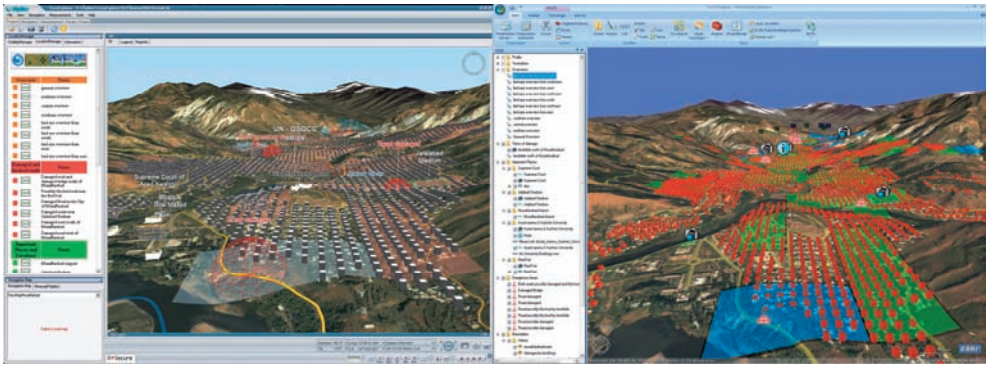

Fig. 3: Virtual Environment of the Pakistan 2005 earthquake. Left: Skyline TerraExplorer; Right: ArcGIS Explorer.

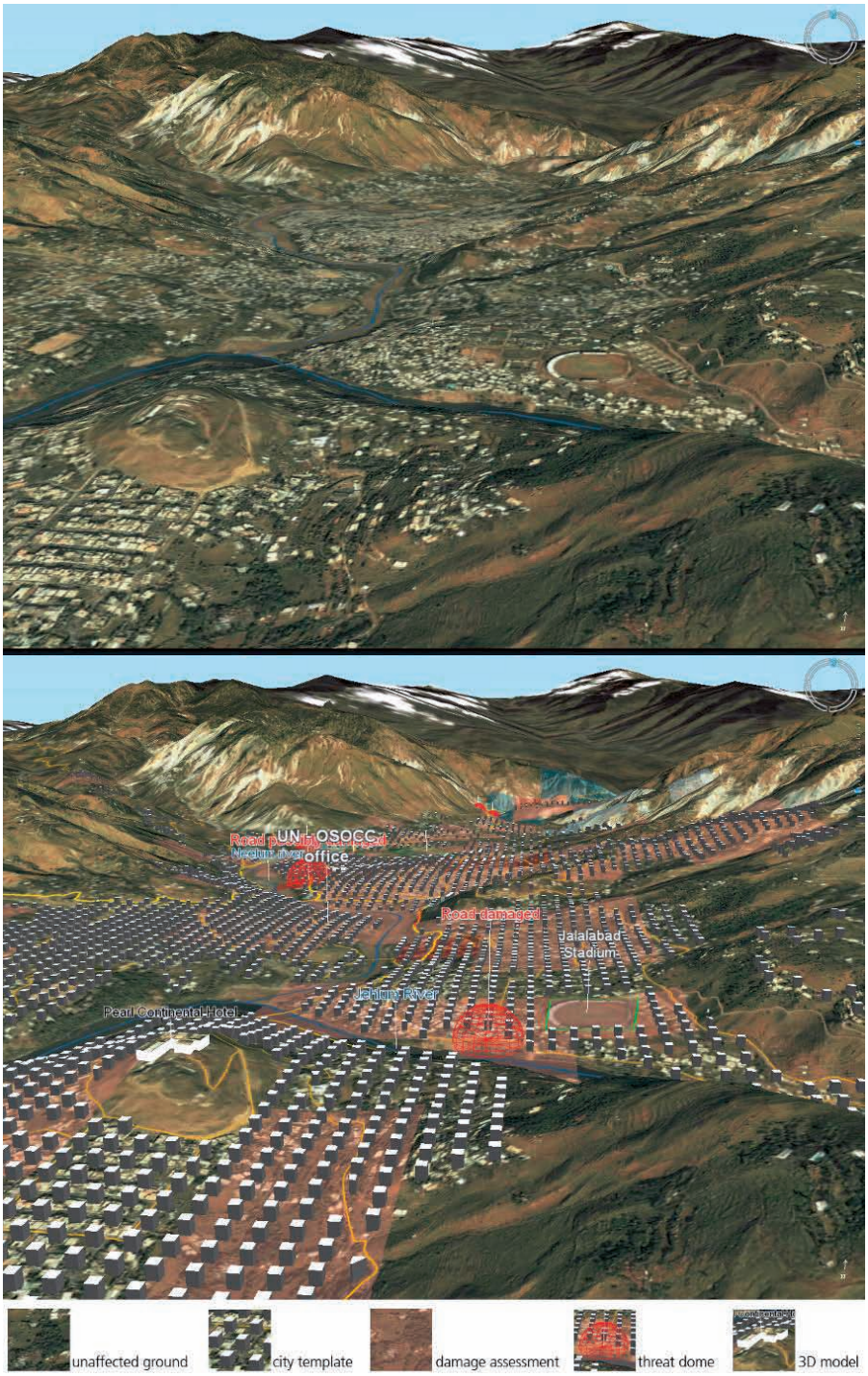

Fig. 4: Development of the virtual Pakistan 2005 scenario according to the phases of the process concept. *Upper image*: Phase 2 – basic scenario with satellite data only; *lower image*: Phase 4 – construction of 3D objects such as threat domes and text labels.

tor to Google Maps was created to allow the exploitation of other sources. Based on user requirements a static map legend using the existing ZKI layout was also added (cf. Woditsch 2010).

Based on the experience described above, a concept for a process chain to create interactive 3D virtual environments was generated using the Pakistan 2005 scenario. This concept was tested during a second DeSecure crisis scenario, the Okavango flooding in 2009, and in a third real-time crisis exercise during the Assessment Mission Course 2009 in Cyprus (LIMES project, cf. Gstaiger et al. 2009) The process chain was modified as necessary and a timeline was derived during those scenarios.

The concept consists of four steps (see Fig. 4):

1. 3D oriented geo- data pre-processing
   Availability: recurring during all following steps
2. Basic scenario – e. g., only basic geo-information for a first orientation
   Availability: within 2–3 hours online or on DVD ready for the on-site teams before deployment
3. Crisis scenario – containing the basic scenario, additional vector data, on-site data, 3D objects
   Availability: within 3–7 hours online or on DVD
4. Update – permanent update of geo-data, adding new data sets, e. g., results from other geo-processing/classifications
   Availability: > 7 hours online

All tests during the exercises showed that the basic VGE could be created during the given time frame in phase 2, provided that earth observation data sets are available. Also, the crisis scenario with updated information, additional 3D objects and improved vector data as well as classified information could be delivered within seven hours of phase 3.

The concept of the process chain was also applied to other freely available 3D software packages such as ArcGIS Explorer and OSSIM Planet. Neither is comparable to Skyline in terms of speed, multi-users and collaboration services. The ArcGIS Explorer has advantages because of its simple user interface and its close integration into the ESRI software environment and thus it could easily connect to a variety of GIS services. The already developed virtual 3D crisis scenarios will also be applied to this software.

During the exercises collaborative work within the 3D interactive virtual world was realized using standard PC workstations. Four partners, the ZGIS in Salzburg, Joanneum Research in Vienna, EURAC in Bozen and DLR Oberpfaffenhofen worked simultaneously in the VGE, added new datasets and "discussed" online in a collaborative session inside the VGE. For presentation purposes mobile computers with slow graphics hardware were used. A streaming feature server using Skyline or Leica software (during GNEX)) was installed at DLR and the virtual environment was streamed both via internal high bandwidth LAN connections as well as via relatively slow internet wireless LAN connections.

The minimum requirements to use real-time 3D crisis scenarios are LAN or W-LAN connections, standard PC workstations or laptops. Recent research initiatives try to establish ad-hoc networks even on-site in the emergency region (Frassl et al. 2010, OASIS consortium 2005).

The next step will be the generation of an operational generic process chain applicable to different real-time 3D packages to create and update 3D VGEs automatically from available remote sensing and other geo-data sets. Integrating web mapping and a web-feature service as described above is one of the future key elements to ensure up-to-date satellite based information availability also in interactive virtual 3D environments.

4 Conclusion

Dissemination of satellite based crisis information in a timely manner during a crisis is crucial for relief organizations and teams in situation rooms to support rapid and reliable decision making. The experience gained in DeSecure concerning the development of new dissemination channels for satellite based crisis information can be summarized as follows:

- The information provided by both 2D web-mapping products and 3D environments can be interactively explored and exploited by the user and thus new information can be generated.
- Digital mapping products can be updated either permanently or when new information/maps are available. Thus the most up-to-date product can always be delivered.
- Time consuming decoding of map information will be reduced to a minimum, which accelerates the decision making process based on the same high quality information.
- Supplementary, 3D interactive environments support situation rooms and very likely enable the staff in charge to intuitively understand the on-site environment and geography.
- Decision making will be conducted on a more consolidated basis, e. g., teams in situation rooms as well as on-site teams can now share a common operational picture (COP) without having to decode the information from printed maps.
- Because the authors work in close cooperation with the ZKI, the 2D and 3D solutions developed can be constantly tested during real crisis scenarios and further improved.

References

COGIC, 2010: Protéger la forêt contre les incendies – dossier de presse. – Direction de la sécurité civile.

DeSecure Consortium, 2009: DeSecure: Nutzer- und Nutzeranforderungen. – Internal project report.

Frassl, M., Lichtenstern, M., Khider, M. & Angermann, M., 2010: Developing a System for Information Management in Disaster Relief – Methodology and Requirements. – 7th International ISCRAM Conference.

Fritsch, D. & Kada, M., 2004: Visualisation using Game Engines. – International Archives of the Photogrammetry, Remote Sensing and Spatial Information Sciences **35** (B5): 626 ff.

Gstaiger, V., Kranz, O. & Förster, A., 2009: A training exercise in Cyprus puts GMES in action. – BOSS4GMES. Windows on GMES, ISSUE 3, Infoterra Ltd.

Häberling, C., 2003: «Topografische 3D-Karten»: Thesen für kartografische Gestaltungsgrundsätze. – Dissertation Eidgenössische Technischen Hochschule Zürich.

Lin, H. & Zhu, Q., 2006: Virtual Geographic Enviionments. – Large-scale 3D Data Integration. Challenges and Opportunities. CRC Press, Boca Raton.

MacEachren, A.M. & Kraak, M.J., 1997: Exploratory cartographic visualization: Advancing the agenda. – Computers & Geosciences **23** (4): 335–343.

Meng, L., 2003: Rahmenbedingungen beim Einsatz von Geovisualisierungsmethoden und -techniken. – Visualisierung und Erschließung von Geodaten. Kartographische Schriften **7**, Kirschbaum Verlag, Bonn.

Mitchell, T., Emde, A. & Christl, A., 2008: Web-Mapping with Open Source-GIS Tools. – O'Reilly Verlag GmbH & Co. KG, Köln.

OASIS consortium, 2005: OASIS User Requirements synthesis, – www.oasis-fp6.org/documents/OASIS_TA22_REQ_003_DSF_3_1.pdf, September 2005 (19.8.2010).

O'Coill, C & Doughty M., 2004: Computer Game Technology as Tool for Participatory Design. – eCAADe 2004 22nd conference: Architecture in the Network Society.

O'Connor, A., 2007: Automatic Virtual Environments from Spatial Information and Models. – Thesis, Cooperative Research Centre for Spatial Information, Department of Geomatics, University of Melbourne, Australia.

Peters, D., 2007: System Architecture Design and Capacity Planning. – ESRI Southeast User Group Conference, ESRI Technical Presentations, May 24th Jacksonville, Florida, USA.

Slocum, T.A., Blok, C., Jiang, B., Koussoulakou, A., Montello, D.R., Fuhrmann, S. & Hedley, N.R., 2001: Cognitive and Usability Issues in Geovisualization. – Cartography and Geographic Information Science **28** (1): 61–75.

Tiede, D. & Lang, S. (2010): Analytical 3D views and virtual globes – scientific results in a familiar spatial cover. – ISPRS Journal of Photogrammetry and Remote Sensing **65:** 300–307.

Tiede, D. & Lang, S., 2007: Pseudo-realistic and Analytical 3D Views – Conditioned Information for Security Scenarios. – In: Global Monitoring for Security and Stability (GMOSS). – Integrated Scientific and Technological Research Supporting Security Aspects of The European Union, JRC Scientific and Technical Reports.

Tüngerthal, S., 2009: Fernerkundungsbasierte 3D-Visualisierung im Katastrophenmanagement". – Diploma Thesis, Institute of Geography, University of Göttingen.

Tufte, E.R., 2007: The visual display of quantitative information. – 2nd ed., 5th printing Graphics Press, Cheshire.

Voigt, S., Trnka, J., Kemper, T., Reidlinger, T. & Husson, A., 2009: Satellite Based Information to Support European Crisis Response. – Remote Sensing from Space. Supporting International Peace and Security, Springer-Science, Heidelberg.

Woditsch, S., 2010: Die 3D Visualisierung von Notfallkarten am Beispiel der Software „Terra Explorer". – Diploma Thesis, Catholic University Eichstätt-Ingolstadt.

Zlatanova, S., 2008: SII for Emergency Response: the 3D Challenges – International Archives of the Photogrammetry, Remote Sensing and Spatial Information Sciences **37** (B4): 1631–1637.

Address of the Authors:

Dr. Thorsten Andresen & Felix Stracke, Deutsches Zentrum für Luft- und Raumfahrt, Deutsches Fernerkundungsdatenzentrum, D-82234 Wessling-Oberpfaffenhofen, e-mail: Name.Vorname@dlr.de

Manuskript eingereicht: Juni 2010
Angenommen: September 2010

Berichte von Veranstaltungen

Gottfried Konecny – 80 Jahre jung

Am 17. Juni 2010 beging Gottfried Konecny, Professor für Photogrammetrie und Fernerkundung und ehemaliger Leiter des Instituts für Photogrammetrie und GeoInformation der Leibniz Universität Hannover, seinen 80. Geburtstag. Konecny war und ist ein Weltbürger der Geodäsie und Geoinformatik und war u.a. von 1984–1988 Präsident der Internationalen Gesellschaft für Photogrammetrie und Fernerkundung (ISPRS). Mit 80 Jahren erfreut er sich bester Gesundheit und ist immer noch voll Energie und Engagement für seinen Beruf, der ihm schon vor langer Zeit zur Berufung wurde, und darüber hinaus ein weltweites Vorbild für die jüngeren Generationen. Sein Vortrag zur Geschichte der ISPRS anlässlich der 100-Jahrfeier der Gesellschaft am 4. Juli 2010 in Wien und das zugehörige Buch sind nur die jüngsten Beweise seiner nie endenden Schaffenskraft. Auf Leben und Werk Konecnys soll an dieser Stelle jedoch nicht weiter eingegangen werden, siehe dazu die Würdigung anlässlich seines 70. Geburtstages in der zfv (6/2000, pp. 218–220).

Aus Anlass von Konecnys Geburtstag veranstaltete die Fachrichtung Geodäsie und Geoinformatik der Leibniz Universität am 29. Juni 2010 ein Festkolloquium, an dem mehr als 150 Freunde und Kollegen Konecnys aus nah und fern teilnahmen. Nach Grußworten des Präsidenten der Universität, Prof. Erich Barke, und der Präsidentin der DGPF, Prof. Cornelia Glässer, beleuchteten zwei eingeladene Vorträge Leben und Leistungen von Gottfried Konecny.

Den ersten Vortrag hielt Ammatzia Peled von der Universität Haifa in Israel, der derzeitige 2. Vizepräsident der ISPRS, mit dem Titel “Gottfried Konecny – ein Geomatics Weltwunder wird 80”. Peled berichtete in lebhaften und persönlichen Worten über seine Verbindung zu Konecny, die 1980 beim ISP Kongress in Hamburg ihren Anfang nahm; Konecny war damals Kongressdirektor. Insbesondere betonte Peled die globale Präsenz über mehr als 50 Jahre und die breiten Interessen des Jubilars, die weit über dessen Fachgebiet hinausreichen. Er schloss mit der Bemerkung, dass Konecny nie und nimmer 80 Jahre alt sein könne, und eher zum vierten Mal seinen 20. Geburtstag gefeiert habe (oder, wie die Franzosen sagen, dass er 4 x 20 Jahre alt sei).

Prof. Fritz Ackermann, der ehemalige Leiter des Instituts für Photogrammetrie der Uni-

Jubilar Prof. G. Konecny (im Vordergrund rechts) und Prof. F. Ackermann (im Vordergrund links).

Festvortragender Prof. F. Ackermann (links) und Prof. G. Konecny (rechts).

versität Stuttgart und langjährige gleichaltrige Wegbegleiter Konecnys, hielt den zweiten Festvortrag, der überschrieben war mit „Gottfried Konecny – der Visionär". Gemeinsam hatten beide lange Zeit entscheidenden Einfluss auf unsere Disziplin, einer der Teilnehmer brachte es auf den Punkt: die Weltformel der Photogrammetrie und Fernerkundung habe über lange Jahre gelautet:

PH&FE = Ackermann + Konecny

Ackermann gab zunächst einen kurzen Überblick über Konecnys Leben und die ersten Schritte seiner Karriere. Dann kam er auf seine wohl größte Leistung zu sprechen, die Einführung von Satellitenbildern für die topographische Kartierung, und zwar zu einer Zeit, in der die beste geometrische Auflösung bei 80 m pro Pixel lag. Vor seiner Hannoveraner Zeit hatte Konecny in Nordamerika u.a. guten Kontakt mit der dort schnell wachsenden Weltraumindustrie. Das daraus erwachsene Wissen sowie die Kontakte hat er dann in Deutschland und Europa konsequent und visionär umgesetzt, zuerst im Metric Camera Experiment und danach in unzähligen weiteren Weltraummissionen und Projekten. Ackermann erwähnte auch Konecnys Aktivitäten der letzten Jahre, also nach Eintritt in den (so genannten) Ruhestand, so z.B. die weltweite Beratertätigkeit. Ackermann schloss mit den besten Wünschen zum Geburtstag und der Hoffnung, Konecny möge sich seine robuste Gesundheit möglichst lange erhalten, um auch zukünftig seinen weit gesteckten Aufgaben und Interessen mit viel Freude und Engagement nachgehen zu können. Alle Anwesenden schlossen sich diesen Wünschen an.

Christian Heipke, Hannover

ISPRS Commission VII Symposium "Thematic Processing, Modeling and Analysis of Remotely Sensed Data" vom 5.–7. Juli 2010 in Wien, Österreich

In Verbindung mit der Dreiländertagung der DGPF, der Österreichischen Gesellschaft für Vermessung und Geoinformation (OVG) sowie der Schweizerischen Gesellschaft für Photogrammetrie und Fernerkundung (SGPF) und den Feierlichkeiten zum 100-jährigen Bestehen der ISPRS fand vom 5. bis 7. Juli das Symposium der ISPRS Kommission VII an der TU Wien statt. Nach dem ISPRS Kongress in Peking ist die Kommission VII mit den Arbeitsgruppen VII/1 „*Physical Modelling and Signatures in Remote Sensing*", VII/2 „*SAR Interferometry*", VII/3 „*Information Extraction from Hyperspectral Data*", VII/4 „*Methods for Land Cover Classification*", VII/5 „*Methods for Change Detection and Process Modelling*", VII/6 „*Remote Sensing Data Fusion*", VII/7 „*Theory and Experiments in Radar and Lidar*", und der kommissionsübergreifenden Arbeitsgruppe ICWG III/VII „*Pattern Recognition for Remote Sensing*" an

den Start gegangen. Das diesjährige Symposium bot einen Überblick zur Halbzeit der Arbeitsphase zwischen den Kongressen.

Zum ersten Mal gab es – wie in anderen Kommissionen bereits auch – unterschiedliche Modalitäten zur Einreichung von Beiträgen: Zum einen als vollständige Beiträge („Full reviewed paper“) zur Veröffentlichung im Teil A, zum anderen wie bisher als Zusammenfassungen zur Veröffentlichung im Teil B des Tagungsbandes. Von den eingereichten 87 vollständigen Beiträgen wurden – zum Teil mit kleinen Änderungen – 63 zur Veröffentlichung angenommen. Mehr als 250 Beiträge wurden für den Teil B registriert. Die Beteiligung war kontinentbezogen gemischt, auch wenn die größte Gruppe von Autoren – sicherlich auch aufgrund der räumlichen Nähe – aus Deutschland kam, direkt gefolgt von China.

Das Symposium wurde von eingeladenen Vorträgen zu den Themen „Recent Advances in Local and Global Environmental Remote Sensing“ (W.P. Menzel) und „Assimilation of Satellite Data into Land Surface Models“ (S. Quegan) eröffnet. Den Kern bildeten dann anschließend die Vortrags- und Postersitzungen. Die Vortragssitzungen mit jeweils fünf bis sechs Beiträgen waren als dreizügige Veranstaltungen vor- und nachmittags organisiert. Zwischen diesen Vortragsblöcken fanden die Postersitzungen der jeweiligen Arbeitsgruppen zusammengefasst statt. Die Überschriften der Sitzungen umreißen grob die diskutierten Themen (in zeitlicher Reihenfolge): „Remote Sensing Applications“ (zwei Vortragssitzungen und eine Postersitzung mit mehr als dreißig angenommenen Beiträgen), „Data Fusion and Data Assimilation“ (eine Vortragssitzung und eine Postersitzung mit 13 angenommenen Beiträgen), „Lidar and Laser Scanning“ (zwei Vortragssitzungen und eine Postersitzung mit 17 angenommenen Beiträgen), „Change Detection and Process Modelling” (eine Vortragssitzung und eine Postersitzung mit 15 angenommen Beiträgen), „Multi-Spectral and Hyperspectral Remote Sensing“ (zwei Vortragssitzungen und eine Postersitzung mit mehr als zwanzig angenommenen Beiträgen), „Land Cover Classification“ (zwei Vortragssitzungen und eine Postersitzung mit dreißig angenommenen Beiträgen), „Microwave Remote Sensing“ (zwei Vortragssitzungen und eine Postersitzung mit mehr als zehn angenommen Beiträgen), „Operational Remote Sensing Applications“ (eine Vortragssitzung und eine Postersitzung mit fünf angenommenen Beiträgen), „Image Processing and Pattern Recognition“ (zwei Vortragssitzungen und eine Postersitzung mit zwanzig angenommenen Beiträgen), „Physical Modelling and Signatures“ (eine Vortragssitzung und eine Postersitzung mit drei angenommenen Beiträgen), „Earth Observation Programmes“ (eine Vortragssitzung) und „Geometric Modelling“ (eine Vortragssitzung und eine Postersitzung mit neun angenommenen Beiträgen). Die Postersitzungen umfassten somit im Allgemeinen mehr Beiträge als die Vortragssitzungen. Leider ist zu vermerken, dass eine Reihe von Stellwänden leer blieb. Den Abschluss des Symposiums bildeten wiederum eingeladene Vorträge zu den Themen „Generating 1 km Land Surface Radiation Product Suite from MODIS: Algorithms and Validation“ (S. Liang), „Persistent Scatterer Interferometry based on TerraSAR-X Imagery: The Barcelona Test Area“ (M. Crosetto) und „Analysis of Full-Waveform ALS Data by Simultaneously Acquired TLS Data: Towards and Advanced DTM Generation in Wooded Areas“ (M. Doneus). Die Auswahl der eingeladenen Vorträge trägt der Tatsache Rechnung, dass Laser- und Radartechniken bei dem diesjährigen Symposium einen breiteren Raum eingenommen haben, auch wenn Themen wie Landbedeckungsklassifizierung, Klassifizierungsverfahren und Monitoring auf der Basis von multi- und hyperspektralen Daten weiterhin einen Großteil der Beiträge ausmachen. Zudem ist festzuhalten, dass die Zuordnung der Beiträge zu den Themen bei der Einreichung durch die Autoren nicht immer einfach ist, da viele der Beiträge eine Reihe von Aspekten umfassen. Mit einem ähnlichen Problem sieht sich der Zuhörer konfrontiert, wenn bei einer dreizügigen Veranstaltung die Entscheidung zu treffen ist, welche Vortragssitzung man besucht. Ein Wechsel zwischen parallel laufenden Sitzungen ist immer schwierig, auch wenn die Vortragsräume wie in den Räumlichkeiten in Wien nah beieinander lagen. Die wie bei fast allen ISPRS-Veranstaltungen enge Zeitvorgabe von 15 Minuten stellte eine Herausforderung an die Zeitdisziplin der Vortragenden, so

dass trotz Einberaumung eines Zeitfensters für eine allgemeine Diskussion im Rahmen der Themensitzungen durch die Organisatoren zum Teil am Ende doch keine Zeit hierfür verblieb. Ein kleiner Wehrmutstropfen ergab sich auch durch die Tatsache, dass die Postersitzungen nicht in unmittelbarer Nachbarschaft zu den Vortragssitzungen stattfanden. Ihnen wurde genügend Zeit eingeräumt, jedoch ergibt sich bei unmittelbarer Nähe von Vortrags- und Postersitzungen die Möglichkeit der Diskussion am Poster auch über die eigentliche Sitzung hinaus.

Insgesamt betrachtet war das ISPRS Kommission VII Symposium eine gelungene Veranstaltung. Die Einführung des Reviews von vollständigen Beiträgen ist eine richtige Entscheidung und es ist zu begrüßen, wenn hiervon in Zukunft von den Autoren mehr Gebrauch gemacht wird, auch wenn dies einen größeren Aufwand bei der Vorbereitung einer solchen Tagung bedeutet. Den Organisatoren um Wolfgang Wagner, dem Kommissionspräsidenten, den Arbeitsgruppenleitern und insbesondere dem örtlichen Organisationsteam ist für die Durchführung des diesjährigen Symposiums herzlich zu danken.

Uwe Weidner, Karlsruhe

9th International Symposium on Spatial Accuracy Assessment in Natural Resources and Environmental Sciences ("Accuracy 2010") 20.–23. Juli 2010 in Leicester, England

The symposium is held on behalf of the International Spatial Accuracy Research Association (ISARA) and takes place every two years. This year, the symposium was hosted by the University of Leicester, Department of Geography, situated in the 'Heart of England'. 131 participants from all parts of the world discussed how to measure, model, and manage uncertainty in spatial data, especially the one from natural resource inventories. 33 sessions, with four presentations each, took place in three locations of the conference building at the same time. In addition, four keynote speeches and 24 posters were presented. Five workshops were held before the start of the symposium.

The symposium was structured in the themes remote sensing, digital elevation models, GIS, geostatistics, geoprocessing, environmental quality, ecology and forestry, land use/land cover, small area concerns, and visualization. Other session were dedicated to statistical topics, e.g., fuzzy uncertainty, uncertainty in space and time, uncertainty propagation, spatio-temporal uncertainty, and sampling design. Highlights at "Accuracy 2010" were three **keynote addresses** from the USA: "*A new look at semantic accuracy*" by O. Ahlqvist, "*The effect of map accuracy on estimates of terrestrial carbon budgets*" by C. Woodcock, and on "*Geostatistical modeling of the spatial distribution of soil dioxin*" by P. Goovaerts. A fourth keynote was presented on "*Statistical interference and local spatial modeling – living and working with uncertainty*" by C. Brunsdon, UK.

In the following contributions regarding remote sensing, DEMs and GIS will be mentioned and partially summarized. In the sessions on remote sensing and image interpretation, the following papers were presented:

"*Uncertainty in image interpretation as reference for accuracy assessment in object-based image analysis*" by F. Albrecht, Austria. "*Overall accuracy estimation of geographic object-based image classification*" by J. Radoux, P. Bogaert & P. Defourny, Belgium. "*Random and spatially autocorrelated sensor noise effects on image classification*" by T. K. Remmel & S.W. Mitchell, Canada. "*Assimilation of remote sensing data into land-surface models: the importance of uncertainty estimation to the filter performance*" D. Ghent, H. Balzter & J. Kaduk, UK. "*Web-based assessment of operator performance and variability in remote sensing image analysis*" by S. Gardin, S. Van Laere, F. Van Coillie, F. Anseel, W. Duyck & R.R. De Wulf, Belgium. "*Raster data transformation for land change analyses: Combined impacts of reprojecting and rescaling categorical maps on landscape composition and configuration*" by Z. Christman & J. Rogan, USA. "*Improving image classification accuracy: a method to incorporate uncertainty in the selection of training sample sets*" by L. Gonçalves, Luisa, C.

The participants of 'Accuracy 2010' listen to a keynote speech together with the organizer Dr. Nick Tate from Leicester University in the first row.

Fonte, H. Carrão & M. Caetano. "*Spatial entropy for the measurement of the accuracy of classified remote sensing imagery at multiple scales*" by D.G. Leibovici, G.M. Foody & D. Boyd, UK. "*Object-oriented remote sensed image classification accuracy assessment*" by Z. Wu, L. Yi & G. Zhang, China. "*Significance analysis of multitemporal Rapideye satellite images in a land cover classification*" by M. Foerster, C. Schuster & B. Kleinschmit, Germany.

The ISPRS working group II/4 (Uncertainty modeling and quality control of spatial data) also held a session where the following papers were presented: "*On the reproducibility of reflectance factors: Implication for Earth observation science*" by K. Anderson, E.J. Milton, V. Odongo, UK & J.L. Dungan, USA. "*Sources of uncertainty in predicting land surface fluxes using diverse data and models*" by J.L. Dungan, W. Wang, A. Michaelis, P. Votava & R. Nemani, USA. "*Challenges associated with integrating data from multiple scales to assess relationships*" by L.J. Joung, C.A. Gotway & K.K. Lopiano. "*An Iterative Dichotomiser 3-improved approach for optimum rule mining through granular computing search algorithm*" by H.S. Alinia, M.R. Delavar, Iran & Y. Yao, Canada.

The sessions on DEM uncertainty consisted of the following papers among others:

M. Gallay, C. Lloyd & J. McKinley, UK, presented the paper "*Using geographically weighted regression for analyzing elevation errors of high-resolution DEMs*". The authors investigated DEMs derived by four different methods (photogrammetry, airborne LIDAR, interferometric SAR, and contour digitizing) in order to find a relationship between DEM errors and DEM surface roughness for each of the acquisition method. It was concluded that large errors occur at DEM artifacts and sharply defined landforms and that the assumption that DEM errors are normally distributed is questionable.

In the contribution "*Increasing the accuracy of DEMs by means of geostatistical conflation*", authored by C.U. Parady-Hernándy, N. Tate, K.J. Tansey, P. Fisher, UK & W.E. Salinas-Castillo, México, it is shown that a DEM may be improved by means of a set of sparely distributed accurate ground control points. Various Kriging methods are applied whereby "Kriging with External Drift" (KED) produced the most accurate results. The error analysis used quantiles of different probability beside the standard accuracy measures. The Inter Quartile Range (IQR), which is defined as the difference between the quartiles of 75% and 25% probability, was also used as accuracy measure. A 49 ha large DEM derived from a spaceborne Interferometric SAR system

(TerraSAR-X) could considerably be improved using 184 ground control points and the KED method. The IQR improved from 12.7 m to 3.1 m, the standard deviation from 9.2 m to 4.2 m. That means that 50% of the errors were in the range of ±1.5 m. Reference was a dense and accurate DEM derived by LIDAR. Its accuracy was assessed by means of a large number of check points of superior accuracy.

The contribution of S. Wise, UK, "*Assessing the spatial characteristics of DEM interpolation errors*", studied the influence of the point density and interpolation type (bilinear and spline) on the spatial autocorrelation properties in various terrain types. Furthermore, it was concluded that the RMSE of elevation is a good predictor for the RMSE for aspect and gradient. These findings are based on resampling a DEM of 50 m spacing to a DEM of much lower resolution and resampling it back to several DEMs of higher resolution. The usual assumptions that elevation errors have a Gaussian distribution and that they are strongly correlated are thrown into doubt by these investigations.

J. Oksanen & T. Sarjakoski, Finland, discuss in their contribution the *non-stationary modelling and simulation of LIDAR DEM uncertainty*. Simulations of DEM uncertainty takes into account elevation errors, vagueness, and ambiguity. Such simulations can derive the boundaries of catchments, which collect water of that area after rainfalls, and enable to model flood risks. The DEM uncertainty was derived by means of the process convolution method. Tests with the new Finnish DEM, which is based on airborne LIDAR, and additional LIDAR acquisitions of lower altitudes (and thereby higher density) have been carried out. The derived catchments boundaries of both simulations differed in location by a few hundred meters.

A. Jalobeanu, Portugal, proposed a new method for *generation of DEMs from stereo image pairs*. The spatial accuracy of the derived elevations is also estimated in this approach. The sources of uncertainty present in the images and in the orientation data are modelled.

A method for *checking the planimetric accuracy of DEMs derived by airborne laser scanning* was presented by J. Höhle & C.Ø. Pedersen, Denmark. The approach uses roofs of buildings and derives points by intersection of three roof planes. The roof planes are determined by means of robust adjustment. Reference points are determined by means of photogrammetry. The reliability of the results is checked by means of confidence ellipses for the intersected points, Normal-Quantile plots of the error distribution and confidence intervals for robust accuracy measures (Median, Normalized Median Absolute Deviation and 95% Quantile). Practical tests proved the feasibility of the method.

A paper on "*Quality evaluations of photogrammetrically derived DEMs*" by H. Papasaika & E. Baltsavias, Switzerland, is also contained in the proceedings. Accordig to experiences of the authors the quality of DEMs depends on land cover and morphological features. One single number, e.g., the RMSE value, is not enough to characterize DEMs. A validation of break lines, which may be derived by edge detection algorithms, should also be carried out. Experiences were gained by assessment of DEMs derived from satellite imagery (IKONOS and PRISM) and using dense DEMs derived from LIDAR as a reference. The co-registration revealed considerable horizontal displacements. The geomorphologic characteristics analysis included slope, aspect, and entropy, which proved as useful quality measures. The land cover analysis revealed bigger differences in shadowed and water areas than in bare ground areas.

"*Land-cover class as a qualifier for quoted elevation error in aerial LIDAR*" was the topic of S. Coveney, Ireland. The vertical accuracy of bare earth DEMs depends very much on the land cover. Three official DEMs of the same area, all derived by airborne laser scanning, were assessed using accurate reference data. Accuracy measures were determined for five land cover classes (open terrain, brush lands and low trees, tall weeds and crops, forested areas, urban areas). The obtained accuracies varied according to the vegetation canopy density and depth and were in all three data sets much lower than in open terrain. The use of airborne laser scanning for modelling flood risk may become difficult for land cover classes with vegetation.

The conference building with lecture and dining rooms.

In the session on visualization, M. Gousie, USA, & M. Smith, UK, presented a new program for the visualization of DEMs and DEM errors. DEMVIEW visualizes differences to reference DEMs, height class frequency, curvature and calculates quantitative statistics. A 'profile cutter' displays dynamically movable profiles in context with a 3D surface. Glyphs show accuracy levels compared to source contours. The program is freeware and can be downloaded from cs.wheatonma.edu/mgousie/research.html.

There were many more presentations to mention. The proceedings of the conference contain 109 papers on 436 pages and may be of interest for those who like to know more about uncertainty and statistical methods in remote sensing and GIS.

The symposium was held outside Leicester in new conference facilities with accommodation and meals close by. It was well organized and took place in a very stimulating atmosphere.

Joachim Höhle, Aalborg, Dänemark

Hochschulnachrichten

Otto-Friedrich-Universität Bamberg

Prof. Dr. rer. nat. Matthias Möller (Otto-Friedrich-Universität Bamberg, Institut für Geographie, Lehrstuhl Humangeographie (i.V.) und Österreichische Akademie der Wissenschaften, GIScience, Salzburg) habilitierte sich am 21. April 2010 an der Otto-Friedrich-Universität Bamberg, Fakultät Geistes- und Kulturwissenschaften, für das Fachgebiet Geographie mit der Habilitationsschrift „*Semantisch-quantitative Modellierungsansätze für das synoptische Monitoring Urbaner Räume*".

Habilitationskommission: Prof. Dr. Thomas Blaschke (Paris Lodron Universität Salzburg), Prof. Dr. Manfred Buchroithner (TU Dresden) und Prof. Dr. Klaus Greve (Universität Bonn)

Kurzfassung:
Urbane Gebiete, also menschliche Agglomerationsräume im weiteren Sinn, sind die Knotenpunkte des Informationszeitalters. Mittlerweile lebt mehr als die Hälfte aller Menschen in urbanen Gebieten, wir haben uns von einer Agrar- zu einer Urbangesellschaft entwickelt. Urbane Gebiete sind die Zentren, in denen annähernd alle menschlichen Aktivitäten zusammenlaufen. Sie weisen ein stark verdichtetes Netz an Kommunikations-, Transport- und sozialer Infrastruktur auf und decken damit die vielfältigen Bedürfnisse des modernen

Menschen ab. Für schnell wachsende, dicht besiedelte Regionen kann rückwärts betrachtet das Wachstum über die vergangenen ca. vier Dekaden auf Basis von frei verfügbaren Satellitenbilddaten durchgeführt werden. Diese liegen seit ca. 1972 vor, aufgezeichnet von den Satelliten und Sensoren des U.S.-amerikanischen Landsat Systems; entsprechend ausgewertet lassen sich Wachstumsphasen raum-zeitlich daraus rekonstruieren. Mit zuverlässigen Ergebnissen arbeitet diese Methode auf einem Maßstabsniveau von ca. 1 : 7 500 und kleiner insbesondere in urbanen Gebieten mit regulären Strukturen, wie sie beispielsweis in den USA anzutreffen sind.

Die Land – Stadt Migration trifft für Länder mit einem sehr hohen HDI (Human Development Index) zweifelsfrei zu, der Trend zu wachsenden Agglomerationen kann aber insbesondere auch bei Ländern mit geringem und sehr geringem HDI beobachtet werden, den so genannten weniger entwickelten Ländern. Hier gelten aber als Auslöser für die Wanderung grundsätzlich andere Faktoren, die urbane Regionen für diese Menschen attraktiv erscheinen lassen. Vorrangig sind die bessere Aussicht auf Arbeit und Verdienst verglichen mit ländlichen Regionen, der bessere Gesundheitsdienst und insgesamt die Perspektive auf ein höher abgesichertes Leben. In weniger entwickelten Ländern wird das Wachstum der urbanen Regionen nicht mit der Ausführlichkeit erfasst und dokumentiert, wie wir es in westlichen Ländern kennen, i.d.R. sammeln sich dort die Zugezogenen in Slums, informellen Siedlungen, die nur über geringe, oftmals keine Ver- und Entsorgungseinrichtungen verfügen. Urbane Infrastruktur ist dort ebenfalls nur in deutlich reduzierter Form vorhanden. Dabei ist es gerade in diesen, meist extrem dicht besiedelten urbanen Regionen, notwendig, eine solide Grundversorgung mit sauberem Trinkwasser sicherzustellen, ebenso muss das Abwasser kontrolliert entsorgt und gereinigt werden, um Krankheiten und Epidemien, vorzubeugen. Eine Anbindung an das Elektrizitätsnetz sollte für jeden Haushalt im 21. Jahrhundert obligatorisch sein. Um diesen Minimalforderungen gerecht zu werden, müssen einzelne Gebäude und deren Einwohnerzahl über eine Adresse verfügen, die an eindeutige Geokoordinaten gekoppelt ist und damit räumlich auffindbar ist. Ein digitales Kataster mit validen Geoinformationen erfüllt diese Basisanforderung.

Dafür ist zunächst eine Grundaufnahme der urbanen Objekte, hier vor allem der Gebäude, in schnell wachsenden Regionen notwendig. Dies kann zuverlässig über eine Erfassung vor Ort erfolgen, was zwar langwierig ist, aber zu präzisen Ergebnissen führt und auch weitere Attributwerte aufnimmt, wie die exakte Einwohnerzahl pro Gebäude. Ein Dilemma entwächst allerdings aus der Tatsache, dass die Agglomerationsräume in gering entwickelten Ländern schnell wachsen und sich laufend ändern, eine Dokumentation des IST-Zustandes eines Gebietes entsprechend schnell veraltet und nur eine zeitlich äußerst begrenzte Aussagekraft hat. Effizienter kann die Erfassung von Gebäuden auf Basis aktueller Fernerkundungsaufnahmen mit einer hohen räumlichen Auflösung im Anwendungsmaßstab von ca. 1 : 5 000 erfolgen. Hierfür sind Bilddaten mit einer Bildpunktauflösung von ca. 1,0 m geeignet, die zunächst weitgehend manuell ausgewertet werden. Da diese Satelliten eine Wiederholung der Aufnahme desselben Gebietes in kurzen Zeiträumen sicherstellen, kann auch eine Analyse der Änderung auf Basis dieser Bilddaten erfolgen. Die Änderungsanalyse (engl. Change Detektion) kann mit objekt-orientierten Methoden der Bildauswertung (engl. OBIA, Object Based Image Analysis) semi-automatisch zu guten Ergebnissen führen. Hierbei ist es wichtig, standardisierte Regelsätze und Methoden für die verschiedenen Naturräume der Erde zu entwickeln, die dann mit kleineren Änderungen, Anpassungen der Variablenwerte übertragbar sind. Dabei sind die folgenden Grundvoraussetzungen zu erfüllen: Die Bilddaten sollen ähnliche spektrale Eigenschaften in den verwendeten Kanälen aufweisen und sie sollen in etwa zur selben phänologischen Ausprägung aufgenommen werden. Sind diese Regelsätze und Methoden etabliert, lassen sich urbane Regionen objektiv und weltweit miteinander vergleichen. Anhand von Bilddaten des U.S.-amerikanischen ASTER Sensors (Advanced Spaceborne Thermal Emission and Reflection Radiometer) konnten bereits beeindruckende Ergebnisse – bezogen auf die Übertragbarkeit von Regelsätzen und Methoden – für die Regi-

onen Phoenix und Las Vegas in den USA erzielt werden.

Als interaktives Web 2.0, Nutzer – generierter „Geocontent" im (mobilen) Internet, zusammengefasst unter dem Schlagwort „Neogeography", versteht sich eine neue Art von Geoinformationsdiensten (GID), die die klassischen Karten und Kartendienste revolutionieren. Die Nutzerfreundlichkeit dieser GID wird zunehmend optimiert, als Folge rücken diese stark in den öffentlichen Fokus. Getrieben wurde diese Entwicklung z.B. durch Google Earth, Google Maps, Microsoft Bing Maps u.a. Weitere wichtige Entwicklungen finden im Bereich der freien Mapping-Community statt: Am Open Streetmap Projekt beteiligen sich über 250 000 Nutzer und generieren permanent validierte, detaillierte Geodaten. Dies kann in Zukunft ganz entscheidend auch die Erfassung und Aktualisierung von urbanen Gebieten etwa in informellen Siedlungen unterstützen. Umso wichtiger ist es, dass gerade in der schulischen Ausbildung, also im Erdkundeunterricht, diese Inhalte nicht fehlen dürfen, denn hier formiert sich die kommende Generation engagierter Kartierer.

Die kumulative Habilitationsschrift verbindet den neuesten Forschungsstand der Stadtgeographie, insbesondere das Wachstum von Megastädten, mit der angewandten Geoinformation und gibt didaktische Anleitungen für die Umsetzung im Schulunterricht. Sie stellt damit eine gelungene Synthese aller Geographischen Teildisziplinen dar. Die digitale Version der Arbeit ist publiziert und kann heruntergeladen werden unter dieser URL: typo3.urz.uni-bamberg.de/fileadmin/gi/habil_moeller/habilschrift_moeller.pdf

Karlsruher Institut für Technologie (KIT)

Herr Dipl.-Ing. Christian Lucas promovierte am 11.2.2010 an der Fakultät für Bauingenieur-, Geo- und Umweltwissenschaften des Karlsruher Institutes für Technologie mit der Arbeit *„Modellierung verbal repräsentierter Geoinformation im Anwendungsbeispiel des Katastrophenmanagements"* zum Dr.-Ing.

Referent: Prof. Dr.-Ing. habil. Dr. h.c. Hans-Peter Bähr, Karlsruhe; Korreferenten: Prof. Dr.-Ing. habil. Monika Sester, Hannover; Prof. Dr.-Ing. habil. Stefan Hinz, Karlsruhe

Kurzfassung:
Um die Integration sprachlicher Information in geographische Informationssysteme zu ermöglichen, wurde eine Methodik zur Überführung verbal repräsentierter räumlicher Zusammenhänge in eine formale Darstellung entwickelt. Diese umfasst neben einer funktionalen ebenfalls eine semantische Modellierungsebene, welche sich durch die differenzierten Betrachtungen begründet, die für eine zuverlässige und robuste Verarbeitung unscharfer Geoinformation notwendig sind. So erfordern die verschiedenen Abstraktionsstufen der verbalen Repräsentation semantische Modellierungsstrukturen. Diese erlauben es, fehlende Information durch einschränkende Bedingungen sowie heuristische Annahmen zu ergänzen. Ferner wurde die der Information zugrunde liegende Raumvorstellung, sowie die Semantik der zur Beschreibung genutzten linguistischen Terme einbezogen. Die Berücksichtigung der semantischen und topologischen Objektrelationen bei der Modellbildung ermöglichte es ferner, die sprachlich bedingten semantischen Mehrdeutigkeiten aufzulösen. Formalisiert wurden diese Aspekte in einer ontologischen Wissensbasis, unter Nutzung der Web-Ontologie Sprache OWL, welche es auf Grund einer Beschreibungslogik erlaubt, die konkrete Domäne semantisch korrekt abzubilden. Die Nutzung einer Inferenzmaschine gestattete es darüber hinaus, ausgehend von dem modellierten Wissen, erforderliche Zusammenhänge abzuleiten.

Die quantitative Beschreibung der verbalen Information erfolgte auf Basis eines funktionalen Modells. Dieses ermöglichte es, unter Berücksichtigung diverser Einflussterme, einen Gültigkeitsraum der verbalen Information aufzuspannen. Ausgehend von diesem Gültigkeitsraum wird ein konkretes intervallwertiges Bewertungsmaß für ein beschriebenes, intendiertes Objekt abgeleitet. Einbezogen werden dabei die Art und Aktualität der Erfassung, die Glaubwürdigkeit des Verfassers sowie die räumliche Unschärfe der Information. Überdies wird die wiederholte Beschrei-

bung der Lage eines intendierten Objektes stützend berücksichtigt. Der konkrete Einfluss der jeweiligen Terme konnte auf Basis eines vorliegenden Meldungskorpus sowie empirisch gestützt ermittelt werden. Das darauf aufbauend entwickelte Bewertungsmaß gestattet es, im Weiteren für jedes Objekt die Konsistenz mit der Meldungsmenge zu bestimmen. Dies erfolgt intervallwertig im Sinne einer Positiv- und Negativ-Hypothese, sowohl für als auch gegen die Konsistenz mit der Meldungsmenge.

Eine konkrete Anwendungsschale des Verfahrens bietet die raumbezogene Auswertung freitextlicher Meldungen von katastrophalen Ereignissen. Der entwickelte Prototyp namens Seneca wertet unter Nutzung des vorgestellten Verfahrens die textuell vorliegenden Meldungen vollautomatisch aus und generiert die entsprechende Lagedarstellung. So ist es dem Stabspersonal möglich, auf Basis des Bewertungsmaßes konkrete Entscheidungen zu treffen.

Karlsruher Institut für Technologie (KIT)

Herr Dipl.-Ing. Mauro Alixandrini promovierte am 10.6.2010 an der Fakultät für Bauingenieur-, Geo- und Umweltwissenschaften des Karlsruher Institutes für Technologie mit der Arbeit *„Land Cover Change Analysis from Historical Remote Sensing Images: Case Study Itaipu“* zum Dr.-Ing.

Referent: Prof. Dr.-Ing. habil. Dr. h.c. Hans-Peter Bähr, Karlsruhe; Korreferenten: Prof. Dr.-Ing. Carlos Loch, Florianópolis, Brasilien; Prof. Dr.-Ing. habil. Joaquim Vogt, Karlsruhe

Abstract:
On the basis of the increasing demand of energy in Brazil, a series of projects involving large hydroelectric power plants will be settled in the next decade. In spite of the renewable energy generated by these enterprises, some phenomena can be observed in the regions where these hydroelectrics are established, for example, reorganization in the land structure, changes in typical economic activities and rural estate appreciation. Accordingly, the analyses of old cases are crucial for planning and management of future projects. In this work we investigate the evolution of the forest distribution in areas with strong deforestation in the period since the construction of the Itaipu hydroelectric power plant until the current day. The focus of this research is the analysis of the forest distribution and its relation to historical aspects regarding the socioeconomic reorganization and the construction of the Itaipu hydroelectric. In order to recognize the phenomena responsible for these changes, we proposed the use of remote sensing as investigation tool. The scenes available for this work are restricted to the medium resolution of 20m to 80m and are derived from the following sensors: LANDSAT 1, 2, 5 TM, 7 ETM and CBERS II. In the first stage we performed the spatial and thematic association of the different sensors. We defined a methodology based on classical techniques, like the Maximum Likelihood classifier and the Thematic Map comparison. The evaluation of the results of the automatic classifications considers two principles developed in this work: i) the random selection into reference groups for the training and the evaluation samples, and ii) the images of evidence. The images of evidence define a minimum situation of acceptance for the thematic maps, which allows the generation of consistent classifications among the applied sensors. In the next step we performed a comparison between these maps. The compatibility of the spatial resolutions takes place with the generalization of these maps. With the results obtained from the set of adopted images, we proceeded with the correlation with a historical perspective of the region. Based on the analysed documents we can define the main anthropogenic phenomena responsible for the changes in the vegetation cover in the region. We identified the Paraguayan agricultural expansionism and the predominantly agricultural Brazilian migratory movements to the border region between Brazil and Paraguay. The results show that the systematic process of deforestation had already been established before the beginning of the construction of Itaipu. Migratory processes associated with previous factors to the construction of hydroelectric show mainly corre-

lations with the deforestation observed in the region. Furthermore, the analysis verifies the incoherent documentation about the current situation in the protected areas. The conclusions prove the characteristics of the employed method showing that its use is valid in a context of the analysis of the regional development.

Karlsruher Institut für Technologie (KIT)

Frau Dipl.-Geol. Eike-Marie Nolte promovierte am 15.7.2010 an der Fakultät für Bauingenieur-, Geo- und Umweltwissenschaften des Karlsruher Institutes für Technologie mit der Arbeit *„Anwendungsmöglichkeiten optischer Satellitenbilder und Zensusdaten zur Bevölkerungsmodellierung am Beispiel der indischen Stadt Ahmedabad“* zum Dr. rer. nat.

Referent: Prof. Dr. Friedemann Wenzel, Karlsruhe; Koreferent: Prof. Dr.-Ing. habil. Stefan Hinz, Karlsruhe

Kurzfassung:
Die Bevölkerungsschätzungen für indische Städte sind meist auf die Daten des indischen Zensus, der alle zehn Jahre durchgeführt wird, beschränkt. Vor dem Hintergrund der hohen Bevölkerungsdynamik indischer Städte sind diese Daten nicht ausreichend, um die Bevölkerungsentwicklung für die Jahre zwischen zwei Bevölkerungszählungen mit hinreichender Genauigkeit abzubilden. Für die Erfassung der räumlichen Verteilung der Bevölkerung in diesen Zeiträumen, spielen Fernerkundungsdaten als Datenquelle für flächenhafte, großräumige Information eine wichtige Rolle, da traditionelle Techniken zur Datenerfassung an ihre Grenzen stoßen. Die zentrale Fragestellung dieser Dissertation ist daher, wie die räumliche Bevölkerungsverteilung in indischen Großstädten mit Hilfe optischer Satellitendaten, geokodierten Informationen und statistischen Daten modelliert werden kann.

In dieser Dissertation wurde eine hierarchische Methode entwickelt, die die Modellierung der Bevölkerungsverteilung für unterschiedliche, administrative Ebenen ermöglicht. Die Hierarchie der entwickelten Methode umfasst drei räumliche Ebenen: Stadt-, Distrikt- und Gebäudeebene. Für jede administrative Ebene wurden verschiedene Modelle zur Modellierung der Bevölkerungsverteilung entwickelt. So ist es möglich, je nach Datenverfügbarkeit Datensätze mit unterschiedlicher Detailgenauigkeit zu entwickeln.

Die Methode wurde beispielhaft an der Stadt Ahmedabad in Nordwestindien getestet. Die Stadt Ahmedabad ist ein gutes Beispiel einer Millionenstadt mit sehr komplexen Bebauung und stark variierender Bevölkerungsdichte, die einer hohen Dynamik mit schnellen strukturellen und sozioökonomischen Wandel unterworfen ist.

Karlsruher Institut für Technologie (KIT)

Frau Karin Hedman (M.Sc.) promovierte am 15.7.2010 an der Fakultät für Bauingenieur-, Geo- und Umweltwissenschaften des Karlsruher Institutes für Technologie mit der Arbeit *„Statistical Fusion of Multi-Aspect Synthetic Aperture Radar Data for Automatic Road Extraction“* zum Dr.-Ing.

Referent: Prof. Dr.-Ing. habil. Stefan Hinz, Karlsruhe; Korreferenten: Prof. Dr.-Ing Uwe Stilla, München; Prof. Dr.-Ing. habil. Dr.h.c. Hans-Peter Bähr, Karlsruhe

Abstract:
In this dissertation, a new statistical fusion for automatic road extraction from SAR images taken from different looking angles, i.e., multi-aspect SAR data, is presented. The main input to the fusion are extracted line features. The fusion is carried out on decision-level and is based on Bayesian network theory.

The developed fusion fully exploits the capabilities of multi-aspect SAR data. By means of Bayesian network theory, a reasoning step could be modelled which describes the relation between the extracted road, neighbouring high objects, and the sensor geometry. For instance, an extracted road oriented in the looking angle of the sensor (range) is considered more reliable than other detections closer to the azimuth. Furthermore, information about

neighbouring high objects (local context information) could be integrated since these objects could be detected by bright line extraction. Examples of neighbouring high objects are trees and buildings. By incorporating this into the reasoning step, contradicting hypotheses, e.g., detection of a road in the first image, detection of parallel shadow and layover regions caused by neighbouring high objects in the second image, could be solved. Furthermore, integrating local context information enables the fusion to distinguish between different pre-defined types of road, e.g., highways, roads with vegetation nearby, open roads, etc.

Information about the scene context (global context information) was obtained by a textural classification of large image regions. In this work the image was classified into built-up areas, forests, and fields. This information is incorporated as prior knowledge into the fusion.

The development of the fusion contains the following steps: Defining a road and local context model in multi-aspect SAR data, analysing the feature extraction (i.e., dark and bright line extraction and textural classification), setting up a Bayesian network structure, learning the fusion, and implementing an association step. Some network structures of varying complexity are presented and discussed. The learning is carried out by estimations of conditional probability functions and conditional probability tables based on manually collected training data. Each step is described in detail.

Two different fusions were developed and tested: One developed for extracted dark linear features only and one designed for both dark and bright linear features. Both fusions consider the sensor geometry, while the last one is based on a more complex road and local context model. The performance of these two fusions was compared by evaluating the results from a data set of multi-aspect SAR data. In addition the transferability of the fusion concept was also tested on data acquired from a second SAR sensor. A discussion on the behaviour of the two fusions follows. The advantages and disadvantages of using Bayesian network theory for this application are also discussed. Finally, some ideas for improving the fusion are presented.

Veranstaltungskalender

2011

1.–3. Februar: 10. **Oldenburger 3D-Tage**. www.fh-oow.de/institute/iapg/workshop/

13.–19. Februar: 16. **Internationale Geodätische Woche** in **Obergurgl**, Tirol, Österreich. geodaetischewoche@uibk.ac.at oder geodaesie.uibk.ac.at/obergurgl.html

3.–4. März: **GeoMonitoring:** Ein Paradigmenwechsel zur Beherrschung von Georisiken in **Clausthal-Zellerfeld**. www.geo-monitoring.org

10.–11. März: **GeoViz Hamburg 2011:** Linking Geovisualization with Spatial Analysis and Modeling an der HafenCity Universität **Hamburg**. www.geomatik-hamburg.de/geoviz/

21.–24. März: 16. **Münchner Fortbildungsseminar Geoinformationssysteme** in **München**. www.rtg.bv.tum.de/

4.–8. April: 8th **IAA Symposium on Small Satellite for Earth Observation** in **Berlin**. www.dlr.de/iaa.symp

11.–13. April: **JURSE 2011** – Joint Urban Remote Sensing Event (URBAN 2011 + URS 2011) in **München**. www.jurse2011.tum.de

13.–15. April: **EOGC 2011** – 3rd Conference on Earth Observation for Global Changes in **München**. www.eogc2011.tum.de

13.–15. April: 30. **Wissenschaftlich-Technische Jahrestagung der DGPF** in **Mainz**. www.dgpf.de/neu/jahrestagung/informationen.htm

3.–8. Mai: **Gi4DM – GeoInformation for Disaster Management** in **Antalya**, Türkei. www.gi4dm2011.org/

12.–13. Mai: **7. GIS-Ausbildungstagung 2011** in Potsdam. gis.gfz-potsdam.de/

23.–26. Mai: **SPIE Optical Metrology – Videometrics, Range Imaging, and Applications** in **München.** spie.org//app/program/index.cfm?fuseaction=conferencedetail&export_id=x12518&ID=x6511&redir=x6511.xml&conference_id=940248&event_id=918522

26.–29. Mai: ISPRS **ICWG V/I joint ICA/ISPRS/FIG International Symposium on Lidar & Radar Mapping: Technologies & Applications (LIDAR & RADAR 2011)** in **Nanjing,** China. www.lidar2011.org/

30. Mai – 1. Juni: **Symposium Königslutter 2011.** Info/Anmeldung: www.angewandte-kartographie.de

13.–16. Juni: 7th **International Symposium on Mobile Mapping Technology (MMT11)** in **Cracow**, Polen. www.mmtcracow2011.pl/

14.–17. Juni: ISPRS WG IV/2 **Workshop on High Resolution Earth Imaging for Geospatial Information** in **Hannover**. www.commission4.isprs.org/wg2/

15.–17. Juni: **GEOINFORMATIK 2011** in **Münster**. www.geoinformatik2011.de/

26.–27. Juni: ISPRS **WG V/4, III/2+4, IV/4+8 joint Workshop on 3D City Modelling & Applications** in **Wuhan**, China. www.lmars.whu.edu.cn/3DCMA2011/

3.–8. Juli: 25th **International Cartography Conference (ICC2011)** in **Paris**, Frankreich. www.icc2011.fr/

29.–31. August: ISPRS **WG V/3 Laser Scanning 2011** in **Calgary**, Kanada. e-mail: ddlichti@ucalgary.ca

12.–16. September: XXIIIth **International CIPA-HD Symposium** in **Prague**, Tschechien. cipa.icomos.org/index.php?id=9

27.–29. September: **INTERGEO 2011** in **Nürnberg**. www.intergeo.de/de/deutsch/index.php

5.–7. Oktober: **Photogrammetric Image Analysis 2011 (PIA11)** in **München.** www.pia11.tum.de

2012

24. August – 3. September: **XXII ISPRS Congress 2012** in **Melbourne**, Australien. www.isprs2012-melbourne.org/

Vorstand der DGPF

Präsidentin
Prof. Dr. Cornelia Gläßer
Martin Luther-Universität Halle-Wittenberg, Institut für Geographie, Von-Seckendorff-Platz 4, D-06120 Halle, Tel.: 0345-55-26020, Fax: -27168, e-mail: praesident@dgpf.de

Vizepräsident
Prof. Dr. rer. nat. Thomas H. Kolbe
Technische Universität Berlin, Sekr. H 12, Institut für Geodäsie und Geoinformation, Straße des 17. Juni 135, D-10623 Berlin, Tel.: 030-314-23274/23206, Fax: -21973, e-mail: kolbe@igg.tu-berlin.de

Sekretär
Dr.-Ing. Manfred Wiggenhagen
Leibniz Universität Hannover, Institut für Photogrammetrie und GeoInformation (ipi), Nienburger Straße 1, D-30167 Hannover, Tel.: 0511-762-3304, Fax: -2483, e-mail: sekretaer@dgpf.de

Schatzmeister
Dr.-Ing. Herbert Krauss
Rodenkirchener Str. 47, D-50997 Köln, Tel.: 02233-22514, e-mail: mh.krauss@t-online.de

Hauptschriftleiter
Prof. Dr.-Ing. Helmut Mayer
Universität der Bundeswehr München, Institut für Angewandte Informatik, D-85577 Neubiberg, Tel.: 089-6004-3429, Fax: -4090, e-mail: Helmut.Mayer@unibw.de

Beirat
Prof. Dr.-Ing. Monika Sester
Leibniz Universität Hannover, Institut für Kartographie und Geoinformatik (ikg), Appelstr. 9A, D-30167 Hannover, Tel.: 0511-762-3588, Fax: -2780, e-mail: monika.sester@ikg.uni-hannover.de

Beirat
Prof. Dr.-Ing. Hans-Gerd Maas
Technische Universität Dresden, Institut für Photogrammetrie und Fernerkundung, Helmholtzstr. 10, D-01062 Dresden, Tel.: 0351-463-32859, Fax: -7266, e-mail: hans-gerd.maas@tu-dresden.de

Beirat
Dr. rer. nat. Klaus Komp
EFTAS Fernerkundung Technologietransfer GmbH, Oststraße 2-18, D-48145 Münster, Tel.: 0251-1330-70, Fax: -733, e-mail: klaus.komp@eftas.com

Beirat
Dr.-Ing. Eckhardt Seyfert
Landesvermessung und Geobasisinformation Brandenburg, Heinrich-Mann-Allee 103
D-14473 Potsdam, Tel.: 0331-8844-506 Fax: -126, e-mail: eckhardt.seyfert@geobasis-bb.de

Ehrenpräsident – Ehrenmitglieder der DGPF

Ehrenpräsident
Prof. Jörg Albertz, Berlin

Ehrenmitglieder
Prof. Friedrich Ackermann, Stuttgart
Prof. Heinz Draheim, Karlsbad
Prof. Gerd Hildebrandt, Freiburg
Dr.-Ing. Otto Hofmann, Brunnthal
Prof. Gottfried Konecny, Hannover
Direktor Fritz Erich Krause, Münster
Prof. Hans-Karsten Meier, Königsbronn
Dipl.-Ing. Horst Schöler, Stadtsteinach
Prof. Klaus Szangolies, Jena

Arbeitskreise der DGPF

- **Aus- und Weiterbildung**
Prof. Dr.-Ing. Jochen Schiewe
HafenCity Universität Hamburg, Department Geomatik, Hebebrandstraße 1, D-22297 Hamburg, Tel.: 040-428-27-5442
e-mail: jochen.schiewe@hcu-hamburg.de

- **Bildanalyse und Bildverstehen**
Prof. Dr.-Ing. Frank Boochs
Fachhochschule Mainz, Holzstr. 36, D-55116 Mainz, Tel.: 06131-262-843/812, Fax:-815, e-mail: boochs@geoinform.fh-mainz.de

- **Geoinformatik**
Prof. Dr. Thomas H. Kolbe
Technische Universität Berlin, Sekr. H 12, Institut für Geodäsie und Geoinformation, Straße des 17. Juni 135, D-10623 Berlin, Tel.: 030-314-23274/23206, Fax: -21973, e-mail: kolbe@igg.tu-berlin.de

- **Standardisierung und Qualitätssicherung**

Prof. Dr.-Ing. Wolfgang Kresse
Fachhochschule Neubrandenburg, Fachbereich BV, Brodaer Straße 2, D-17033 Neubrandenburg, Tel.: 0395-5693-355, Fax: -399, e-mail: kresse@fh-nb.de

- **Auswertung von Fernerkundungsdaten**

Dr. habil. Horst Weichelt
Sperberhorst 3, D-14478 Potsdam, Tel.: 0331-861707, Mobil: 0162-1003158, e-mail: dgpf-akfe@h-weichelt.de oder: horst@h-weichelt.de

- **Nahbereichsphotogrammetrie**

Prof. Thomas Kersten
HafenCity Universität Hamburg, Labor für Photogrammetrie & Laserscanning, Hebbrandstraße 1, D-22297 Hamburg, Tel.: 040-42826-5343, Fax: -5399, e-mail: thomas.kersten@hcu-hamburg.de

- **Fernerkundung in der Geologie**

Dr. Hans-Ulrich Wetzel
GeoForschungsZentrum Potsdam, Telegraphenberg A 17, D-14473 Potsdam, Tel.: 0331-288-1194, Fax: -1192, e-mail: wetz@gfz-potsdam.de

- **Sensoren und Plattformen**

Prof. Dr. Norbert Haala
Universität Stuttgart, Institut für Photogrammetrie, Geschwister-Scholl-Str. 24D, 70174 Stuttgart, Tel.: 0711-685-83383, Fax: -83297, e-mail: norbert.haala@ifp.uni-stuttgart.de

- **Hyperspektrale Fernerkundung**

Dr. András Jung
SphereOptics GmbH, Remote Sensing Technology, Bergstr. 36, D-88690 Uhldingen, Tel.: 07556-9299666, Fax: -50108, e-mail: ajung@dgpf.de

- **Radar-Fernerkundung und Flugzeuglaserscanning**

Prof. Dr. Uwe Sörgel
Leibniz Universität Hannover, Institut für Photogrammetrie und Geolnformation (ipi), Nienburger Straße 1, D-30167 Hannover, Tel.: 0511-762- 2981, Fax: -2483, e-mail: soergel@ipi.uni-hannover.de

- **3D-Stadtmodelle**

Dipl.-Ing. Bettina Petzold
Stadt Wuppertal, Ressort Vermessung, Katasteramt und Geodaten, Johannes-Rau-Platz 1, D-42275 Wuppertal, Tel.: 0202-563-5428, Fax: -8158, e-mail: bettina.petzold@stadt.wuppertal.de

Dipl.-Ing. Ekkehard Matthias
Freie und Hansestadt Hamburg, Landesbetrieb Geoinformation und Vermessung, Sachsenkamp 4, 20097 Hamburg, Tel.: 040-428-26- 5750, Fax: -5966, e-mail: Ekkehard.Matthias@gv.hamburg.de

Berichterstatter für ISPRS und CIPA

Kommission I – Image Data Acquisition – Sensors and Platforms
Dr.-Ing. Franz Kurz
D-82230 Oberpfaffenhofen
e-mail: Franz.Kurz@dlr.de

Kommission II – Theory and Concepts of Spatial Information Science
Prof. Dr.-Ing. Monika Sester
D-30167 Hannover
e-mail: monika.sester@ikg.uni-hannover.de

Kommission III – Photogrammetric Computer Vision and Image Analysis
Prof. Dr.-Ing. Stefan Hinz
D-76128 Karlsruhe
e-mail: Stefan.Hinz@kit.edu

Kommission IV – Geodatabases and Digital Mapping
Dr.-Ing. Volker Walter
D-70174 Stuttgart
e-mail: volker.walter@ifp.uni-stuttgart.de

Kommission V – Close-Range Sensing: Analysis and Applications
Dr.-Ing. Danilo Schneider
D-01062 Dresden
e-mail: danilo.schneider@tu-dresden.de

Kommission VI – Education and Outreach
Dipl.-Inf. Gert König
D-10623 Berlin
e-mail: gerhard.koenig@tu-berlin.de

Kommission VII – Thematic Processing, Modeling and Analysis of Remotely Sensed Data
Dr.-Ing. Uwe Weidner
D-76128 Karlsruhe
e-mail: weidner@ipf.uni-karlsruhe.de

Kommission VIII – Remote Sensing Applications and Policies
Prof. Dr. Irmgard Niemeyer
D-09599 Freiberg
e-mail: Irmgard.Niemeyer@tu-freiberg.de

CIPA – Internationales Komitee für Architekturphotogrammetrie
Prof. Dr.-Ing. Michael Scherer
D-44780 Bochum
e-mail: michael.scherer@ruhr-uni-bochum.de

Gutachter der PFG im Jahr 2010

Gutachter im Jahr 2010

Der Wert einer wissenschaftlichen Zeitschrift hängt stark von der Qualität der Gutachten ab. Die Schriftleiter der PFG möchten sich hiermit bei folgenden Gutachtern herzlich bedanken, die neben dem Editorial Board ihre Arbeitszeit der dreifachen „blind“ Begutachtung gewidmet haben:

- Karl-Heinrich Anders, Villach, Österreich
- Stefan Auer, München
- Martin Bachmann, Oberpfaffenhofen
- Ulrich Beisl, Heerbrugg, Schweiz
- Ludwig Braun, München
- Claus Brenner, Hannover
- Michael Breuer, Berlin
- Thomas Brinkhoff, Oldenburg
- Thomas Brox, Berkeley, USA
- Manfred Buchroithner, Dresden
- Frank Canters, Brüssel, Belgien
- Vittorio Casello, Pavia, Italien
- Christopher Conrad, Würzburg
- Wolfgang Förstner, Bonn
- Georg Gartner, Wien, Österreich
- Markus Gerke, Enschede, Niederlande
- Michael Gertz, Heidelberg
- Görres Grenzdörffer, Rostock
- Eberhard Gülch, Stuttgart
- Karin Hedman, München
- Sören Hese, Jena
- Stefan Hinz, Karlsruhe
- Volker Hochschild, Tübingen
- Joachim Höhle, Aalborg, Dänemark
- Eija Honkavaara, Masala, Finnland
- Jürgen Jäger, Weßling
- Ekkehard Jordan, Düsseldorf
- Martin Kappas, Göttingen
- Hartmut Kenneweg, Berlin
- Thomas Kersten, Hamburg
- Birgit Kleinschmit, Berlin
- Barbara Koch, Freiburg
- Michael Köhl, Hamburg
- Klaus Komp, Münster
- Herbert Krauß, Köln
- Jukka Krisp, München
- Werner Kuhn, Münster
- Tobia Lakes, Berlin
- Christian Lucas, Karlsruhe
- Jose Antonio Malpica, Alcalá de Henares, Spanien
- Ioannis Manakos, Chania, Griechenland
- Ulrich Michel, Heidelberg
- Matthias Möller, Bamberg
- Andreas Müterthies, Münster
- Maik Netzband, Bochum
- Stefan Pickl, München
- Martin Raubal, Santa Barbara, USA

- Peter Reinartz, Oberpfaffenhofen
- Frank Riffel, Weßling
- Mathias Schardt, Graz, Österreich
- Michael Schmitt, München
- Thomas Schneider, Freising
- Monika Sester, Hannover
- Martin Smith, Nottingham, Großbritannien
- Uwe Sörgel, Hannover
- Christoph Strecha, Lausanne, Schweiz
- Hans Peter Thamm, Berlin
- Antje Thiele, Karlsruhe
- Markus Ulrich, München
- Sebastian van der Linden, Berlin
- Horst Weichelt, Potsdam
- Uwe Weidner, Karlsruhe
- Carsten Weyand, Köln
- Manfred Wiggenhagen, Hannover
- Marcel Ziems, Hannover

Daneben geht besonderer Dank an Michael Cramer und Cornelia Gläßer für die Organisation der Begutachtung für die PFG 2/10, Birgit Kleinschmit und Horst Weichelt für die PFG 4/10 sowie Monika Gähler und Stefan Hinz für die PFG 6/10.

Zum Titelbild

Satellitengestützte Kriseninformation mit RapidEye und TerraSAR-X Daten

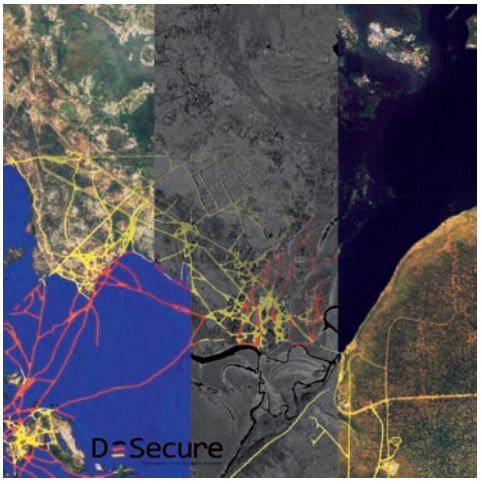

Die Caprivi Region im Nordosten Namibias wird eingegrenzt durch die Flussläufe des Zambezi im Norden und Linyanti im Süden. Überflutungen kommen in dieser Region zur Regenzeit regelmäßig vor. Im Frühjahr 2009 führten außergewöhnlich starke Regenfälle jedoch zu extremen Überflutungen: Zahlreiche Straßen waren unpassierbar und auch Siedlungsbereiche waren von den Überflutungen betroffen.

Im Projekt DeSecure wurde dieses Flutereignis als Basis für die Bearbeitung eines gemeinsamem Datenszenario genommen, durch das die Weiterentwicklungen des Projektes über die verschiedenen Aspekte von der Satellitenaufnahme über die Auswertung bis hin zur Dissemination der Ergebnisse gut dokumentiert werden konnten.

Das Titelbild zeigt eine Kombination von Satellitenszenen zum Zeitpunkt der Flut (links & rechts RapidEye vom 14.4.2009) sowie Referenzdatensätzen (Mitte: TerraSAR - X vom 1.9.2009) im Bereich der Siedlung Ngoma, Namibia. Darüber hinaus sind Teile einer extrahierten Flutmaske (blau) (auf Basis RapidEye vom 14.4.2009) sowie das abgeleitete Straßennetz (gelb) inkl. der überfluteten Teilstrecken (in rot) dargestellt. Diese Daten sind als interaktive Kartenanwendung über die DeSecure Homepage (www.desecure.info/desecure_webclient_de.html) abrufbar.

Weitere Informationen:
Dr. Monika Gähler, DeSecure Projektleitung, Deutsches Zentrum für Luft- und Raumfahrt Oberpfaffenhofen, 82234 Weßling, Tel.: +49-8153-28 -3309, www.desecure.info

Korporative Mitglieder

Firmen
AEROWEST GmbH
AICON 3D Systems GmbH
Alpha Luftbild GmbH
aphos Leipzig AG
Becker GeoInfo GmbH
Bernhard Harzer Verlag GmbH
Blom Deutschland GmbH
Brockmann Consult
bsf swissphoto
Büro Immekus
CGI Systems GmbH
con terra GmbH
Creaso GmbH
DEFINIENS AG
DELPHI IMM GmbH
Deutsches Bergbau-Museum
EFTAS Fernerkundung Technologietransfer GmbH
ESG Elektroniksystem- und Logistik-GmbH
ESRI Geoinformatik GmbH
EUROPEAN SPACE IMAGING
Eurosense GmbH
fokus GmbH
fpi Fuchs Ingenieure GmbH
g.on experience gmbh
GAF GmbH
GeoCad GmbH
GeoCart Herten GmbH
GeoContent GmbH
Geoinform. & Photogr. Engin. Dr. Kruck & Co. GbR
geoplana Ingenieurgesellschaft mbH
GEOSYSTEMS GmbH
GGS - Büro für Geotechnik, Geoinformatik, Service
Hansa Luftbild AG
IGI - Ingenieur-Gesellschaft für Interfaces mbH
ILV Ing.-büro für Luftbildausw. und Vermessung
Imetric 3D GmbH
Infoterra GmbH
INVERS - Industrievermessung & Systeme
J. Linsinger ZT-GmbH
Jena-Optronik GmbH
KAZ Bildmess GmbH
Leica Geosystems GmbH
Luftbild Brandenburg GmbH Planer + Ingenieure
Luftbilddatenbank-Würzburg
Messbildstelle GmbH
Microsoft Photogrammetry
MILAN Geoservice GmbH
PHOENICS GmbH
PMS - Photo Mess Systeme AG
RWE Power AG, Geobasisdaten/Photogrammetrie
technet GmbH
TerraVista Umweltdaten GmbH
TRIGIS Vermessung + Geoinformatik GmbH
Trimble Germany GmbH
trimetric 3D Service GmbH
Wichmann, VDE Verlag GmbH
Z/I Imaging Ltd.

Behörden
Amt für Geoinformationswesen der Bundeswehr
Bayerische Landesanstalt für Wald und Forstwirtschaft
Bundesamt für Kartographie und Geodäsie
Bundesmin. für Ernäh., Landw. u. Verbraucherschutz
DB Netz AG
Hess. LA für Bodenmanagement und Geoinformation
Innenministerium NRW, Gruppe Vermessungswesen
Inst. für Umwelt- und Zukunftsforschung
LA für Geoinformation u. Landentw., Baden-Württem.
LA für Vermessung und Geoinformation, Bayern
LB Geoinformation und Vermessung, Hamburg
LB f. Küstenschutz, Nationalpark u. Meeresschutz, SH
Landesvermessung und Geobasisinformation Nieders.
Märkischer Kreis, Vermessungs- und Katasteramt
Regierungspräs. Tübingen, Abt. 8 Forstdirektion
Regionalverband Ruhr
Staatsbetrieb Sachsenforst Pirna
Stadt Bocholt, Fachbereich 31
Stadt Düsseldorf, Vermessungs- und Katasteramt
Stadt Köln, Amt für Liegensch., Verm. und Kataster
Stadt Wuppertal, Verm., Katasteramt und Geodaten
Thüringer LA für Vermessung und Geoinformation

Hochschulen
BTU Cottbus, Lehrstuhl für Vermessungskunde
FH Frankfurt a.M., FB 1, Studiengang Geoinformation
FH Mainz, Inst. f. Raumbez. Inform.- und Messtechn.
FH Oldenburg, Inst. für Angew. Photogr. und Geoinf.
HCU HafenCity Universität Hamburg, Geomatik
HfT Stuttgart, Vermessung und Geoinformatik
HS Bochum, FB Vermessung und Geoinformatik
HS Karlsruhe, FB Geoinformationswesen
HTW Dresden, FB Vermessungswesen/Kartographie
Ruhr-Uni Bochum, Geographisches Institut
RWTH Aachen, Geodätisches Institut
TU Bergak. Freiberg, Inst. f. Markscheid. u. Geodäsie
TU Bergak. Freiberg, Inst. für Geologie, RSG
TU Berlin, Computer Vision & Remote Sensing
TU Braunschweig, Inst. für Geodäsie und Photogr.
TU Clausthal, Inst. für Geotechnik und Markscheidew.
TU Darmstadt, Inst. für Photogrammetrie und Kartogr.
TU Dresden, Inst. für Photogrammetrie und Fernerk.
TU München, FG Photogrammetrie und Fernerk.
TU Wien, Inst. für Photogrammetrie und Fernerk.
Uni Bonn, Inst. für Photogrammetrie
Uni Göttingen, Inst. für Waldinv. und Waldwachstum
LUH Hannover, Inst. für Kartogr. und Geoinformatik
LUH Hannover, Inst. für Photogrammetrie und GeoInf.
Uni Heidelberg, IWR Interdis. Zentr. f. Wiss. Rechnen
Uni Karlsruhe, Inst. für Photogrammetrie und Fernerk.
Uni Kassel, FB Ökologische Agrarwissenschaften
Uni Kiel, Geographisches Institut
Uni Stuttgart, Inst. für Photogrammetrie
Uni Würzburg, Geographisches Institut
Uni zu Köln, Geographisches Institut

PFG – Jahrgang 2010, Heft 1 – 6
Inhaltsverzeichnis Jahrgang 2010

Originalbeiträge, alphabetisch nach Autoren

Aus Wissenschaft und Technik

Prof. Friedrich Ackermann zum 80sten Geburtstag

Berichte und Mitteilungen

PFG · Photogrammetrie · Fernerkundung · Geoinformation
Jahrgang 2010 · Heft 6

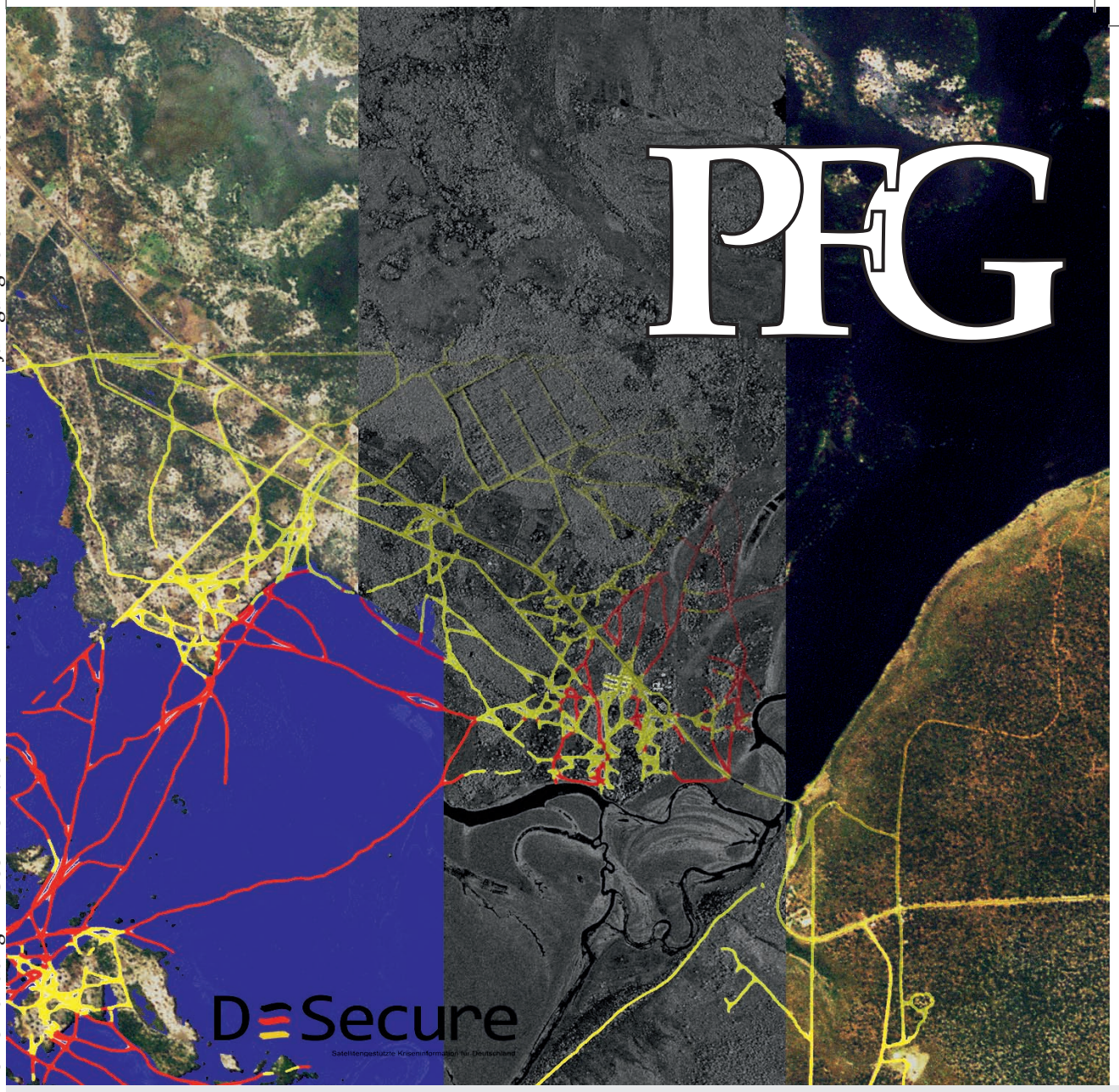

Photogrammetrie Fernerkundung Geoinformation

Jahrgang 2010
Heft 6
Organ der Deutschen Gesellschaft für Photogrammetrie, Fernerkundung und Geoinformation (DGPF) e.V.
Indexed in Science Citation Index Expanded (SciSearch®) Journal Citation Reports / Science Edition

E. Schweizerbart'sche Verlagsbuchhandlung (Nägele u. Obermiller) Stuttgart

PFG_Heft_5_2010.indd 1 07.10.2010 15:18:30 Uhr

Am 28. Oktober 2010 verstarb im Alter von 74 Jahren unser

Ehrenpräsident

Prof. Dr.-Ing. Jörg Albertz

* 29.02.1936 † 28.10.2010

Die Gesellschaft für Photogrammetrie, Fernerkundung und Geoinformation trauert um ihren Ehrenpräsidenten. Mit ihm verlieren wir eine stark prägende Persönlichkeit unserer Gesellschaft, einen großartigen Menschen und einen wertvollen Freund.

Jörg Albertz hat als langjähriger Schriftleiter unserer Fachzeitschrift, Vorstandsmitglied, Präsident und Ehrenpräsident mit großer Umsicht und Kompetenz, hohem persönlichen Einsatz und seinen menschlichen Qualitäten Außergewöhnliches für die Entwicklung unserer Gesellschaft geleistet

Jörg Albertz bleibt uns Vorbild. In Ehrfurcht verneigen wir uns vor seinen Leistungen und nehmen in tiefer Trauer Abschied. Er wird uns unvergessen bleiben und sein Andenken werden wir bewahren.

Vorstand der
Deutschen Gesellschaft für Photogrammetrie,
Fernerkundung und Geoinformation

Prof. Dr. Cornelia Gläßer
Präsidentin

10 Jahre
Oldenburger 3D-Tage

02./03. Februar 2011

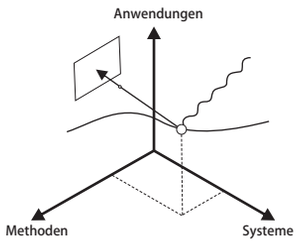

Photogrammetrie - Laserscanning
Optische 3D-Messtechnik

- ⇨ *Feierlichkeiten am 01.02.*
- ⇨ *über 40 Fachvorträge*
- ⇨ *große Firmenausstellung*
- ⇨ *Anwender, Dienstleister*
  Wissenschaftler, Hersteller

www.jade-hs.de/3dtage

Institut für Angewandte Photogrammetrie und Geoinformatik
Jade Hochschule Wilhelmshaven/Oldenburg/Elsfleth
Ofener Str. 16-19 26121 Oldenburg (Oldb)

Studienbücher der Geographie

Geographie und Fernerkundung

von Ernst Löffler, Ulrich Honecker
und Edith Stabel

3. vollst. überarb. u. erg. Aufl., 2005. 287 S., 105 Abb.,
9 Tab., 16 Farbtaf., ISBN 3-443-07140-6, € 29,00

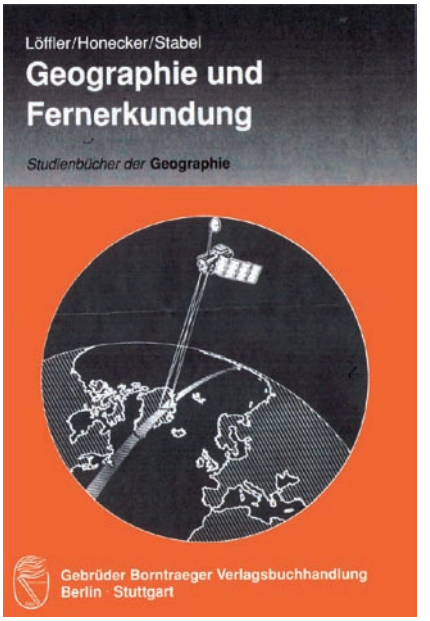

Seit dem Erscheinen der 1. Auflage dieses Buches vor 20 Jahren hat sich die Fernerkundung mit ungebrochener Dynamik weiterentwickelt. Besonders beeindruckend sind dabei ohne Zweifel die damals kaum für möglich gehaltenen Fortschritte in der Satellitentechnologie und insbesondere der digitalen Aufnahmetechnik. Gleichzeitig haben die digitale Datenverarbeitung und Bildklassifizierung, zusammen mit dem Einsatz geographischer Informationssysteme, die Möglichkeiten der Integration, Verschneidung und Repräsentation von Daten unterschiedlichster Art erheblich gesteigert. Es war daher notwendig, das Buch nicht nur zu überarbeiten und zu aktualisieren, sondern ihm auch eine etwas andere Schwerpunktsetzung zu geben. Dies gilt vor allem für die stark erweiterten Ausführungen über die digitale Bildverarbeitung und -klassifikation und die Radarerkundung. Am Charakter des Buches als Studienbuch wurde nichts geändert; es wird Wert gelegt auf eine verständliche Darstellung, ohne Vollständigkeit anzustreben.

Gebrüder Borntraeger · Stuttgart
Tel. +49 (0)711 351 456-0, mail@schweizerbart.de, www.schweizerbart.de

Kein Detail bleibt unerkannt – auch nicht das Kleinste.

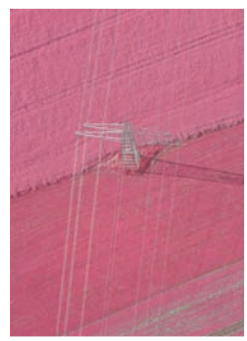

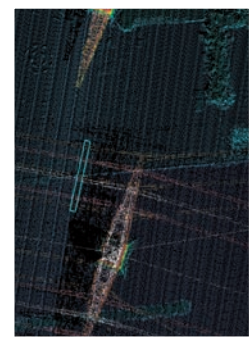

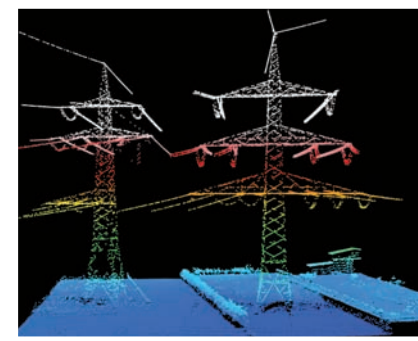

Jeder weiß, dass in der Steigerung der Effizienz der Weg zum Erfolg liegt. Darum kombinieren wir, bei Trimble GeoSpatial, erstklassige flugzeug- und landgestützte Geodatenerfassungssysteme mit weltweit führender Auswertesoftware, um Ihnen eine Vielfalt von Lösungen zur erfolgreichen Produktion von Geodaten anbieten zu können.

Zuverlässige und detaillierte Geodatenerfassung, mit bis vor kurzem unerreichbarer Geschwindigkeit, bildet die Grundlage für eine effiziente Bestandsdatenhaltung.

Trimble setzt auf innovative Geschäftsideen. Mit unseren GeoSpatial-Produkten bieten wir Ihnen stets den neuesten Stand der Technik, um den Anforderungen der sich ständig ändernden Bedingungen des Marktes gerecht zu werden. Weitere Informationen finden Sie auf unserer Website www.trimble.com/geospatial.

Besuchen Sie uns bei der Intergeo im Oktober und bei der Trimble Dimensions im November. Erfahren Sie, wie Sie von einer besseren Datenqualität in jeder Phase Ihrer Projekte profitieren können.

Trimble

© 2010, Trimble Navigation Limited. All rights reserved. Trimble and the Globe & Triangle logo is a trademark of Trimble Navigation Limited, registered in the United States and in other countries. All other trademarks are the property of their respective owners. GEO-007G

Trimble_GEOSPTL_PFG_DIM.indd 1 7/19/10 8:16 AM